

4-D Trajectory Prediction and Its Application in Air Traffic Management

by Zhiyuan Shi

Thesis submitted in fulfilment of the requirements for
the degree of

Doctor of Philosophy

under the supervision of Min Xu

University of Technology Sydney
Faculty of Engineering and Information Technology

September 2020

Acknowledgements

My sincere gratitude is first to my supervisor Associate Prof. Min Xu for her continual support, guidance, help and encouragement during my Ph.D. study. Min has brought me into the area of deep learning, and provided brilliant insights in my research works. It is my honour to have a supervisor who always inspires me to achieve higher targets. Her conscientious and meticulous attitude on research have significant influence on my research work.

I am grateful to Prof. Quan Pan in Northwestern Polytechnical University for his kind help. He encouraged me to be creative in academic research and guide me to make my research practical. He attaches great importance to international cooperation among universities and research groups. Every progress I made is closely related to Prof. Pan.

I would also like to demonstrate great appreciation to my co-supervisor Dr. Xiaoying Kong for her valuable comments and feedback on my research topic. Thanks for Ms. Jing Zhao and the officers in GRS for their patient guidance and help since I enrolled in UTS. I am grateful to all the staff in the School of Electrical and Data Engineering for their help on Ph.D. skills development.

Special thanks to my colleagues in Min's group, in particular, Haimin Zhang, Lingxiang Wu, Tianrong Rao, Zhongqin Wang, Lei Sang, Ruiheng Zhang, Yukun Yang Wanneng Wu, for their selfless help. My duration in UTS with the friends, Zhichao Sheng, Ye Shi, Hairong Yu, Yao Huang, Xilin Li and Hanjie Wu will be a good memory.

My deepest gratitude goes to my parents for their immeasurable support and encouragement throughout my graduate studies.

Abstract

Safety is assigned with the highest priority in Air Traffic Management. Trajectory prediction is the most crucial task in the increasing aviation activities. Situation of an aircraft can be assessed according to the predicted intention. Massive data contributes a lot for training a trajectory predictor, but cannot guarantee better decisions. While data visualization helps us understanding information well. Therefore, we carried out the following works in this thesis.

Points of interests play an important role in most land traffic prediction algorithms. Compared with land traffic, the sparse way-points and shared airways make it difficult for flight trajectory prediction. Practical information including landmarks, navigation facilities, and flight rules is fused and embedded in LSTM networks, namely the constraint LSTM network is proposed. Density-based Spatial Clustering of Applications with Noise and airports' locations segment the flight trajectories into climbing, cruising and descending/approaching phases. Linear Least Square fits the relationship of the constraint items. Sliding windows bridge the input sequences of LSTM network and help maintain the continuity of trajectory. Multiple ADS-B ground stations contribute to the historical flight trajectories for our experiment. The widely used LSTM network, Markov Model, weighted Markov Model, Support Vector Machine and Kalman Filter are used for comparison. Experimental results demonstrate that our trajectory predictor outperforms the above-mentioned state-of-the-arts models.

In addition to the trajectories, airports, pilots and geographical environment contribute a lot to stable and safe air traffic, especially during the climbing/descending phases. We increased of LSTM network to predict the flight trajectory in the climbing phase. Geographical environment, weather information, and dynamic performances of aircraft are modelled comprehensively in the proposed cubic A* search algorithm

for 3-D path planning when encountering an emergency. Real-time states of aircraft, including speed, altitude and track angle, are constructed as three threat factors, which are applied to assessment of the planned optimal path.

Finally, an auxiliary decision support system is developed based on ArcGIS 10.0, to graphically provide the intuitive and quick assistance for air traffic controllers. Multi-scale and multi-modal data is encoded as visual symbols and mapped on GIS to display geographical situations. Based on the predicted intention of an aircraft and scheduled flight plans, two cases are studied and analysed on our system, i.e., path planning for collision avoidance with mountains and rerouting suggestion for getting around the bush-fire, respectively. The system can provide timely auxiliary support for controllers to make decisions.

Publications

The contents of this thesis are based on the following papers that have been published, accepted, or submitted to peer-reviewed journals and conferences.

Journal Papers:

1. Zhiyuan Shi, Quan Pan, Min Xu. "LSTM-Cubic A*-based Auxiliary Decision Support System in Air Traffic Management," *Neurocomputing*, 2020. DOI: 10.1016/j.neucom.2019.12.062.
2. Zhiyuan Shi, Min Xu, Quan Pan. "4-D Flight Trajectory Prediction with Constrained LSTM Network," *IEEE Transactions on Intelligent Transportation Systems*. 2020. DOI: 10.1109/TITS.2020.3004807.

Conference Papers:

1. Zhiyuan Shi, Min Xu, Quan Pan, et al. "LSTM-based flight trajectory prediction", *2018 International Joint Conference on Neural Networks (IJCNN)*. July, 2018.

Table of contents

List of figures

List of tables

1	Introduction	1
1.1	Background	1
1.2	Problems in Aviation Activities Analysis	4
1.2.1	Differences in Data Quality	4
1.2.2	Special Geographical Terrains	7
1.2.3	Influences of Natural Environment	9
1.3	Motivation and Scope	11
1.4	Main Contributions	12
1.5	Dissertation Outline	14
2	Literature Review	17
2.1	Overview	17
2.2	Flight Trajectory Prediction	17
2.2.1	Performance-based Models	18
2.2.2	Trajectory-based Models	20
2.3	Path Planning	21

2.4	Decision Support System	22
2.5	Summary	24
3	Definitions in Air Traffic Management	25
3.1	Overview	25
3.2	Definitions in Air Traffic Management	26
3.2.1	Acronyms	26
3.2.2	Flight Phases Definition	27
3.2.3	Way-points	28
3.2.4	Air Routes	31
3.2.5	Flight Plans	33
3.3	Aeronautical Chart	36
3.4	Summary	37
4	4-D Flight Trajectory Prediction with Constrained Long Short-Term Memory Networks	39
4.1	Overview	39
4.2	Preliminary	40
4.3	Construction of Physical Constraints	42
4.3.1	Top of Climb	43
4.3.2	Way-points	44
4.3.3	Runway Direction	46
4.4	Constrained LSTM Network Building	48
4.5	Experiment and Discussion	51
4.5.1	Data Description	52
4.5.2	Trajectory Clustering	54

4.5.3	Coordinate Transformation	56
4.5.4	Constrained LSTM Network Building	58
4.5.5	Evaluation Methods	59
4.5.6	Experimental Results	60
4.5.7	Quantitative Analysis	68
4.6	Summary	72
5	Situational Awareness and Path Planning	73
5.1	Overview	73
5.2	4-D Trajectory Prediction in Climbing Phase	74
5.3	Path Planning Model	75
5.4	Threat Assessment Model	80
5.5	Experiment and Discussion	82
5.5.1	Data Collection	83
5.5.2	4-D Trajectory Prediction in Climbing Phase	85
5.5.3	Path Planning	88
5.5.4	Threat Assessment	89
5.6	Summary	92
6	Auxiliary Decision Support System and Its Case Studies	93
6.1	Overview	93
6.2	Visualization of Knowledge	95
6.3	Development of Auxiliary Decision Support System	98
6.4	Case Studies	101
6.4.1	Case 1: Path Planning in HKG Airport	101
6.4.2	Case 2: Rerouting Suggestion in SYD Airport	102

6.5	Summary	105
7	Conclusions and Future Work	107
7.1	Conclusions	107
7.2	Future work	108
	References	111

List of figures

1.1	Statistics on aviation accidents and casualties around the world in recent 20 years.	2
1.2	Airports that are constructed at special geographical locations (labelled with ICAO code).	8
1.3	The outline of this thesis.	12
3.1	Flight phases defined in ICAO.	28
3.2	Symbols of navigational facilities on aeronautical chart.	30
3.3	Schematic diagram of airway model in geographical environment.	33
3.4	Schematic diagram of flight plan.	36
3.5	IFR chart of Sydney Kingsford Smith Airport.	37
4.1	Chain structure of vanilla LSTM cells.	41
4.2	Construction of the constraint TOC.	43
4.3	Linear least square for approximating line equation of way-points.	45
4.4	Constraints applied by WPT.	46
4.5	A schematic diagram of descending/approaching phase.	47
4.6	Constrained LSTM network for 4-D flight trajectory prediction.	49
4.7	ADS-B assisted ATM system.	53

4.8	Visualization effect of trajectory prediction in Climbing phase with cLSTM, LSTM, MM, wMM, SVM and KF. (Constraint TOC)	62
4.9	Absolute errors of trajectory prediction in Climbing phase with cLSTM, LSTM, MM, wMM, SVM and KF. (Constraint TOC)	62
4.10	FFT on absolute errors of trajectory prediction in Climbing phase with cLSTM, LSTM, MM, wMM, SVM and KF. (Constraint TOC)	63
4.11	Visualization effect of trajectory prediction in Cruising phase with cLSTM, LSTM, MM, wMM, SVM and KF. (Constraint WPT)	64
4.12	Absolute errors of trajectory prediction in Cruising phase with cLSTM, LSTM, MM, wMM, SVM and KF. (Constraint WPT)	64
4.13	FFT on absolute errors of trajectory prediction in Cruising phase with cLSTM, LSTM, MM, wMM, SVM and KF. (Constraint WPT)	65
4.14	Visualization effect of trajectory prediction in Descending/Approaching phase with cLSTM, LSTM, MM, wMM, SVM and KF. (Constraint TOC, WPT and RWD)	66
4.15	Absolute errors of trajectory prediction in Descending/Approaching phase with cLSTM, LSTM, MM, wMM, SVM and KF. (Constraint TOC, WPT and RWD)	66
4.16	FFT on absolute errors of trajectory prediction in Descending/Approaching phase with cLSTM, LSTM, MM, wMM, SVM and KF. (Constraint TOC, WPT and RWD)	67
4.17	Prediction effect on the whole voyage with cLSTM and MM models.	67
4.18	Errors on the whole voyage with cLSTM and MM models.	68
4.19	Process of weights selection in loss functions of each constraint.	70
5.1	Commonly used three types of path search directions.	77
5.2	Force analysis of the aircraft during climbing phase.	78
5.3	Node expansion of the cubic A* search algorithm.	79

List of figures

5.4	Two classic data fusion models: JDL and DFIG.	81
5.5	The DEM data near Hong Kong International Airport.	83
5.6	Structure of SRTM-3 data.	84
5.7	Predictions of trajectory in climbing phase by LSTM, Markov Model, weighted Markov Model and Gaussian Hidden Markov Model.	85
5.8	Projection of the optimal path on the 762-meter-high horizontal plane.	89
5.9	Optimal path planned by cubic A* search algorithm.	90
5.10	Threat assessment on the optimal path.	91
6.1	Data visualization process.	96
6.2	Functions of our auxiliary decision support system.	98
6.3	Fundamental functions of our auxiliary decision support system.	100
6.4	Climbing flight path planning for obstacle avoidance in Hong Kong International Airport.	101
6.5	Flight volume and on-time rate of Sydney Kingsford Smith Airport in the year 2019.	103
6.6	Rerouting suggestion for the departure and landing aircraft around Sydney Kingsford Smith Airport.	104

List of tables

1.1	Differences of different data types in air traffic.	7
3.1	Altitude thresholds for TO, IC, AP and LD phases in BADA models. .	28
4.1	Performance comparison among cLSTM model and state-of-the-arts models.	71
5.1	Similarity evaluations of the predicted trajectories and ground truth of the LSTM, MM, wMM and G-HMM models.	86

Chapter 1

Introduction

This chapter starts with the background of this thesis, then introduces the problems related to the research topic, which inspires the motivation and scope. The main contributions and outline of the thesis are provided in the end of this chapter.

1.1 Background

As one of the major ways of public transportation, civil aviation plays a vital role in both personal life and social development. According to International Civil Aviation Organization (ICAO) [1], the growth rate of air traffic has expanded twice every 15 years since the mid-1970s. In the year 2014, the number of passengers reached 330 million. While the air freight value exceeded \$ 6.4 trillion annually [2]. As reported in IATA-annual review [3], the world's airlines provided about 4.4 billion passengers travelling on 46.1 million flights between almost 22,000 routes in the year 2018. Aviation supports 65 million jobs and \$ 2.7 trillion in global GDP. Accordingly, many problems exist in current air traffic. Rapidly increasing flight volumes have put heavy pressure on airspace, which results in the saturation of airspace usage. In addition, chartered plane, low altitude unmanned aerial vehicle, helicopters are very active in the low altitude airspace in recent years, which makes the situations worse. Furthermore, frequent aviation activities brought by increasing aircraft in a fixed amount of airspace also result in certain burdens and potential risks, as they can cause severe air traffic jam,

resources consumption and even accidents. The congested and busy airspace increases workload of air traffic controllers. In the year 2019, there were approximately 37.12 million departures around the world with 75.58% on-time rate. The average take-off delay was 26.47 minutes [4]. Accidents occur frequently when the aircraft take off and land. Even small errors can lead to serious consequences. MH370 crashed in March, 2014, which shocked the whole world but does not stop worldwide aviation accidents. ET302 disappeared from radar and dropped in six minutes after departure in March, 2019. Once a civil aircraft crashes, it will inevitably cause loss of lives and properties. Fig. 1.1 illustrates statistics on the accidents and casualties around the world since year 2000 [5]. Though in recent years, these data have decreased with the advancement of modern technologies, accidents have not been completely prevented. In 2020, until now there were 2 fatal accidents that resulted in 179 fatalities. These problems will greatly affect the safe, orderly and efficient operation of air traffic.

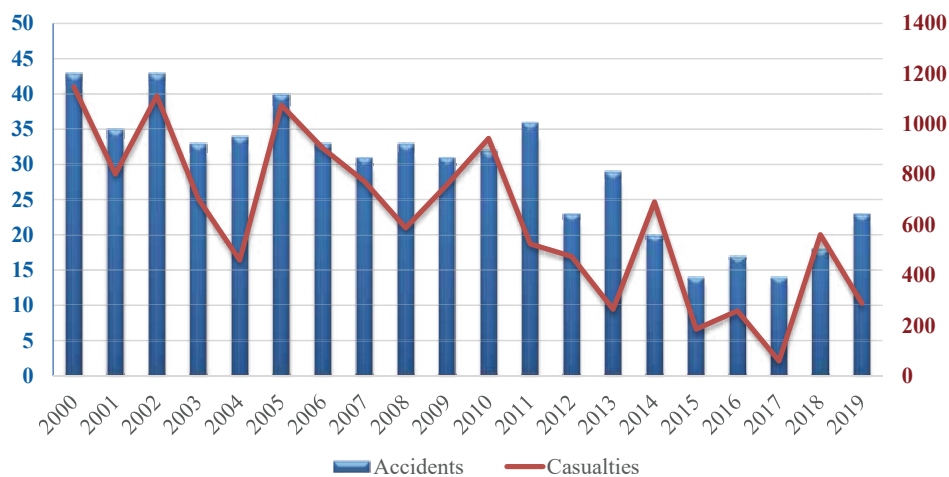


Fig. 1.1 Statistics on aviation accidents and casualties around the world in recent 20 years.

Air traffic management (ATM) applies technologies including communications, navigation and monitoring to ensure safety and orderly flight during the aviation tasks. ATM models have gradually become data-driven and request significant increasing computing resources in recent decades. Data is being generated on an unprecedented scale and aviation data is no exception. As is pointed out in [6], current ATM system has reached a limit to safely manage the numerous aircraft at the same time. It might suffer a lot to provide efficient services in the coming decades. According to

the 2017-2019 strategic objectives in ICAO, safety is assigned with the first priority in ATM. In addition, ATM should also increase capacity and improve efficiency, enhance security and facilitation, promote economic development, and minimize the short-term or continuous impact on the ecosystem caused by civil aviation activities. ICAO obliges countries to formulate their programs according to the 2016-2030 global air navigation plan (GANP) [7] for better management.

Forecasting is vital to avoid mistakes or reduce errors when making risk assessment and decisions. Flight trajectory prediction lays a solid foundation for tasks including air traffic flow and capacity management, conflict detection, flight planning, rerouting suggestion and arrival/departure management. Especially with the increasing amount of air traffic, there is an urgent requirement on efficient and accurate trajectory predictors, which will precisely indicate the short/long-term intent of aircraft so that to provide arrival information. Multi-modal information of multiple fields (sources) need to be considered comprehensively in trajectory prediction. The aircraft performance, regulations of air traffic management organizations, geographical terrain, meteorological conditions and (active/passive) detection information vary during a flight task. Trajectory predictor is not only the basis of complex airspace and high-density traffic flow management, but also a critical part of ATM systems. The significances of four-dimensional trajectory prediction (4DTP) lie in but not limited to the following aspects:

- For the nations and passengers, 4DTP will guarantee the safe flight during the tasks. Predicting the intention of the aircraft in advance can effectively reduce the accident rate so that improve the safety.
 - Pilots will realize in advance the traffic and weather conditions of the airspace that is about to arrive. They can make some decisions under certain traffic conditions or report and wait for guidance from ground-based control centre.
 - Air traffic controllers (ATC controllers) will tell the situations with accurate prediction, such as conflict and abnormal detection, alert on dangerous terrain and severe weather. They can make timely decisions on the forecast intention of an aircraft in advance, for example, path planning for collision avoidance and rerouting for unexpected influence of natural phenomena.

- For the ATC controllers, 4DTP can significantly reduce their burden on trajectory management, which include flow and capacity management, and arrival/departure management. While data visualization can accelerate the process of knowledge understanding to assist decision-making. Air traffic flow can be reasonably arranged, which can accordingly increase the utilization of airspace, thereby improving the efficiency of ATM systems.
- For the airlines, 4DTP will relieve the congestion and guide the aircraft performing its task with less cost, for example fuel consumption.

1.2 Problems in Aviation Activities Analysis

There are a series of factors that have influence on aviation activities analysis. We summarize them as differences of data quality, special geographical terrains and influences of natural environment.

1.2.1 Differences in Data Quality

Flight trajectory is a kind of spatial point set, which raises a unique challenge for prediction. As summarized in [8], spatial data is characterized in spatial dependency and heterogeneity with limited ground truth. GPS-based devices record the living habits and trajectories of pedestrians and vehicles with large scale and high frequency. These densely distributed and accurately located points of interest (POI) greatly assist the trajectory prediction in land traffic. POIs, including living habitats, hospitals, schools, supermarkets and gas stations, improve the accuracy a lot in pedestrian and land traffic trajectory prediction. Spatial-temporal location can be well predicted by Markov Model, in terms of the Markovian property of POIs transitions. The state-of-the-art Hidden Markov Model works well in the ground spatial-temporal prediction with robust performance [9]. Way-points in aviation are the navigation aids at are pre-set strategic location with latitude/longitude coordinates, which provide guidance for the aircraft within their coverage. They could be rare and far apart. Airways are defined as segments consisting of way-points and constructed with certain corridor width. Ideally,

an aircraft should fly along the centreline within corridor width. Sometimes, due to the bad weather, traffic conditions and geometry environment, the intent of an aircraft should adapt to different conditions.

Different communities concern differently about the civil aviation, which results in different data structures when collecting information for each community. Passengers focus more on the punctuality of flights. Airlines mainly care about attendance and fuel consumption. While ATM systems consider the safety as the most important factor for safe and orderly flight. In addition, different organizations/regions define the concept baseline differently, which make the representation of same data inconsistent. Taking the airport code as an example, ICAO uses the four-letter code, while IATA with a three-letter code. We take Sydney Kingsford Smith Airport as an example, it is referred as YSSY in ICAO rules, while SYD in IATA. Trajectory prediction is tightly related to the data quality, which mainly includes the accuracy, update frequency, dataset size, data volume, data dimensions, accessibility and to name but a few. It is difficult for us to build an accurate trajectory predictor without sufficient data.

Generally, when referring to aircraft trajectories, flight phases are the first to be considered in a task. Though ICAO has made detailed definitions on flight phases, it is difficult for us to identify the accurate phase without being able to access the status dataset of aircraft [10]. While in the flight trajectory prediction, way-points are too sparse to label a trajectory in the ascending, cruising and descending phases, which are usually located at a strategic position to estimate the arrival time for the ground-based ATM systems. Localization with Time of arrival (ToA) / Time difference of arrival (TDOA) is the simplest way to achieve an optimal traffic synchronization in ground-based ATM systems. ToA relies heavily on the positioning accuracy of navigational facilities and the allocated system resources [11]. Besides, multi-path caused by the terrain will bring distress and impact on the accurate positioning. The number of aircraft at large/busy airports and their surrounding areas has increased dramatically. High-density traffic reduces the distance between aircraft and airport, especially during the climbing and approaching phases, which may result in runway incursions and conflicts. Multilateration (MLAT) is a proven technique for locating aircraft by using TDOA. Instead of detecting the absolute distance or angle, MLAT measures the difference between two stations at known locations. In order to expand

the scope of measurement and enhance the tracking effectiveness, a number of ground stations are employed in MLAT. They are built in strategic locations around airport. Huge distance measurement error can be introduced by multi-path and non-line-of-sight (NLOS) conditions. However, it is still disturbed by problems such as signal interference, radio emission frequency, the optimal positions and data transmission.

Flight plans are generally made up of way-points and airways (with multiple flight levels/altitudes). They divide the airspace into discrete gridded spatial spaces. Compared with the way-points, in addition to the constraint on reporting position, flight plans also constrain the trajectory prediction on both time and span (airway direction) intervals. These scheduled flight tasks can help a lot for trajectory prediction, but fail to provide identification information for the high-density flight tasks, as they will not update with time. Air traffic control detectors and controllers will take over the aircraft, once they submit the flight plans. The diverse methods on detection and rich data content make the monitoring data more suitable for training a trajectory predictor. However, data may be stored in multi-modal, such as regulations and rules of air traffic management are usually published by procedures, which are not described with equations and triggered by certain events. Both actual flight plans and ATC data are not public for the researchers, organizations or personal applications.

Automatic dependent surveillance broadcast (ADS-B) services [12] are open to the public. It can provide as much data as possible for ATM systems to provide assistance or correct system deviations for detection equipment. Limited by the coverage of single device, a group of ground stations is needed to monitor certain regions. Since the ADS-B data is completely open, it cannot be directly introduced to ATM systems. Currently, it acts as an auxiliary source in ATM. Pilots and ATC controllers can see the data in a separately screen to judge the situation. In addition, the ADS-B data needs to be verified by ATM systems before being accepted.

In summary, the differences of different data types are concluded in Table 1.1. As it implies, we have the full access to way-points and ADS-B messages and can obtain all the information they can provide. ADS-B messages stand out from these data categories due to their integrity and accessibility. In many research works, the updating interval of ADS-B trajectories is set to be 15 seconds [13]. Though ATC data is perfect

Table 1.1 Differences of different data types in air traffic.

Data Type	Content	Amount	Integrity	Real-time	Accessibility
Way-points	★	★★	★★★★	/	★★★★
Flight plans	★★★	★	★	★★★	*
ADS-B messages	★★★★	★★★★	★★★★	★★★★	★★★★
ATC data	★★★★	★★★★	★★★★	★★★★	/

★ indicates the rank of data quality, the more the better of this attribute.

* means that we can get some information similar to the data item.

/ stands for the absence of attribute item.

as or better than ADS-B messages, it is not public for the safety reasons. Flight plans are the files that transmit flight tasks between pilots/airliners and ATC controllers, which are also not publicly available. However, we can get the expected departure and landing airports/time from certain websites. As a traditional navigational way, although the way-points contain less amount of information, they still play vital role in current ATM systems. We take the route "Hong Kong - Sydney" as an example to make the star more clear. The straight-line distance between these two airports is about 3980 nautical miles. There are 48 way-points in the whole voyage, which constitute a route mileage of 4032 nautical miles according to the historical flight plans. While ADS-B messages or ATC data can report over 2000 track points for each aircraft.

1.2.2 Special Geographical Terrains

Flight plans are mandatory documents to submit before or not long after take-off, which specify the spatial-temporal constraints during the flight phases. Most current flight trajectory predictors are trajectory-based operations, which face the challenge raised by the grid-structured geographical environment.

Geographical region poses certain influence on aviation safety. It is quite challenging for pilots to fly over mountains or complex terrains due to the changing visibility during flight phases [14]. As briefly described in Section 1.1, although the number is now reduced, every accident is a tragedy. Take-off and landing are proved to be the phases with high accident rate according to the statistics [15]. To maintain airspace safety, the intention of aircraft can be predicted with its flight envelopes, which are dynamic and

vary with altitude. In turn, accurate trajectory prediction can give a positive feedback to the location-aware computing.

Infrastructures of airports are also crucial, including the construction sites, surrounding environment and corresponding emergency facilities. Therefore, most of the world's airports are well-designed to provide the most comprehensive protection for the aircraft, except for some special cases. There are such airports around the world, some of which are located in the mountains, some are located in the middle of a big city, some runways extend straight into the ocean. We list four selected airports that are located at special/dangerous geographical positions as shown in Fig. 1.2.

**RJBB****LPMA****TNCM****MHTG**

Fig. 1.2 Airports that are constructed at special geographical locations (labelled with ICAO code).

Despite their special geographical locations, some of these airports are irreplaceable in daily air traffic.

- Kansai International Airport (RJBB). It is a large maritime international airport that located on an artificial island five kilometres offshore. As reported, Kansai International Airport has over 30 million passengers on international and domestic routes in 2019.
- Maderia Airport (LPMA). The airport was known for its short runways, and it is surrounded by mountains and oceans. It is considered as one of the most dangerous airports around the world.
- Princess Juliana International Airport (TNCM). The runway of this airport is extremely close to the shore and beach, which requires very low-altitude flyover landing approaches.
- Toncontín International Airport (MHTG). It is located in a valley surrounded by mountains with relatively short runway. Poor visibility makes it difficult to take off and land, especially in inclement weather conditions. It was ranked as the second most extreme airport in the world.

In summary, geographical locations mainly have serious influence on the visibility of pilots and the surrounding weather of aircraft. The intention of aircraft will change according to the terrain features and weather conditions under the guidance of ATC controllers. Therefore, in the work of trajectory management, we must take the terrain (at least elevation) into consideration, and infer the possible diversion paths in dangerous situations, such as collisions and adverse weather conditions.

1.2.3 Influences of Natural Environment

Almost half of the abnormal flights are directly or indirectly related to the natural environment, including weather conditions and natural disasters. They are key reasons that threaten the safety of air transportation and cause heavy delays. Aviation weather generally includes airport and en-route weather. Wind, visibility and cloud base height are the main indicators that have important influence on airport operations. While thunderstorms, lightning, low-altitude wind shear and volcanic ash can pose a threat to safe flight. Terrain and weather are sometimes inseparable and even affect each other.

Weather conditions have important influence on airports before they can serve for the air traffic. Runway direction is determined once a new airport is selected, which may be affected by many factors including wind conditions, airspace conditions, type and number of aircraft operations, topography of the site and some other aspects. Among them, wind conditions are the first and most important item to be considered. Severe weather conditions at departure and arrival airports will not only affect the flight task, but also have influence on passengers, airports, airlines and the ATM systems. As we know, weather has a certain degree of diffusivity, thereby disrupting the aircraft on certain route or area.

Wind shear is extremely harmful to aviation, especially during the take-off and landing phases. For the flights with low speed, wind shear can make a strong impact on the airspeed of the aircraft, which results in a large deviation from the scheduled routes. In the low-altitude airspace, this change can sometimes be catastrophic. There are two main causes of wind shear:

1. **Atmospheric motion.**

- Severe convection. It is usually referring to weather such as thunderstorms and cumulonimbus.
- Frontal weather.
- Low-level jet of radiation inversion. This type of wind shear is usually very weak, so it is easy to be ignored. But it will be dangerous if not handled properly.

2. **Geographical/environmental factors.** It mainly includes mountainous terrain, tall buildings, groves of trees and natural/man-made factors. Wind shear caused by geographical/environmental factors is related to prevailing wind conditions, size and complexity of the mountain terrain, shape of buildings, etc. The wind scale usually increases with elevation difference, water area and the height of building.

Sometimes it is a combination of the two factors.

Almost all the natural disasters are closely related to weather, water and climate. The factors that cause disasters are complex, which usually are combinations of different

items. Some disasters will have a series of lasting effects with wide range and heavy impact. While some disasters are obvious regional, such as bush-fire, which is influenced by distribution of combustible.

Taking the aviation meteorology into consideration, we can ensure the flight safety, punctuality, and save fuel. In trajectory prediction and path planning, natural environment can be considered as an obstacle. However, the location, shape and severity of this obstacle vary with time. In addition, the reactions/measures for various situations are different, accordingly.

1.3 Motivation and Scope

Trajectories should be predicted in the ground-based ATM systems for better management according to the instructions of Base of Aircraft Data (BADA) in EUROCONTROL [16]. Modern equipment has been greatly improved in terms of type and data capacity, thereby enhancing their capabilities in monitoring and managing trajectories. A large number of multi-modal data is generated and accumulated in data processing centres. However, massive data contributes a lot for forecasting, but cannot guarantee better decisions. Decision-making is closely related to threat assessment. Geographic information system (GIS) manages data by indexing spatial-temporal location. Both related and unrelated information can be integrated by using location as the key index variable in GIS, which makes it able to provide auxiliary decision-making in wide-area applications.

We aim to provide precise short/medium-term intentional perception for the flight task in case of unexpected situations, such as conflicts, crashes or collisions. Both dynamic performance of aircraft and static navigational information are considered when constructing constraints for constrained Long Short-Term Memory (cLSTM) network. Terrains and airspace around designated airport are modelled as discrete gridded spaces by digital elevation model and the dynamic performance of aircraft, respectively. A cubic A* algorithm is proposed for obstacle avoidance based on the predicted state in 4-D space. Threats between aircraft and the mountains are assessed along the optimally planned path. Natural environment is constructed as polygons,

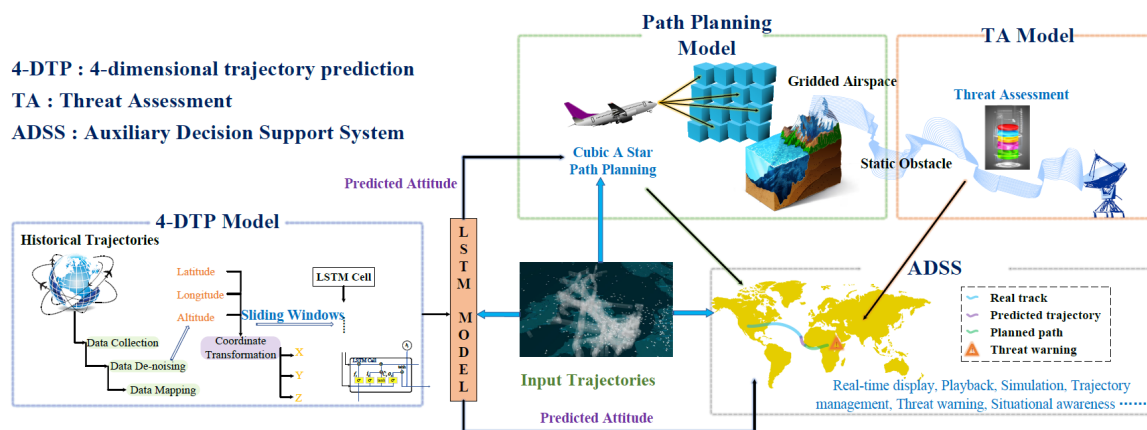


Fig. 1.3 The outline of this thesis.

which helps the rerouting flight path before the aircraft entering the dangerous area. Overall, the above-mentioned functions are embedded to our auxiliary decision support system, which is built based on ArcGIS 10.0 to provide Geo-environment information and spatial-temporal mapping, as is shown in Fig. 1.3. Our system has been proven to provide stable and effective assistance in practical circumstance by multiple tests.

1.4 Main Contributions

The thesis mainly contributes in following aspects:

1. Static ground-based navigational information and dynamic performance of aircraft are modelled as three types of constraints, i.e., Top of Climb (TOC), Way-Points (WPT) and Runway Direction (RWD), respectively. These constraints are taken into consideration as part of loss functions of the LSTM networks.
 - TOC is constructed based on the climbing/descending performance of an aircraft, which mainly applies restriction on attitude angle to limit the spatial span along the altitude direction.
 - WPT fits the discrete sparsely distributed way-points into a line through linear least square. It corrects the heading of the aircraft and drags it towards the specified way-points at the horizontal plane. Attitude adjustments are accomplished in the cruising level.

- RWD models departure/entry points around airports and the direction of runways as constraint in direction. Combined with TOC and WPT, the constraints adjust both descending altitude and heading.
2. Considering the behaviours and performance of each flight phase, we design an unique cLSTM network. LSTM network embedded with TOC leads our forecast to specified location. LSTM network embedded with WPT drags the predicted positions from deviations of the centreline of airways. LSTM network embedded with RWD guides the predictions to land accurately. These three LSTM networks with corresponding constraints are concatenated, which enables our model to achieve accurate prediction on the whole voyage. Taylor's expansion and linear least square guarantee a fast and low-complexity process. Sliding windows help maintain continuity of the predicted trajectory with control on the spatial span. Our model outperforms the state-of-the-arts models in short/medium-term 4-D flight trajectory prediction.
 3. In order to shorten the time required for data analysis and provide a reliable path for obstacle avoidance. Airspace is divided into discrete adjacent cubes according to the maximum yaw angle and Rate of Climb (RoC) of specified type of aircraft (A320).
 - Cubic A* search algorithm is proposed considering the dynamic performance of aircraft. In the climbing phase, maximum yaw angle and RoC limits the spatial span of the aircraft, which makes our model able to generate the optimal 3-D path in a very short time.
 - Threat factors consist of real-time speed, altitude and track angle of the aircraft along with the planned path. Threats caused by mountains and no-fly zones are assessed to ensure reliability of the optimal path.
 4. Knowledge of multi-modal dataset is visualized and mapped on the geographic information system. Data that cannot be expressed by equations (regulations/rules) are represented by visual shapes. With the help of ArcEngine, an auxiliary decision support system is designed and built on this basis. Practical cases, including collision avoidance in Hong Kong International Airport and rerouting over bush-

fire in Sydney Kingsford Smith Airport, are tested and verified on our system, which shows good robustness and high efficiency.

1.5 Dissertation Outline

The outline of the dissertation is as follows:

Chapter 1

This chapter presents the background, problems in the research topic, motivation and scope, contributions and the outline of the dissertation.

Chapter 2

An overview of air traffic management including 4-D trajectory prediction, path planning and decision support system is presented in this chapter.

Chapter 3

Regulations and definitions used in air traffic management and our thesis are introduced in this chapter. In the limited controlled airspace, ATM systems apply navigational facilities to aid the control and management for the operators. Navigational facilities, airways and flight plans are the foundations of ATM systems, which are presented by multi-modal data. We will use these basic data under the rules of ICAO.

Chapter 4

We model the navigational facilities mentioned in Chapter 3 as physical constraints to be applied to our trajectory prediction model. Specifically, top of climb, way-points and runway direction are generalized as distance and angular constraints. Multiple ADS-B ground stations contribute to our historical trajectory database. The Density-Based Spatial Clustering of Applications with Noise segments the trajectory database into climbing, cruising and descending/approaching phases. We build our 4-D trajectory predictor based on constrained LSTM network for each phase which is embedded with corresponding constraint item. The networks are concatenated to provide prediction for the whole flight phase. In the quantitative analysis part, we compare our performance with conventional methods and practical systems. Our model outperforms the listed models and most of the practical variants.

The work in this chapter has been published in:

- Zhiyuan Shi, Min Xu, Quan Pan, et al. "LSTM-based flight trajectory prediction," *2018 International Joint Conference on Neural Networks (IJCNN)*. July, 2018.
- Zhiyuan Shi, Min Xu, Quan Pan. "4-D Flight Trajectory Prediction with Constrained LSTM Network," *IEEE Transactions on Intelligent Transportation Systems*. 2020. DOI: 10.1109/TITS.2020.3004807.

Chapter 5

Precise 4-D trajectory predictor is key important for the airports that are located at special geographical environment. Terrains (mountains) raise certain threat for the take-off and landing aircraft, due to poor visibility of pilots, unstable airflow, the frequent manoeuvring and heavy traffic flow. Airspace is divided into adjacent cubes according to the dynamic performance of aircraft. We model the airport and its surroundings as a gridded space during the climbing and descending phases. The intent of an aircraft can be judged by our 4-D trajectory predictor, then we will assess the geographical environment on its predicted way. Once potential threat appears, the path plan and threat assessment models will be triggered to guide the aircraft performing its task safely. The proposed cubic A* path planning model can provide an optimal path in a very short time for the ATC controllers. Meanwhile, the safety of planned path is also evaluated to present numerical safety indicators for decision-making.

The work in this chapter has been published in:

- Zhiyuan Shi, Quan Pan, Min Xu. "LSTM-Cubic A*-based Auxiliary Decision Support System in Air Traffic Management," *Neurocomputing*, 2020. DOI: 10.1016/j.neucom.2019.12.062.

Chapter 6

Decision is the last but important work when dealing with any cases. Massive data contributes a lot for forecasting, but cannot guarantee better decisions. In this chapter, we build a database for ATM system as priori information to judge the situations. However, multi-modal data can be confusing and complex for a decision-maker to take a right reaction. We map the knowledge that appeared within the scope of ATC into visual GIS shapes. Based on the ArcEngine, we develop an auxiliary decision support system for ATC controllers. It will provide us an intuitive and controllable way to

manage the messages. We test and verify our system by several practical cases, which are added following the system description. This system will reduce the burden on the ATC controllers and speed up the information processing.

The work in this chapter is part of the published journal in:

- Zhiyuan Shi, Quan Pan, Min Xu. "LSTM-Cubic A*-based Auxiliary Decision Support System in Air Traffic Management," *Neurocomputing*, 2020. DOI: 10.1016/j.neucom.2019.12.062.

Chapter 7

This chapter summarizes the works of this Ph.D. dissertation and presents the future research developments.

Chapter 2

Literature Review

2.1 Overview

Literature reviews on flight trajectory prediction, path planning and decision support systems are introduced in this chapter.

2.2 Flight Trajectory Prediction

Air traffic management systems based on 4-D trajectory-based operations (TBO) were proposed successively in the United States and Europe, which were named as the Next Generation Air Transportation System (NextGen) [17] and Single European Sky ATM Research (SESAR) [18], respectively. Modern technologies and equipment made the aircraft visible and provided a more accurate report of their positions. The cooperation between ADS-B and ATM systems enables increased capacity, safety and efficiency of air traffic and benefits both pilots and ATC [19–21]. Most of current researches on trajectory prediction are trajectory-based, which relies on navigation-aid gridded planning. In terms of the structure and parameters of algorithms, ground-based 4-D trajectory prediction can be mainly divided into aircraft performance-based and trajectory-based models. Flight trajectory prediction is an attractive but complex research. Aircraft operation models [22], flight plans [23] and external environment should be considered comprehensively. Among these factors, civil aviations may

be influenced heavily by meteorological conditions, which attract much attention of scholars and institutes [24][25].

Data provides the foundation for researches in ATM systems. Detection equipment, ground stations, satellites, and other facilities supply a sufficient amount of data for modern traffic and management systems. Aircraft performance, sensing equipment and meteorology have a heavy influence on aircraft trajectory prediction. Base of Aircraft Data (BADA) families are able to provide precise aircraft performance and operating procedure coefficients for over 399 different aircraft types [26]. These coefficients can be used to formulate aircraft state (mass), intent (thrust and drag laws, speeds) and fuel flow. Historical trajectory dataset can be automatically collected by ADS-B ground stations so that provide data foundation. Precise trajectory-based trajectory prediction can be achieved based on ADS-B data [27]. In [13], the machine learning method, Gradient Boosting Machines, was applied on point-mass parameters learning to improve climb prediction with ADS-B data. Short/mid-range intention prediction was performed for conflict detection in [28]. Meteorological data is not as easy to access as ADS-B. But it has a serious impact on aircraft trajectory prediction. Both Japan Meteorological Agency (JMA) [29] and BADA model contributed meteorological data for the optimal trajectory-based prediction in [27].

2.2.1 Performance-based Models

Hundreds of research and operational papers related to Separation Management were reviewed in [30]. According to the author, classical mathematical models for trajectory prediction can be summarized as Point-Mass, Kinematic, Kinetic and other models. The kinetic aircraft performance model, earth model and aircraft intent were involved in Trajectory Computation Interface in [31]. Thrust model [32] and total energy model [33] of BADA were also used to estimate aircraft mass in recent researches. In order to avoid the impact of wind, a non-linear LASSO controller was designed for an UAV for trajectory tracking in [34]. Effects of wind should be taken into consideration especially for speed estimation [35]. The Residual-Mean Interacting Multiple Model (RMIMM) was proposed to achieve aircraft conflict detection by switching continuous dynamics and discrete modes in [36]. Motions of aircraft were expressed by equations to enable

CTAS to make spatial and temporal arrangements in case of potential conflicts [37]. With the assumption on point-mass aircraft model, the equation of motion can describe the aircraft motion in a simulation environment in a short time [38]. An intent-based trajectory prediction combined state estimates and intent was proposed in [39], which was simulated to be effective and better than RMIMM. But only horizontal intent was considered in this work.

Currently, most research on 4-D trajectory prediction built aircraft operation models with the knowledge of a profile, which assumes a flight task consist of several discrete phases. Then accurate kinematics for each phase can be established accordingly. Trajectories were modelled and straight lines or arcs in the horizontal plane with segmented altitudes in the vertical direction [37]. A dynamic space warp model was applied to extract the flight intention from historical data. Cressman interpolation was employed to weaken the effect of meteorological factors, thereby improving the accuracy of 4-D trajectory estimation in [40]. Flight plans are essential in ATC, though there is no connection with the aircraft performances, they provide spatial-temporal constraints to predict aircraft behaviour. Aircraft performances are influenced by a series of factors, among which may be interdependent. It is impossible for us to predict/analysis all of these parameters. While the hidden patterns can be discovered from flight plans. In some prediction research based on flight plans, they assumed aircraft behaved similarly if they were assigned with similar flight plans [41]. Aircraft performance can be predicted by mining historical data by machine learning methods. Although flight plans indicate the intent of an aircraft, in the future free flight environment, aircraft will be flying according to their performance and pilots' decisions, which raise a challenge for intention prediction. In [42], aircraft-related data, airspace and weather were used on trajectory prediction. A motion-based trajectory prediction function was implemented and evaluated to strengthen the robustness of flight management [43]. In [44], practicality of Continuous Descent Arrival/Approach (CDA), including feasibility, availability and variability, was analysed and simulated using Future ATM Concept Evaluation Tool based on BADA total energy model.

2.2.2 Trajectory-based Models

Precise models are inseparable from accurate parameters. Sometimes, the key parameters are quite difficult to be estimated, observed or inferred. Benefiting from modern monitoring methods, trajectory data is easier to obtain than the core parameters of models. Aircraft performance parameters can also be mined with large amounts of historical trajectories collected by ADS-B devices, which were demonstrated to be very close to coefficients presented in BADA family 3 in [45]. Trajectory prediction could also be data-driven. Transportation modes can be learned by mining the knowledge hidden in the sensors data [46]. The real-time simulation environment built based on BADA models [47] showed that trajectory-based operations can significantly reduce complexity. Uncertainties in the climbing phase can result in unexpected prediction errors. Ground-based infrastructure for trajectory prediction has limited access to aircraft intent and parameters. In [33], the uncertainties were quantified and analysed by model-driven data statistics based on airborne recorded dataset.

A hybrid ARIMA-SVM model [48] was presented to predict the remaining useful life of aircraft engine based on the observed data. Kalman Filters are typical algorithms for state estimation by observing the objects over certain time span, which were used for traffic flow [49] and wind speed prediction [50]. Markov Model is a widely used strategy in location forecasting [51][52], due to its chain structure. Chain structure of Markov models made them practical in both discrete and continuous time with countable state space. They were widely used in many scenarios, including aircraft trajectory prediction [53][54] and sequences generation [39]. HMM was applied to learn the hidden patterns from observed sequences on trajectories and weather conditions, a variant of Viterbi algorithm guaranteed a conflict free trajectory to settle the long-term aircraft CD&R problem in [55]. SVM can also serve to predict air traffic delays and traffic flow prediction [56]. Nowadays, Recurrent Neural Network (RNN) [57] and LSTM [58–60, 41] are famous for their ability and performance in sequential data processing. They were popular with natural language processing [61], speech recognition [62], machine translation [63], image captioning [64] and traffic flow forecasting [65]. RNNs could be used in location prediction [66], however, they have problems with long-term

dependencies [67]. The purposes of pedestrians were analysed and predicted by an LSTM network with attention model in [58].

As is pointed out by some research, real-time airborne parameters and meteorological data are not easy to access. In our research, besides the historical trajectories, we also fully consider various types of public data, including navigational/guiding way-points/airways in ATM system and dynamic performance of certain type of aircraft (BADA family 3), which are embedded into our model to improve the accuracy of flight trajectory prediction.

2.3 Path Planning

Path planning [68], trajectory monitoring [69] and attitude restoration can be achieved with the help of GIS [70]. From the perspective of civil aviation, airspace is divided into high-altitude, medium-low altitude, terminal (approaching) and airport tower control zones by airway and civil airports. Airports or terminal manoeuvring areas are the busiest spaces with the highest accident rate. Timely decisions are needed for various emergencies including conflicts, crashes and congestions. In the climbing phase, situations become more complicated, which results in complex optimization with multiple factors [71][72]. Optimal path algorithms usually can be labelled as optimum and heuristic algorithm. The former one can guarantee the optimum solution at the cost of time-consuming and complexity-increasing, while heuristic methods often find sub-optimal feasible solution within limited time. Path planning, threat detection and collision avoidance in the field of autonomous mobile robotics attracted many researchers' interests [73]. Robust Markov decision process (MDP) [74] modelled bad weathers while model prediction control (MPC) [75] introduced the dynamic model of aircraft in temporary path planning. MDP and MPC were limited by the man-made transition matrices and response time, respectively. In the terminal airspace, genetic algorithm [76] was applied to plan a flexible approaching path. A Star (A*) algorithm [77–80] performs well as a heuristic algorithm. A* search algorithm couples optimal path finding and threat assessing.

Situational awareness (SA) forms certain knowledge on spatial-temporal environment and events. It predicts the future status according to the comprehension of their meaning. Time is an important concept in SA due to its dynamic construction. Endsley [81] illustrated SA by three stages: perception, comprehension and projection. Recent years, scholars have studied the key technologies of SA, including Bayesian networks [82], Markov Logic Networks [83], analytic hierarchy process [84], genetic algorithms [85], D-S evidence theory [86] and fuzzy comprehensive evaluation methods [87]. Traffic Collision Avoidance System / Traffic Alert and Collision Avoidance System (TCAS) [88] was born to lower the incidence of collisions between aircraft in the middle air. This research was started since at least the 1950s. It was forced to be installed on large and medium-sized aircraft. It is the last barrier to prevent aircraft conflicts and plays a vital role in safe flying. Aircraft equipped with TCAS or its improved versions can only interact with each other who operates mode C/S transponder correctly. The dynamic performances of aircraft determine the range of protected airspace. In other words, each aircraft can raise a threat to the airspace surrounds it.

For a short flight duration, we need to take the transient state of the aircraft into account. Scene analysis and path planning should be performed according to certain terrain characteristics under the restrictions of the born performance of an aircraft.

2.4 Decision Support System

Decision Support System (DSS) has been developed in various fields including business management, air traffic management, intelligent transportation systems, control system and to name but a few. A DSS provides auxiliary knowledge for decision-makers, which is possible to improve efficiency and quality during the process [89]. Massive data urges fast and reliable decisions, which increases the demand on DSS [90].

Digital geographical data has grown rapidly in scope, coverage and volume. It is gradually available to public and personal applications. There are various types of geographical data, including spatial locations, geographic topologies, terrains, elevations, etc., which can be used to analyse and a series of situations and management occurred in certain scene. GPS-based devices record and store trajectories of moving entities.

These entities could be pedestrians, vehicles, aircraft, vessels, animals, etc. The recorded dataset contributes a lot to trajectory prediction and decision support.

Frequent natural disasters, such as wildfire, earthquakes and floods, bring substantial harm to human survival or damage human living environment, which lead to a high number of fatalities and need quick response. They can also have influence on climate or can be caused by the changing of climate. Social networks and GIS help a lot in early warning system on disasters, as they can provide timely support with Geolocation information [91]. A rule and knowledge-based hybrid decision support system was proposed in [92] to manage the humanitarian relief chain related activities and assess the post-disaster situation. Spatial efficiency is the important factor to be considered in urban construction and transportation network design. Multi-criteria decision-making method with GIS was applied in [93] to provide powerful decision support and evaluation on logistics efficiency. A spatial decision support system was built to model residential water demand in Australia by integrating different factors into maps to clearly display the situations [94].

DSS will help operators handle with anomaly situations [95]. Surface trajectory prediction-based conflict detection and resolution (CD&R) attracts a lot attention of NASA and FAA, as runway accidents are probably the most serious accidents. Constraint-embedded modelling and CD&R logic were applied in the decisions on conflict prevention in [96]. As pointed out in [97], the conflict between high-density requirement on air transportation and limited airspace/airport capacity resulted in flight delays. Moreover, current airspace is not been used rationally by the departure and approach procedures. Area navigation has not been fully exploited worldwide. Consequently, the efficiency of scheduling and traffic flow control is very low in terminal area. The authors proposed point merge route network for parallel runway operations, and modelled the CD&R for merging curved trajectory and radius-to-fix. A causal encounter model could provide auxiliary supports for the TCAS system by considering horizontal resolution and predicting potential collision in the vertical plane in [98]. The work published in [99] provided support service for abnormal flight trajectory with limited knowledge on the flight task and predicted the possible diversions. Alternatives in a decision-making process can be quite different, which need to be considered carefully and reasonably by decision-makers.

Our goal is to develop an open decision support system with strong compatibility, which supports user-defined functions and provides visual services to achieve intuitive and fast management.

2.5 Summary

In this chapter, a lot of literature related to 4-D trajectory prediction (performance/trajectory-based), path planning and decision support system has been studied. We will introduce our research in detail in the following chapters.

Chapter 3

Definitions in Air Traffic Management

3.1 Overview

Airspace is part of the atmosphere that can be mainly divided into controlled and non-controlled airspaces. Controlled airspace is defined differently with different organizations or countries. Generally, the airspace for air traffic control (ATC) services consist of classes A-E [100]. The use of these airspaces should be approved by air traffic controller and has clear and strict regulations on altitude (flight level).

ATC guides aircraft to perform its task safely and smoothly between ground and airspace. This guidance will turn to be consulting services in uncontrolled area. Operators position aircraft in its assigned airspace by monitoring and communication radios. ATC is primarily used to prevent collisions (between aircraft or obstructions) and expedite air traffic flow. Visual observation provided by airport control tower is the main method to monitor the ground and manage flight data to arrange departure and landing. Flight rules including visual-based and instrument-based are applied in en route, centre or area control. Though every airport varies, terminal controller takes charge of traffic in 30-50 nmi from the airport.

ATM contains systems that assist aircraft departing/landing at an airport and flying through the airspace, which includes navigation and guidance services, airspace

and traffic management. Modern ATM emphasizes the interpretable and harmonised systems with minimum performance changing on the aircraft. According to ICAO, the primary operational concept of ATM focuses on its system performance, including safety, operating efficiency and assurance. Situational awareness in the airspace and ground ranks secondary to ensure the orderly flight with the help of collision avoidance and separation regulations. Then it can optimize traffic flows within certain area. Certainly, the air navigation plan keeps updating accordingly.

In this chapter, we will introduce the foundations in air traffic management systems. Section 3.2 presents the basis of ATM, including definitions of flight phases, navigational facilities, airways and flight plans, which are essential for an aircraft to perform its tasks. Section 3.3 describes the basics of aeronautical chart based on the above-mentioned components. We draw the summary in Section 3.4.

3.2 Definitions in Air Traffic Management

3.2.1 Acronyms

We list the acronyms that may exist in our following chapters and sections as follows.

- ICAO: International Civil Aviation Organization,
- IATA: International Air Transport Association,
- NextGen: Next Generation Air Transportation System,
- SESAR: Single European Sky ATM Research,
- FAA: Federal Aviation Administration,
- BADA: Base of Aircraft Data,
- ATM/ATC: Air Traffic Management/Control,
- ADS-B: Automatic Dependent Surveillance-Broadcast,
- GNSS: Global Satellite Navigation System,

- FMS: Flight Management System,
- FMSP: Flight Management System Procedures,
- IFR: Instrument Flight Rules,
- VFR: Visual Flight Rules,
- RNAV: Area navigation, a method of IFR navigation,
- nmi: nautical miles,
- MSL: Mean Sea Level,
- GIS: Geographic Information System,
- ArcGIS: a GIS maintained by ESRI,
- WGS: World Geodetic System. The commonly used version is known as WGS-84.

3.2.2 Flight Phases Definition

The specialized agency ICAO is organized by the United Nations. Up to April 2019, there are 193 members in ICAO. Member states such as Europe (SESAR), American (NextGen), Brazil (SIRIUS), Canada, China (CAAC) and Russia (Russian Federation) have been working hard on improving air navigation programs to guarantee the near/long-term global interoperability of their solutions.

ICAO standardizes certain functions for civil aviation, such as the Aeronautical Message Handling System (AMHS). As required, each country should make their Aeronautical Information Publication (AIP) public, which is stated based on standards defined by ICAO. The ICAO standard atmosphere is widely used in calibrating instruments and designing aircraft [101]. In communication, navigation and surveillance/air traffic management (CNS/ATM) systems, ICAO is ready to provide digital technologies.

Airport codes in ICAO are with 4-letter, while IATA uses 3-letter codes. Airlines are assigned with 3-letter codes in ICAO (2-letter in IATA). Regulations for drones have been creating and improving by ICAO to make airspace be safe.

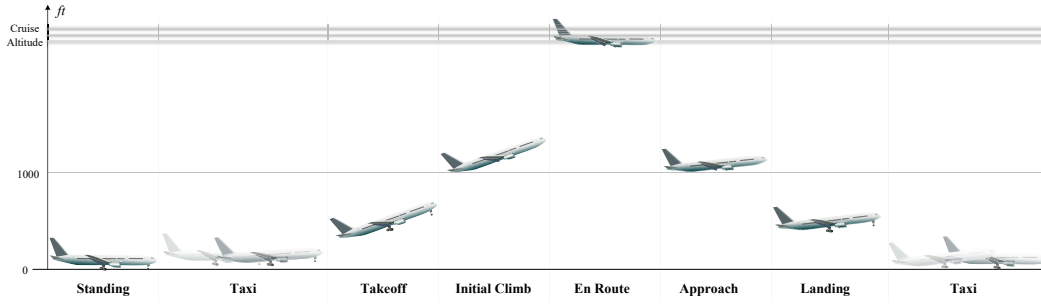


Fig. 3.1 Flight phases defined in ICAO.

According to ICAO taxonomy, phases of flight can be named as standing, taxi, takeoff, initial climb, en route, manoeuvring, approach, landing, emergency descent, uncontrolled descent and post-impact [102], which are defined according to the altitude, as is shown in Fig. 3.1.

Although the flight phases in ICAO are divided in detail, for the users, it is difficult to identify the exact boundaries of each flight phase without the airborne measurement. The Operations Performance Model in BADA family 3 makes a simplification on flight phases based on ICAO definitions. It divides the flight phases into take-off (TO), initial climb (IC), cruise (CR), approach (AP) and landing (LD) phases to specify speeds in each phase. BADA specifies four altitude thresholds for the TO, IC, AP and LD phases as shown in Table 3.1.

Table 3.1 Altitude thresholds for TO, IC, AP and LD phases in BADA models.

Name	Description	Value (ft)
$H_{max,TO}$	Maximum altitude threshold for take-off	400
$H_{max,IC}$	Maximum altitude threshold for initial climb	2000
$H_{max,AP}$	Maximum altitude threshold for initial climb	8000
$H_{max,LD}$	Maximum altitude threshold for landing	3000

3.2.3 Way-points

A large number of navigational facilities are shown on the aeronautical chart. Among which, we mainly focus on facilities that constitute parts of airways. Way-points are

series of coordinates of the navigational facilities, which help create invisible paths for navigation. Navigational facilities basically include NDB, VOR, TACAN:

1. **NDB.** Non-Directional Beacon, is a ground-based radio transmitter that located at specific geographical position. As its name implies, it does not transmit directional information. NDB signals can track the curvature of the Earth, which makes them able to travel further at lower altitudes (compared with VOR). Atmospheric conditions, terrain and coastal refraction have an influence on the signals. According to ICAO Annex 10 [103], there are four types of NDBs servicing the aeronautical navigation:
 - En route NDBs,
 - Approach NDBs,
 - Localizer beacons,
 - Locator beacons.
2. **VOR.** Very High Frequency (VHF) Omni-Directional Range, is a ground-based short-range radio. Phased antenna is applied to send a highly directional signal by a VOR station. An aircraft is able to position itself and stay on course if it has equipped with the receiving unit. It has the following features:
 - VOR signals are much precise and reliable than NDBs mainly due to the bearing from station to the aircraft provided by VOR.
 - VOR relies on the "line of sight", the range will be limited to the horizon or closer if mountain exists.
3. **DME.** Distance Measuring Equipment, is one of the radio navigation methods to measure the distance between an aircraft and certain ground station with the accuracy of 185 m (0.1 nmi). It is characterized as ultra high frequency (UHF) by ICAO. DME usually cooperates with VOR to provide a two-dimensional navigation information.
4. **TACAN.** Tactical Air Navigation, can provide bearing and range information for civil aviation, which is more accurate than the VOR/DME system. Theoretically, it is 9 times in accuracy than VOR and can provide distance up to 390 nmi.

5. **VORTAC**. Combined with VOR and TACAN, VORTAC can also provide the azimuth and distance information for civil aircraft.
6. **RNAV**. It is a kind of IFR navigation methods, which leads aircraft to follow any route within the navigation beacon network. It is not necessary for an aircraft to travel directly from/to the beacon, which will save flight distance reduce congestion and allow aircraft fly to the airport even without beacons. Thus, RNAV used to be known as random navigation.

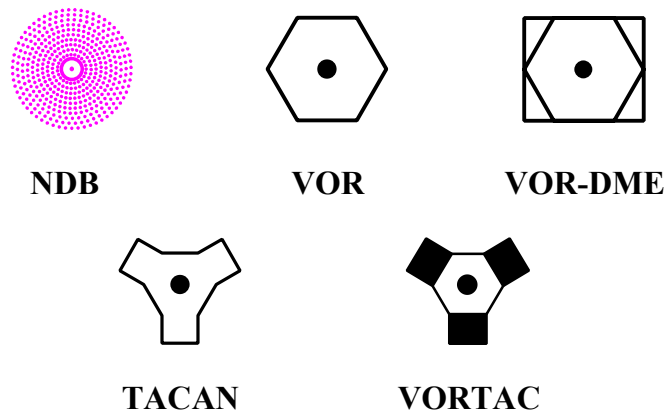


Fig. 3.2 Symbols of navigational facilities on aeronautical chart.

VOR and early NDBs were used as the intersections along airways. Most IFR aircraft equips at least two VOR receivers. When the primary receiver is working, pilots can use the second one to track a radial to/from a VOR station and record the time to cross another VOR. Thus, pilots can position their aircraft accurately. Though some GPS-based products will provide distance and altitude information with at low cost, the GNSS navigation is easy to be disturbed, which results in the retention of VOR stations for use. Different navigational facilities are expressed in different symbols on the aeronautical chart as shown in Fig. 3.2.

Since the VORTAC and VOR/DME provide same function to civil aviation, we treat all types of the navigational facilities uniformly in our work. The geographic locations of these facilities are referred to as way-points.

3.2.4 Air Routes

Departure/Arrival Procedures

An aircraft should take off under strict control with certain procedure, which is known as standard instrument departure (SID). SID is usually formulated for instrumented aircraft according to the actual situation of an airport. SIDs include pilot-guided and radar-guided procedures. Pilots are primarily responsible for navigation in the former type, while the later depends on navigation information by ATC. Compared with pilot-guided method, the radar-guided procedure is more flexible for traffic flow control in ATC. A SID consists of a number of way-points or fixes, which can be located by geographical coordinates or radio beacons (VOR/NDB or with DME). SID is also defined with a climb profile, which requires pilots to fly over certain points with indicated altitude. SID ends at the start way-point of an airway, since where pilots have to fly along the route. SID is applicable to both IFR and VFR aircraft to help maintain the safety separation. Pilots must strictly follow the SIDs with permitted minor errors along the departure route (several kilometres wide according to regulations in each country). Many countries/regions publish their SID procedures of its airports on-line, for example Airservices Australia [104].

Accordingly, the standard terminal arrival route/standard terminal arrival (STAR) procedure is published for IFR flight to use before reaching the destination airport. Though RNAV STAR/FMSP also serves for the landing phase, it requires the aircraft to be equipped with FMS or GPS. A STAR is defined as a flight route that connects the last point of the airway filed in the flight plan and the first point of the approach to the airport. STAR is usually made up of a set of transition points and routes by VORs. Although airways in the flight plan does not change during a task, the STAR might vary according to weather and traffic flow. Thus flight plans end with some distance with touchdown, while STAR starts to guide the pilot to land.

Airways

Airway/air route is usually defined as corridor that connects specified locations with certain altitude to provide routes for the competent aircraft performing its task. The

specified locations are coordinated by GPS, VORs or NDBs. Communication and navigation equipment must be guaranteed along the airways. Airways are conducive to maintain air traffic order, improve the efficiency and ensure safety.

Each airway is specified with limitations on upper and lower altitude. The width of airway is determined by the stability of aircraft to the specified track, the accuracy of the aircraft flying over the navigation facilities, the turning radius of the aircraft at different altitudes and speeds, and the necessary buffer zones, which results in the unfixed width. According to ICAO, when the distance between two omni-directional beacons is within 50 nmi, the basic width of the airway is assigned with 4 nmi on each side of the centreline. In other cases, width is calculated according to the stability of aircraft when tracking the pre-defined flight paths.

During cruising phase, the points on airways are usually assumed to be at the same height. Then the great-circle path between any two way-points is defined as the centreline of an airway. Suppose the starting way-point of the airway is represented by $W_1 = (x_1, y_1, z_1)$, followed by $W_2 = (x_2, y_2, z_2)$. The boundary of airway W_{12} can be determined by extending 10 kilometres to the left and right along the centreline $\overrightarrow{W_1W_2}$. The boundary point $W' = (x, y, z)$ of W_1 should meet the following conditions

$$\begin{cases} x^2 + y^2 + z^2 = (R + h)^2 \\ (x - x_1)^2 + (y - y_1)^2 + (z - z_1)^2 = 100 \\ \vec{n} * \overrightarrow{W_1W'} = 0 \end{cases} \quad (3.1)$$

where, $\vec{n} = \overrightarrow{OW_1} \times (\overrightarrow{OW_1} \times \overrightarrow{OW_2})$. Notations R and h represent the radius of the earth and the altitude of the airway, respectively. We can get two boundary points W'_{11} and W'_{12} corresponding to way-point W_1 by solving Eq. (3.1). Similarly, the boundary points of W_2 can be solved by substituting its coordinates into Eq. (3.1). As is shown in Fig. 3.3, curves $\overrightarrow{W_{11}W'_{21}}$ and $\overrightarrow{W_{21}W'_{22}}$ determine the inner and outer boundaries of the airway, respectively, thus forming the airway shown in the blue shaded part in the figure.

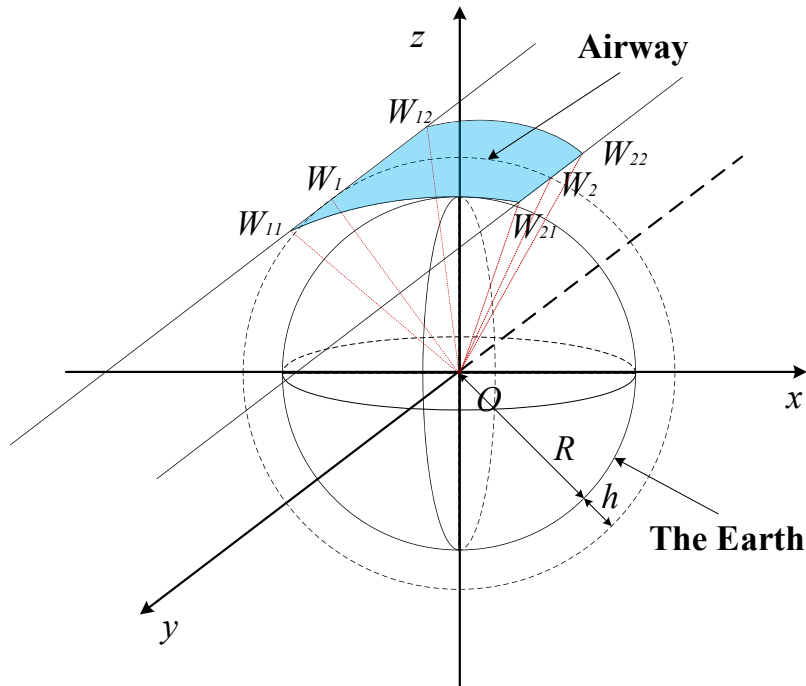


Fig. 3.3 Schematic diagram of airway model in geographical environment.

3.2.5 Flight Plans

Flight plans are the documents that submitted to the local Air Navigation Service Provider by pilot or airline dispatcher before performing the flight tasks, which indicate the pre-planned flight paths. Flight plans should be formatted according to the ICAO Doc 4444 [105]. Generally, a flight plan document contains the information including departure/arrival airports, alternate airports, flight time, plane type (IFR/VFR) and crew information. In most countries/regions, flight plans are required for IFR flights. The detailed information in a flight plan can be concluded as follows:

1. Route. Routes used in flight plans include three types: airway, navaid and direct.
 - Airway. Airways are defined as 3-D airspaces with specified width that connect the departure and arrival airports. Most airways are eight nmi (14 kilometres) wide, but the number is slightly adjusted according to the regulations of countries and the geographical environment. Aircraft keeps separated by at least 1000 feet in the vertical direction when flying along

airways. Airways can be divided into high-altitude and low-altitude routes according to the altitude, they are named with one letter followed by several digits.

- Navaid. Navaids are the points for an aircraft changing from one airway to another. Airways usually intersect at Navaids, both NDBs and VORs can define airways, while Navaids are not always connected by airways.
- Direct. Direct routes are specified by some flight planning organizations according to the checkpoints.

2. SIDs/STARs. SIDs and STARs are procedures for IFR aircraft leaving and arriving. Transition points exist at the intersection of airways and SID/STAR.

- SID. Standard Instrument Departure is also called a Departure Procedure (DP). SIDs are unique in every airport.
- STAR. Standard Terminal Arrival Route indicates the route flying into an airport from the airway. STARs can be shared by nearby airports.

3. Special use airspace. Though airspace is quite broad, only a small part of it is available for civil aviation. When preparing a flight plan, special use airspaces including restricted, warning, prohibited or alert areas should be avoided. In our work, we unify these areas as “no-fly” zones.

4. Flight levels. Flight levels (FL) are used by operators to discretize the vertical space for aircraft. When aircraft climbing/descending under a transitional altitude, it should follow the guidance of air traffic controller, otherwise, it need to reach the specified FL. The transitional altitude varies among countries/states. FL are standardized along airways, which must be followed. ATC will assign FL according to traffic flow. Fuel consumption is associated with FL, airliners will consider the efficiency when taking the task.

5. Alternate airports. One or more airports need to be involved in a flight plan in case of unexpected situation. It should be carefully planned as the fuel load, total weight and type of aircraft need to be considered comprehensively.

6. Fuel. Fuel is an important flight performance that provided by manufacturers, which helps pilots estimate the fuel consumption for flight task. Fuel consumption is calculated by weight due to its critical influence on weight of aircraft. While the dynamic performance (rate of climb/descend) also affects the fuel consumption.
7. Time-line. Flight plans may be submitted before or after departure. They should also include the estimated departure and arrival time with universal coordinated time.
8. Crew information. Contact information of pilots and total number of people on board.
9. Weather conditions. Weather conditions of airports in the flight plans reported as Meteorological Terminal Aviation Routine Weather Report (METAR), which is standardized to universal format by ICAO. The report updates every an hour or half-hour by airports or weather observation stations. It mainly involves temperature, wind (magnitude, speed and direction), visibility, cloud information and barometric pressure. METAR code is jointly regulated by the World Meteorological Organization (WMO) and ICAO.

A complete flight plan is shown in Fig. 3.4, the blue circles indicate the airports, while the labels "DEP" and "Arr" represent the departure and landing airports, respectively. The matrices sets $\{\theta, \mathbf{H}, \mathbf{F}\}$ in SID and STAR mean the heading, altitude, and communication frequency an aircraft should reach when flying over these navigation aids. Each navigational facility in every flight phase has its geographic location and communication frequency. When the aircraft flies over a certain way-point, it will switch its communication frequency and reach the specified altitude of the airway. Flight plans are not exactly the same, even if the same aircraft performs its task along the same route. If the amount of fuel permits, in addition to those fly-over way-points, some airways or way-points will be re-scheduled due to the real-time traffic flow and weather conditions. Flight plans impose non-real-time restrictions on the time-of-flight and spatial span of a flight task.

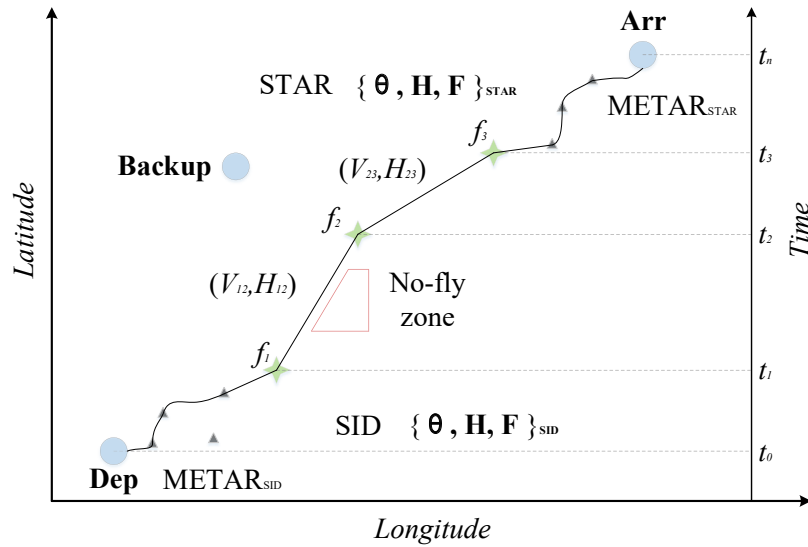


Fig. 3.4 Schematic diagram of flight plan.

3.3 Aeronautical Chart

An aeronautical chart is designed to assist navigation for aircraft. For example, the Jeppesen Chart combines the aerial and topographic maps to provide the navigation information needed in flight. It is mainly applied to make flight plans, identify aircraft positions, maintain safe altitude and ensure smooth communication. Usually, the aeronautical chart contains information as high/low-altitude airways, navigational facilities, reporting points, communication frequencies and special-use airspaces. Fig. 3.5 shows the IFR aeronautical chart of Sydney Kingsford Smith Airport on SkyVector [106].

Geographical location, elevation (above MSL) and magnetic variation of airports are listed in the IFR chart. The green point in the centre of Fig. 3.5 is the location of weather station of Sydney Kingsford Smith airport. It will update the weather conditions hourly in the form of METAR. Frequency, radial/range and name of nearby navigational facilities (NDB, VOR or VORTAC) and airports are also illustrated in this chart. Black and blue lines are the high-/low-altitude airways, which are named with letter and numbers. The solid triangles on the airways stand for the compulsory reporting points, while the hollow triangles are the non-compulsory reporting points. For an undi-

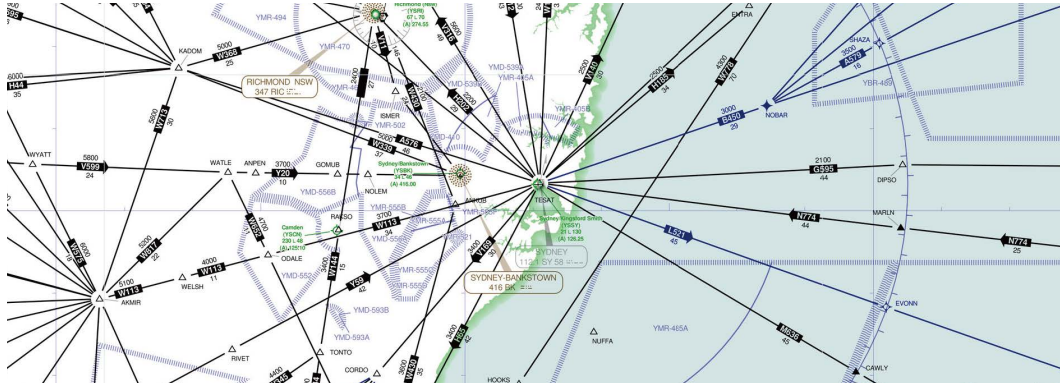


Fig. 3.5 IFR chart of Sydney Kingsford Smith Airport.

rected graph composed of way-points on routes "W113" and "Y20", the degree distribution of the way-points $\{AKMIR, WATLE, WELSH, ODALE, ANKUB, TESAT\}$ is shown in Eq. (3.2).

$$D = \begin{bmatrix} 2 & 0 & 0 & 0 & 0 & 0 \\ 0 & 2 & 0 & 0 & 0 & 0 \\ 0 & 0 & 2 & 0 & 0 & 0 \\ 0 & 0 & 0 & 3 & 0 & 0 \\ 0 & 0 & 0 & 0 & 2 & 0 \\ 0 & 0 & 0 & 0 & 0 & 1 \end{bmatrix} \quad (3.2)$$

3.4 Summary

In this chapter, we introduced the basis of ATM and listed the abbreviations of terms that may be used in the following chapters. We have also outlined how we model them according to the regulations by ICAO in this chapter, such as the way-points, airways and airports.

Chapter 4

4-D Flight Trajectory Prediction with Constrained Long Short-Term Memory Networks

4.1 Overview

Forecasting is a vital and fundamental research problem in ATM to prevent traffic jams and collisions. It mainly includes delay prediction [107–109], flow forecast [110–112] and trajectory prediction [113]. In modern intelligent transportation systems, trajectory prediction is a common but very challenging problem. Many long-term [114][115], medium-term [116][117] and short-term [111, 118, 119] forecasting techniques are presented in aviation [120–122] and land traffic. These methods can generally be divided into parametric and non-parametric groups. Parametric models are based on prior known parameters, such as Origin-Destination matrix (OD) [112] simulation models, Autoregressive Integrated Moving Average (ARIMA) [123] and its improved models, Kalman Filters (KF) [124][125] and Markov Models [126–128]. The typical representatives of non-parametric models are Bayesian networks [107][129], k -Nearest Neighbours (k NN) [130, 131] and Neural Networks (NN) [132].

Although airspace is quite broad, only certain airways and areas are available for civilian activities which are shared by different airlines. Huge flow and intensive

activities bring unexpected dangers to safe travel. To avoid traffic jams and collisions, aviation data processing mainly focuses on trajectory clustering [133], delay prediction [134] and traffic flow prediction [111]. Conventional flight motion methods rely heavily on aircraft performance models [22] for target tracking and state estimation, which are difficult for researchers to get the access/license of these models and related parameters. Recently, the gradually publicized historical trajectories led us to conduct research on this basis. K-means combined with time warp edit distance was put forward for precise extraction of nominal flight profile in [135]. Though it was effective than traditional K-means, the K value was determined by the dataset. HMM combined with Viterbi algorithm was proposed for decision support system of ATM in [53]. Hidden relationships among trajectories, aircraft types and corresponding weather conditions were discovered by HMM-Viterbi during the process of trajectory predicting. However, the increasing amount of trajectories may lead to heavy computational burden. Long Short-Term Memory network embedded with sliding windows was introduced to predict 4-D flight trajectories in our initial research [136]. In this chapter, we further propose a so-called cLSTM network by formulating three constraints and embedding them into the LSTM networks, which significantly improve the prediction accuracy.

The rest of this chapter is arranged as follows. Some basic introductions of LSTM network start the Section 4.2. We construct three kinds of constraint based on the navigational facilities in Section 4.3. A constrained LSTM network is then built in Section 4.4. Experimental design, parameter settings and quantitative analysis on the experimental results are presented in Section 4.5. Finally, we summarize this chapter in Section 4.6.

4.2 Preliminary

Markov Models (MMs) are very famous for their capabilities in sequence processing. This typical strategy uses one-step previous state to predict a future state. Though simple in expressions of MMs, they have powerful performance that makes them competent in many practical systems. However, when dealing with medium-term and long-term prediction problems, shortcomings of MMs are exposed. The Markov process

makes two assumptions: Firstly, the system state at time stamp t is only related to that at $t - 1$ (no after effects). Secondly, state transition probability is independent of time (homogeneity). The strict system models limit their flexibility. While Hidden Markov Model (HMM) also assumes the outputs are independent, which will result in label bias problem.

Recurrent neural network (RNN) does not make the Markovian assumption and has a powerful representation. RNN applies the distributed representation, while HMM uses one-hot way. The number of hidden variables is limited in HMM, so that it can only represent limited states. RNN is able to perform intelligent smoothing by taking syntactic and semantic features into account.

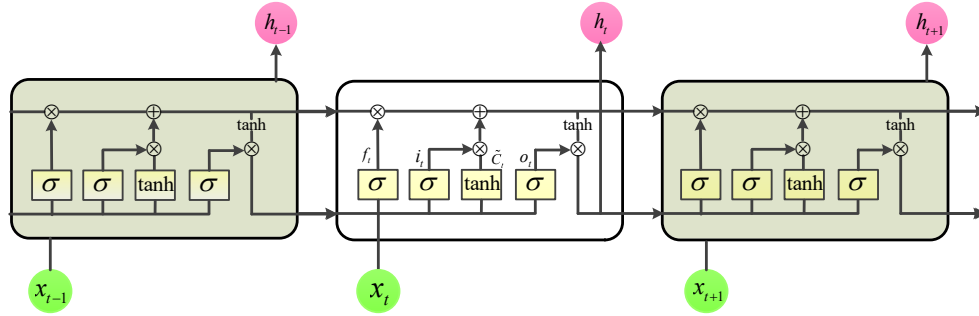


Fig. 4.1 Chain structure of vanilla LSTM cells.

LSTM network is a special form of RNN. It has the same feedback edges as RNN and also considers timing relationships. LSTM adds a special structure to each hidden layer node, the chained LSTM cells can be shown as Fig. 4.1. In the yellow blocks, σ is a logistic sigmoid function with the form of $\sigma(x) = 1/(1 + \exp(-x))$. The forget gate \mathbf{f}_t filters state that transited from the previous cell. New information is stored by the input gate layer \mathbf{i}_t , meanwhile, the tanh layer formulates a new candidature $\tilde{\mathbf{C}}_t$, where $\tanh(x) = 2\sigma(2x) - 1$. The old cell state \mathbf{C}_{t-1} is then updated to $\mathbf{C}_t = \mathbf{f}_t \odot \mathbf{C}_{t-1} + \mathbf{i}_t \odot \tilde{\mathbf{C}}_t$, notation \odot represents the product of vector elements. Output gate \mathbf{o}_t decides the output of current cell according to the input and updated cell state. All these gating units have a sigmoid non-linearity.

4.3 Construction of Physical Constraints

In this section, we will introduce and construct three types of constraints, which consist of static/dynamic components and are embedded into our segmented flight phases.

Definition 1. A continuous flight trajectory can be discretized as time-ordered scatters by sensors. These scatters can be labelled as 4-D spatial-temporal features: time, latitude, longitude and altitude.

The work on flight trajectory prediction is based on the following assumptions:

- Assumption 1. We consider the aircraft as a rigid body and curvature of the earth is omitted.
- Assumption 2. The changes on wind, temperature and pressure are ignored when an aircraft climbs and descends.
- Assumption 3. Airways are supposed to be a cylindrical airspace, with standard radius and certain altitudes.
- Assumption 4. Way-points are considered as circles that perpendicular to the horizontal plane, whose centres are positioned with certain latitude, longitude and altitude. The diameter is set to be equal with that of the airways.

Our research focuses on the long-voyage and large-scale flight trajectory prediction. The intention we mentioned in this thesis refers to the changes on heading, speed and altitude.

We simplify and reorganize the flight stages that defined in ICAO into three phases, i.e., climbing, cruising and descending/approaching phases. Density-based spatial clustering of applications with noise (DBSCAN) algorithm [137] segments trajectories into climbing and non-climbing phases, while the later dataset is split into cruising and descending/approaching phases. We gather the track points that located within $50km$ of the airport into descending/approaching phase.

Static indicators including airways, way-points and other navigational facilities, are responsible for guiding aircraft flying sequentially. They act as static constraints to ensure safe and orderly aviation activities. Dynamic performances of an aircraft, for

example optimum rising angular velocity and minimum turning radius, determine the best time to handle related problems when unexpected situations occur. Both static and dynamic constraints are considered in this section. Specifically, they are Top of Climb (TOC), Way-points (WPT) and Runway Direction (RWD).

4.3.1 Top of Climb

Climbing phase starts at the end of take-off phase, taking economic aspects, ultimate climbing performance of aircraft and traffic flow into consideration comprehensively, aircraft fly towards the airway that at certain altitude. We consider the altitude of the centre of cluster as the value of top of climbing phase. TOC mainly applies its constraint on climbing angle. As is shown in Fig. 4.2.

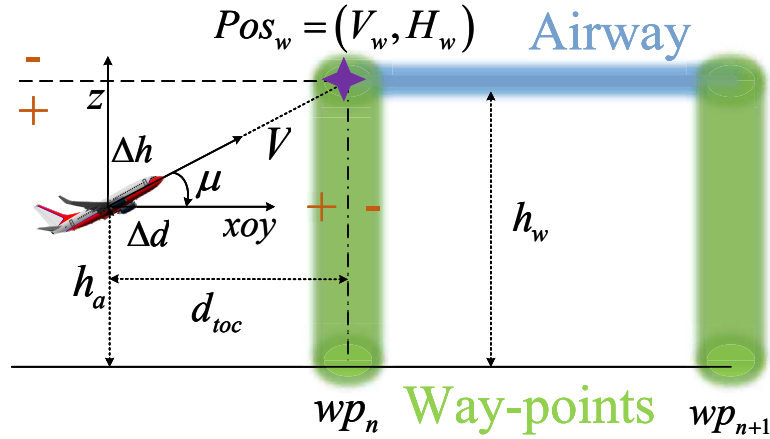


Fig. 4.2 Construction of the constraint TOC.

Suppose the maximum climb angle is θ_{max} , the connection point between climbing and cruising phase is represented by $Pos_w = (V_w, H_w)$, where V_w and H_w are the coordinate components of the connection point along vertical and horizontal directions, respectively. Then, constraint can be expressed as formula (4.1).

$$\begin{cases} \theta_{max} \geq \mu = \tan^{-1} \left(\frac{|h_w - h_a|}{d_{toc}} \right) \\ V \sin \mu \cdot t \pm \Delta d = V_w \\ V \cos \mu \cdot t \pm \Delta h = H_w \end{cases} \quad (4.1)$$

where, h_w represents the altitude of en-routing airway, h_a is recorded altitude of the aircraft in real time. d_{toc} indicates the horizontal distance between aircraft and the start way-point of the designated airway, then $\Delta h = |h_w - h_a|$, $\Delta d = |d_{toc}|$. V , μ are the real-time dynamic variables of the aircraft, which stand for the velocity and track angle, respectively. We define the coordinate be positive, when the aircraft flies below the plane with altitude of h_w and not arrives at H_w . Conversely, the coordinate is negative.

4.3.2 Way-points

Way-points build the foundation of airways, which are required to fly-over or fly-by in RNAV procedures. Airspace is gridded by way-points, as is shown in Fig. 4.3. As is defined in 3.2.5, the air route of an aircraft is composed of different way-points. For a flight f^i , we discrete its scheduled route as a sequence shown in Eq. (4.2) by each navigational point to be reached.

$$Route = \{ \mathbf{wp}_0^i, \mathbf{wp}_1^i, \mathbf{wp}_2^i, \dots, \mathbf{wp}_k^i, \mathbf{wp}_{k+1}^i \} \quad (4.2)$$

where \mathbf{wp}_j^i represent the vector of the navigational facilities. Basically, they are described in a three-dimensional way with latitude, longitude and altitude, some of which may be enriched by communication frequency or special purposes. It is worth noting that \mathbf{wp}_0^i and \mathbf{wp}_{k+1}^i stand for departure and arriving airports in the flight plan, respectively. Accordingly, the take-off and landing head are important features in these vectors.

Multiple discrete flight levels exist in each airway, which are shared by all the airlines. Aircraft cruise stably with the guidance of way-points. We assume that an aircraft cruises within the width of airway. However, if the constraint WPT is calculated segment by segment, it will increase the computing burden. Moreover, sometimes, the airspace where the aircraft flying through cannot clearly correspond to the segment. So we approximate the discrete way-points to a linear function in the sense of minimum error, which is well known as linear least square (LLS). Then multiple segments are fitted to a straight line as is shown in Fig. 4.3.

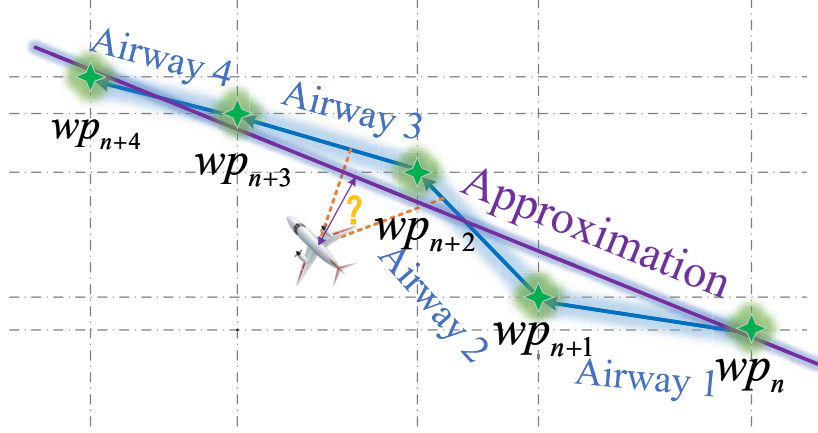


Fig. 4.3 Linear least square for approximating line equation of way-points.

Assumption 1 holds in certain cruising phase that the earth is flat, ignoring the altitude of the airway, we consider a linear relationship existing between longitude and latitude of way-points as Eq. (4.3).

$$lat = a_0 + a_1 lon + e_i \quad (4.3)$$

where, a_0 and a_1 are arbitrary real numbers. lat and lon represent latitude and longitude, respectively. e_i indicates the error of sample (lat_i, lon_i) . We would like to minimize the squared loss e_i^2 .

$$\begin{aligned} Q &= \sum_{i=1}^n e_i^2 = \sum_{i=1}^n (lat_i - \hat{lat}_i)^2 \\ &= \sum_{i=1}^n (lat_i - a_0 - a_1 lon_i)^2 \end{aligned} \quad (4.4)$$

After partially derivate Q by a_0 and a_1 , we can find the pole of squared loss, which determines the equation of the approximate line. Then the constraint WPT is formulated as Eq. (4.5), which is illustrated in Fig. 4.4.

$$\begin{cases} \psi_c = \tan^{-1} \left(\frac{y_m - y_n}{x_m - x_n} \right) \\ d_{wp} = \sqrt{(V \sin(\psi - \psi_c) \cdot t)^2 + (V \cos(\psi - \psi_c) \cdot t)^2} \\ d_w = (a_1 x + a_0 + e_i - y) / \sqrt{1 + a_1 \cdot a_1} \end{cases} \quad (4.5)$$

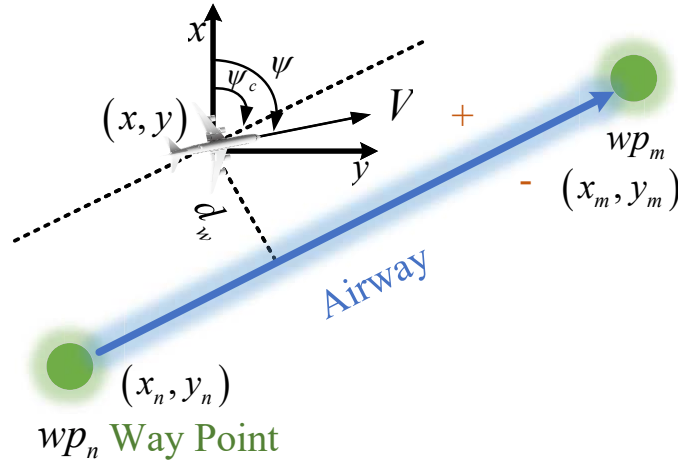


Fig. 4.4 Constraints applied by WPT.

where, ψ_c is the angle between approximate airway and the north direction, while ψ is the angle between the track angle of aircraft and the north direction. (x_i, y_i) represents the coordinate of way-point, where the subscript i indicates the numbering sequence. (x, y) marks the position of aircraft. Under Assumption 1, an aircraft is simplified to be a particle without taking its shape and size into consideration, d_w is the distance from the aircraft to the approximate airway. Notations a_1 and a_0 , e_i are parameters of the fitted line equation. We denote the distance between aircraft and the next way-point to be traversed as d_{wp} , which is a non-linear function about time.

4.3.3 Runway Direction

Runways in an airport are usually named with a number from [01, 36], which generally indicates the magnetic azimuth of the runway direction in deca-degrees. Every airport provides several entry routes with fixed altitude. Entry route starts with a VOR or NDB ground station. Constraints can be added by way-points, VORs/NDBs and runway direction, as shown in Fig. 4.5.

LLS is also applied to fit the way-points and entry routes, separately. Usually, the direction of a runway is not designed according to the true azimuth but the magnetic azimuth. The relationships among true, magnetic and coordinate azimuth are shown

in Eq. (4.6).

$$\begin{cases} \theta_{mag} = \theta_{true} - (\pm\theta_{dec}) \\ \theta_{coo} = \theta_{mag} + (\pm\theta_{dec}) \end{cases} \quad (4.6)$$

where, the θ_{mag} , θ_{true} and θ_{coo} stand for magnetic, true and coordinate azimuth, respectively. Magnetic declination is expressed as θ_{dec} .

We can get the maximum changes of spatial spans based on current dynamic status of aircraft, as described in Eq. (4.7).

$$\begin{cases} \Delta h = V \cos(\mu - 90) \cdot t \\ \Delta l = V \sin(\mu - 90) \cdot t \\ \Delta\theta = \theta_{mag} - \theta_{coo} \end{cases} \quad (4.7)$$

where, Δh and Δl are changes in distance along vertical and horizontal directions, which provide maximum change on distance due to the reduced velocity during descending/approaching phase. V and μ are the dynamic statuses (velocity and track angle). The track angle and runway direction should be ultimately consistent when the flight task finishes.

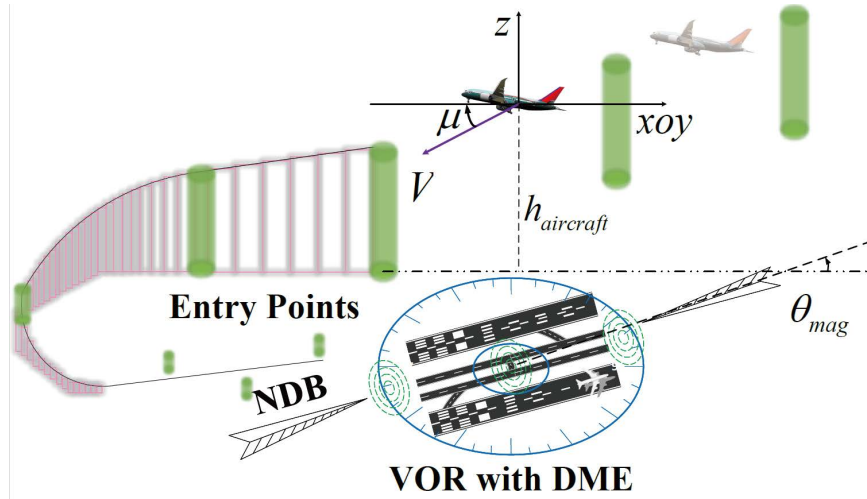


Fig. 4.5 A schematic diagram of descending/approaching phase.

4.4 Constrained LSTM Network Building

In this section, a constrained LSTM network is proposed to predict the flight trajectory. We will introduce the vanilla LSTM network first and then explain in detail how the constraints are constructed and embedded to the LSTM networks.

Trajectories are segmented into climbing, cruising and descending/approaching phases by DBSCAN. Coordinate transform narrows the errors caused by different units used in latitude, longitude and altitude. Input sequences of our cLSTM network is normalized by Min-Max and bridged by sliding windows. The segmented phases determine which constraint is applied to calculate losses correspondingly. LLS fits discrete way-points to lines for convenient calculation when constructing constraints. Adam is selected to optimize our network. Neural networks that suitable for each phase are concatenated to form our cLSTM model. The framework of cLSTM network is shown in Fig. 4.6.

DBSCAN divides region into clusters with arbitrary shapes, which are derived from density-reachable relationship. Clusters are formulated by core, (density-)reachable points and outliers. If all points in a cluster will be reachable from a point, then it is appointed as a core point. It can be guaranteed that, points in the cluster are density-connected with each other. Once a point can be density-reachable from any other points in certain cluster, it is also part of this cluster. In this section, we apply DBSCAN to segment our flight trajectories into climbing and non-climbing phases. The non-climbing dataset is then divided into cruising and descending/approaching phases based on the geographical distance from the airport.

We embed the constraints constructed in Section 4.3 as part of loss functions into the LSTM networks. Different constraints behave differently for 4-D flight trajectory prediction. WPT contributes to adjusting attitudes of aircraft along airways. While TOC and RWD restrict strictly for climbing and descending/approaching phases. Near future intentions can be predicted by current state and corresponding constraints. We design our cLSTM network according to the constraint item we add to each network, as is shown in Fig. 4.6. A linear combination of these constraints is applied to formulate the loss function of our proposed constrained LSTM network. Constraints strengthen

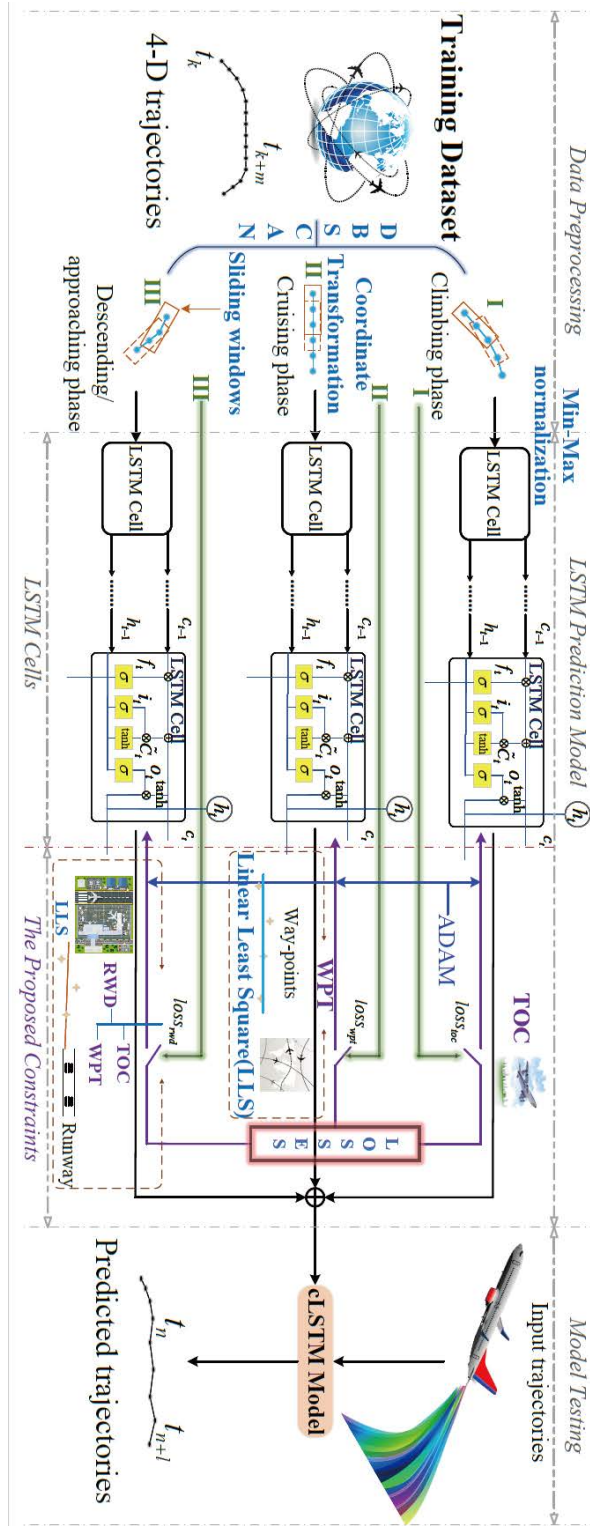


Fig. 4.6 Constrained LSTM network for 4-D flight trajectory prediction.

and refine the losses when iteratively calculating the loss functions.

$$Loss_{func} = w_0 loss_{toc} + w_1 loss_{wpt} + w_2 loss_{rwd} \quad (4.8)$$

where $loss_{toc}$, $loss_{wpt}$ and $loss_{rwd}$ stand for the losses of these three types of constraints, respectively. Weights w_0 , w_1 and w_2 range from 0 to 1, and $\sum_{i=0}^2 w_i = 1$.

The flight phase of input sequences determine the type of constraint to be triggered. TOC guides the output to scheduled position Pos_w in Fig. 4.2, which takes the whole responsibility for calculating loss in climbing phase. Correspondingly, w_0 is assigned to be 1. WPT drags the intention of an aircraft to the centreline of approximated airway to keep orderly fly when aircraft cruises. In this phase, way-points act as the unique component to restrict the activities of aircraft, we set $w_1 = 1$. Situation becomes complicated in descending/approaching phase. Constraint should be enhanced, as heading should be aligned and height should be carefully adjusted. The three constraints work together to ensure a safe descending/approaching phase. We then rewrite Eq. (4.8) into the form of Eq. (4.9).

$$\mathbf{Loss}_{func} = \begin{bmatrix} 1 & 0 & 0 \\ 0 & 1 & 0 \\ 1/3 & 1/3 & 1/3 \end{bmatrix} \begin{bmatrix} loss_{toc} \\ loss_{wpt} \\ loss_{rwd} \end{bmatrix} \quad (4.9)$$

where, the matrix \mathbf{Loss}_{func} stands for the set of loss functions in above-mentioned three phases. In order to guarantee the unbiased allocation of weights in descending/approaching phase, we assign the weights with arithmetic mean [138], i.e., $w_0 = w_1 = w_2 = 1/3$.

Without loss of generality, we summarize and formulate the above three types of constraints as relative distance and angular deviations. A generic expression can be written as Eq. (4.10).

$$loss_* = f(d, \theta) = (w_{dg}(d) + w_{\theta}h(\theta))^2 \quad (4.10)$$

where $*$ indicates the collection of constraints, $f(d, \theta)$ represents a non-linear function of deviations on distance d and track angles θ , it is the square of the weighted sum

of these components. Weights w_d and w_θ can be any value between 0 and 1. The switching of flight phases will result in a change of weights.

We construct the loss functions as brought up in Section 4.3. The distance loss $g(d)$ is constructed by mean absolute error, i.e., $g(d) = \text{mean}(\text{abs}(d_{pre} - d_{truth}))$, where d_{pre} and d_{truth} represent predicted position and ground truth, respectively. Polynomial minimax approximation based on Remez algorithm is applied when calculating the angle loss. Taylor's expansion provides a fast approximation with low complexity. $h(\theta) = \text{mean}(\text{abs}(\theta_{pre} - \theta_{ref}))$. θ_{ref} stands for the angle of line that fitted by LLS. The fitted parameters are selected with 95% confidence level. θ_{pre} indicates the real-time track angle, it is calculated approximately as Eq. (4.11).

$$\begin{cases} \alpha = dy / (dx + \ell) \\ s = \alpha \cdot \alpha \\ \theta_{pre} = ((p_1 \cdot s + p_2) \cdot s + p_3) \cdot s \cdot \alpha + \alpha \end{cases} \quad (4.11)$$

where (dx, dy) labels the relative position to reference point, ℓ is a constant with small value that approaches zero, p_1, p_2, p_3 are the corresponding coefficients.

Our cLSTM model concatenates the three independent LSTM networks with the corresponding constraint embedded to them.

4.5 Experiment and Discussion

There are many other related technologies involved in trajectory prediction. It is a series of data processing processes, including data collection, data preprocessing, clustering and segmentation, and spatial-temporal pattern mining. In this section, we introduce our work gradually. Data collection is first presented, followed by data preprocessing, which includes clustering, segmentation and coordinate transformation. The proposed constrained LSTM network discovers the hidden spatial-temporal pattern of the flight trajectories. We evaluate our model via different indicators. Comparison tests include the following models:

- LSTM network: A recurrent neural network composed of LSTM units, which is suitable for time series processing. The LSTM network with sliding windows in [136] is used for experimental comparison.
- Markov Model (MM): A stochastic model used in probability theory. It assumes that previous occurred events have no influence on future states. They are determined by the current state. This makes it widely used in predictive modelling and probabilistic forecasting.
- weighted Markov Model (wMM): Weights on neighbouring states of Markov Model are redistributed with large value.
- Support Vector Machine (SVM): A supervised learning model that is widely used in binary classification and linear regression analysis [139].
- Kalman Filter (KF): A typical algorithm that produces estimations of unknown variables based on sequential observations. It is frequently applied in guidance, navigation and control in aviation.

We quantitatively analyze the prediction effects of the above models followed by experimental results.

4.5.1 Data Description

Aircraft can be positioned by ground-based ATC monitoring system or airborne sensors. Data-links are used to transfer data from airborne equipment to ground-based ATC. The fundamental data consists of basic and further information.

ATC monitoring systems primarily provide estimated position, altitude and identity of aircraft periodically. Flight plans, arrangement of way-points and workload of pilots are closely related to monitoring performance. The accurate location of aircraft, especially in terminal areas, has a direct influence on the following procedures, alerting systems and separation standards. Pilots report their position to ATC when they drive the aircraft in the areas without electronic monitoring facilities. These systems are evaluated by coverage volume, accuracy, integrity, update rate, reliability and availability.

Airborne equipment is diverse, information that broadcast by ADS-B system is composed of messages from GNSS, INS, IRS, FSM and other sensors, which requires no pilot or external input. This information will be transmitted through air-to-air and air-to-ground data links with certain time period. ADS-B is an important element in NextGen, ASBU and SESAR [140–142]. It is mandatory to equip ADS-B in some areas of Australian airspace (full continental coverage above FL300) [143] and will be equipped by the year 2020 in the United States. Some aircraft in Europe have also been required to equip this device since 2017, while Canada currently uses ADS-B for limited air traffic control. ADS-B is gradually introduced to pilots and the ATM system to provide benefits on both safety and efficiency, as is shown in Fig. 4.7.

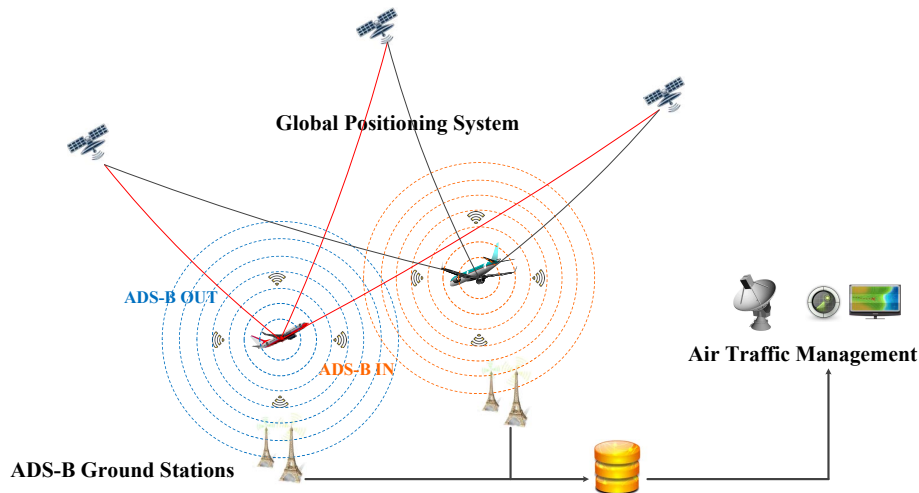


Fig. 4.7 ADS-B assisted ATM system.

ADS-B system is made up of In and Out devices. Aircraft periodically broadcasts its information via ADS-B Out, while ADS-B In receives FIS-B, TIS-B and ADS-B data. The transport protocol (1090ES or 978MHz UAT) enables the communication between pilots and ATC controllers. Information reported by ADS-B devices mainly includes:

- *4-D position:* time stamp, geographical locations,
- *Aircraft:* identification and category information,
- *Additional information:* collision warning, pilot input, track angle, transmission points, heading, air speed, wind speed, wind direction and temperature.

With the help of ADS-B equipment, pilots are able to know the surrounding aircraft and traffic conditions (situational awareness). As ADS-B ground stations are significantly economical and precise compared to ATC monitoring systems, the ATC operators can make efficient guidance for separation and control procedures.

The dataset is obtained by multiple ADS-B ground-based receivers. Trajectories are recorded every 15 seconds. It is round-trip data from an airport that lasts for five months, from June to November 2017. Every flight duration is around two and a half hours. The data consists of static and dynamic components. The static data implies the taking-off and landing airports, call-sign and scheduled airways. While the dynamic one is the 4-D data, mainly includes time stamp, position (latitude, longitude, altitude), velocity and direction.

4.5.2 Trajectory Clustering

Raw data is not available to act as the input of a network as they can be redundant and noised. The geographical span of an aircraft trajectory maybe huge according to its voyage. Different units could result in enormous numerical differences along each dimension. The DBSCAN-based [133] clustering method is used for data segmentation. Coordinate transformation is followed to prepare the data for training the network.

Clusters in DBSCAN are defined with the largest set that with densely connected points. It divides regions with sufficiently high density into clusters and can find the clusters with any shape in the noised spatial database. Compared with k -means clustering method, DBSCAN is parameter-free and can discover clusters of any shape. For a set of points in some space is expressed by $P = (p_1, p_2, \dots, p_n)$. Parameters $(\epsilon, MinPts)$ is used to describe the density of samples in the neighbourhood. Some definitions in DBSCAN algorithm are listed below.

- *ϵ -neighborhood*: for any point p_i in the set P , its ϵ -neighborhood is defined as $N_\epsilon(p_i) = \{p_j \in P \mid distance(p_i, p_j) \leq \epsilon\}$, the number of this subset is recorded as $|N_\epsilon(p_i)|$.
- *Core point*: for any point $p_i \in P$, if its ϵ -neighborhood includes at least $MinPts$ samples (including p_i), i.e., $|N_\epsilon(p_i)| \geq MinPts$, it is defined as a core point.

- *Directly reachable*: if $p_j \in N_\varepsilon(p_i)$, and p_i is a core point, then we say point p_j is directly reachable from core points.
- *Reachable*: for any points p_i and p_j , if the path x_1, \dots, x_m exists, with $x_1 = p_i$ and $x_m = p_j$. If point x_{i+1} is directly reachable from point x_i , then we say p_j is reachable from p_i .
- *Outliers/noise points*: Points that cannot be reached from any other points are considered as outliers or noise points.
- *Density-connected*: if there is a point $o \in P$, which is reachable to both p_i and p_j , we call them density connected. Density-connectedness is symmetric.
- *Reachability*: according to its definition, reachability is not symmetric, as no point can be reached from a non-core point.

DBSCAN is not sensitive to the order of samples in the database. Based on the definitions, a cluster has two features:

1. All points from certain cluster are densely connected with each other.
2. Suppose p can be density-reached from q in a cluster, then it is also part of this cluster.

According to the aforementioned three kinds of constraints added to the network, we utilize the DBSCAN clustering technique to divide our database into two groups: climbing and non-climbing datasets. Different from randomly discrete points, trajectories generally have a fixed path, pattern or discipline. We choose one dimension, altitude, as the basis for clustering. An "inflection" point marks the end of climbing phase and the beginning of cruising phase.

Parameters of DBSCAN are set as follows with consideration of features of our data, $\varepsilon = 100ft$, $Minpts = 15$. The dataset then is divided into climbing and non-climbing phases. After that, track points located in the hemispherical area with a radius of $50km$ of the airport as the centre are assigned to the descending/approaching phase.

The training dataset is segmented into three phases: climbing, cruising and descending/approaching phases with constraints of TOC, WPT and RWD, respectively.

4.5.3 Coordinate Transformation

As we know, GPS uses the Geocentric Coordinate System, which is one of the WGS-84 coordinates. Elements will have different units of measurement. Intuitively, the value of altitude can be hundreds or thousands times of latitude or longitude, as they are limited to $[0, \pm 90^\circ]$ and $[0, \pm 180^\circ]$ respectively. In many cases, especially for the short-range flights, the spatial span along latitude or longitude may be smaller than one degree. Training error of the trajectory predictors will be even larger than the changes of input tensors due to the minor difference between any two positions that recorded by latitude and longitude. We need to transform the data into appropriate expression to reduce model-training error. The unit used in North East Down (NED) coordinate system is meter, which guarantee the small difference in numerical values among different dimensions, thereby decrease error in data processing.

LLA to NED

The ADS-B device broadcasts the aircraft position with plain-text, which is expressed in latitude and longitude. Suppose (L, B, H) represents the geodetic latitude, longitude and altitude (LLA). The transformation starts by finding the changes in latitude and longitude from the initial position (L_0, B_0, H_0) .

$$\begin{cases} \Delta L = L - L_0 \\ \Delta B = B - B_0 \end{cases} \quad (4.12)$$

We then covert geodetic LLA to NED. The radius of curvature in the prime vertical R_N and the meridian R_M can be calculated by

$$\begin{cases} R_N = \frac{R}{\sqrt{1-(2f-f^2)\sin^2 L_0}} \\ R_M = R_N \frac{1-(2f-f^2)}{1-(2f-f^2)\sin^2 L_0} \end{cases} \quad (4.13)$$

where R and f are the equatorial radius and the flattening of the earth, respectively.

Changes in the North and East positions are

$$\begin{cases} \Delta N = \frac{\Delta L}{\text{atan}\left(\frac{1}{R_M}\right)} \\ \Delta E = \frac{\Delta B}{\text{atan}\left(\frac{1}{R_N \cos L_0}\right)} \end{cases} \quad (4.14)$$

The position in NED (x, y, z) can be transformed by equation (4.15). The output units are meters in the three axes.

$$\begin{cases} \begin{bmatrix} x \\ y \end{bmatrix} = \begin{bmatrix} \cos \psi & \sin \psi \\ -\sin \psi & \cos \psi \end{bmatrix} \begin{bmatrix} N \\ E \end{bmatrix} \\ z = -H - H_{ref} \end{cases} \quad (4.15)$$

where, ψ measure the angle between the x-axis and north in degrees. H_{ref} indicates the reference height.

NED to LLA

The reversed output tensors of LSTM networks are with the NED coordinate system after the training process. Though the NED coordinate system can generate fewer errors during the training process, the output is not so intuitive to our habit. For trajectory management, we usually plot/map the trajectories on a GIS system for analysis (ATC monitoring, warning or diversion). Some procedures need the aid from navigational facilities at strategy geographical locations. So we convert the NED to LLA.

We first transform the coordinate (x, y, z) to North and East coordinates with

$$\begin{bmatrix} N \\ E \end{bmatrix} = \begin{bmatrix} \cos \psi & -\sin \psi \\ \sin \psi & \cos \psi \end{bmatrix} \begin{bmatrix} x \\ y \end{bmatrix} \quad (4.16)$$

where, it is same as above, ψ indicates the angle between x-axis and north.

The radius of curvature in the prime vertical R_N and the meridian R_M are also needed to convert the North and East coordinates to geodetic LLA.

$$\begin{cases} R_N = \frac{R}{\sqrt{1-(2f-f^2)\sin^2 L_0}} \\ R_M = R_N \frac{1-(2f-f^2)}{1-(2f-f^2)\sin^2 L_0} \end{cases} \quad (4.17)$$

where R and f are the equatorial radius and the flattening of the earth, respectively.

So, the changes on latitude and longitude are approximated by

$$\begin{cases} \Delta L = \text{atan}\left(\frac{1}{R_M}\right) \Delta N \\ \Delta B = \text{atan}\left(\frac{1}{R_N \cos L}\right) \Delta E \end{cases} \quad (4.18)$$

We can get the coordinate (L, B, H) by adding the initial (*latitude, longitude*) and the changes on them, as stated by equation (4.19).

$$\begin{cases} L = L_0 + \Delta L \\ B = B_0 + \Delta B \\ H = -z - H_{ref} \end{cases} \quad (4.19)$$

where H_{ref} stands for the reference height.

4.5.4 Constrained LSTM Network Building

In our cLSTM model, each LSTM network with different constraint is structured in four layers: input layer, LSTM layer, Dense layer and output layer. Based on Keras [144], with Tensorflow or Theano backend, the input sequences are characterized by time stamps, longitude, latitude, altitude and heading, while the output tensors have the same data structure. In the climbing/descending phases, inputs are set to be 10 steps and output one step (one step lasts for 15 seconds). Prediction accuracy can be guaranteed even extending the length of output tensors in cruising phase. Input sequences are split with equal length, while we insert 0 into tensors of insufficient length. Adam is selected as the optimizer of the network.

Min-Max normalization is applied in our model before inputting the training data, x is transformed to $y = (x - min)/(max - min)$ linearly and is scaled between 0 and 1. Where, notations *min* and *max* are the abbreviations for minimum and

maximum functions, which find corresponding values of the input tensor, respectively. Sliding windows adjust the length of input to control the spatial span, which works for smoothing training process. Steps of the windows need to be set accordingly for precise and smooth prediction.

The coefficients appeared in Eq. (4.10) are determined by experimental tests. Settings and initialization of related parameters are given in Section 4.5.6.

4.5.5 Evaluation Methods

Euclidean distance is the most direct way to measure the resemblance among sequences. The mean absolute error (MAE), the mean relative error (MRE) and the root mean square error (RMSE) are most common indicators in many practical applications. We also use the dynamic time warping (DTW) to measure the similarity between predicted trajectory and the ground truth.

1. Euclidean Distance:

$$\begin{cases} MAE = \frac{1}{n} \sum_{i=1}^n |f_i - \hat{f}_i| \\ MRE = \frac{1}{n} \sum_{i=1}^n \frac{|f_i - \hat{f}_i|}{f_i} \\ RMSE = [\frac{1}{n} \sum_{i=1}^n (|f_i - \hat{f}_i|)^2]^{\frac{1}{2}} \end{cases} \quad (4.20)$$

where f_i is the observation and \hat{f}_i is the prediction.

2. Dynamic Time Warping (DTW)

DTW is known for the successful application in speech recognition. It can be seen as an optimal match between sequences with certain restrictions.

Let $Tra_1 = (tr_1^1, tr_1^2, \dots, tr_1^m)$ and $Tra_2 = (tr_2^1, tr_2^2, \dots, tr_2^n)$ be any two trajectories with different length. A $m \times n$ distance matrix $Dis_{m \times n}$ is constructed with Euclidean distances among the points from trajectories. The element in this distance matrix can be represented by $d_{ij} = |tr_1^i - tr_2^j|$, constrained by $1 \leq i \leq m$ and $1 \leq j \leq n$. $W = (w_1, w_2, \dots, w_k)$ is referred to the warping path on the grid. It should be noted that W must meet the criteria including boundary,

monotonicity and step size conditions [145]. Under these rules, the paths of each grid are limited to three directions. Suppose the grid (i, j) has passed, then the next grid to be passed will be one of $(i + 1, j)$, $(i, j + 1)$ or $(i + 1, j + 1)$. However, there can be exponential paths satisfying above restrictions. The path that minimizes the regularization described in (4.21) is what we try to get.

$$d_{dtw}(Tra_1, Tra_2) = \min \left\{ \frac{1}{M} \sum_{i=1}^M w_i \right\} \quad (4.21)$$

With the help of dynamic programming, an optimal path is generated by minimizing the cumulative distance. Let $R_{m \times n} = [r(i, j)]_{m \times n}$ be the cumulative matrix, which measures the shortest distance between Tra_1 and Tra_2 . It can be calculated as:

$$r(i, j) = d_{ij} + \min \begin{cases} r(i, j - 1) \\ r(i - 1, j - 1) \\ r(i - 1, j) \end{cases} \quad (4.22)$$

Finally, the distance between two sequences can be expressed as s cumulative distance, i.e., $d_{dtw}(L_1, L_2) = r(m, n)$.

4.5.6 Experimental Results

We conduct our experiment on an Alienware laptop, with 16GB RAM, Intel Core i7-7700HQ CPU and NVIDIA Geforce GTX 1060 graphics. 75% of the dataset is used to train the cLSTM network, while the other is used to test the effectiveness of our model. In order to have a concise and intuitive display, we randomly pick out four predicted trajectories to be visualized, while the rest of output is used to calculate the errors.

Length of sliding windows is set to be 10 time stamps, and shift by one to shape the tensors in input layer. The LSTM layer is defined with 10 neurons, and one neuron in the output layer for predicting. Output sequences are restored to tensors with the same dimensions as the original data. Models are compiled with corresponding constraints. The coefficients and parameters in Eq. (4.11) are set as $\ell = 2.2204460492503131e - 016$,

$p_1 = -0.0464964749$, $p_2 = 0.15931422$, $p_3 = -0.327622764$. Validation data is used to track the training and test loss when our model is trained. The cLSTM model is trained with 200 epochs and the batch size is set to be 16. Function $g(d)$ in Eq. (4.10) represents distance deviation between predicted and real positions, which is calculated in the same way as described in 4.4 during the three phases. DTW is initialized as follows,

$$\begin{cases} r(0,0) = 0 \\ r(i,0) = +\infty, i > 1 \\ r(0,j) = +\infty, j > 1 \end{cases} \quad (4.23)$$

Experiment on Climbing Phase

In the climbing phase, manoeuvring along the vertical direction will be more frequently than that in horizontal plane. Distance constraint alone is not able to predict well on altitude changes. We need to concentrate on the significance of angular deviation. TOC restricts both spatial distance and climb angle. Angular constraint component can effectively guide the prediction on altitude changes. Function $h(\theta)$ indicates angular deviation between angle of climb and vertical angle of current position to top of climb, as shown in Fig. 4.2.

According to our design of the matrix $\mathbf{Loss}_{\text{func}}$ in Eq. (4.9), TOC is the only component considered in this phase. The loss function in Eq. (4.8) becomes $Loss_{\text{func}} = loss_{\text{toc}} = (0.1 \cdot g(d) + 0.9 \cdot h(\theta))^2$, where the weights of distance and angular deviation components are assigned experimentally.

Fig. 4.8 depicts the predictive effects on randomly selected four pieces of climbing trajectories, while Fig. 4.9 and Fig. 4.10 record the errors of test data in time domain and frequency domain, respectively.

Experiment on Cruising Phase

In cruising phase, WPT provides unique restricts on heading and distance deviation along the centreline of airway. Medium/long-term intention could be predicted with the assistance of WPT. The weights of losses on distance and angle with the centreline

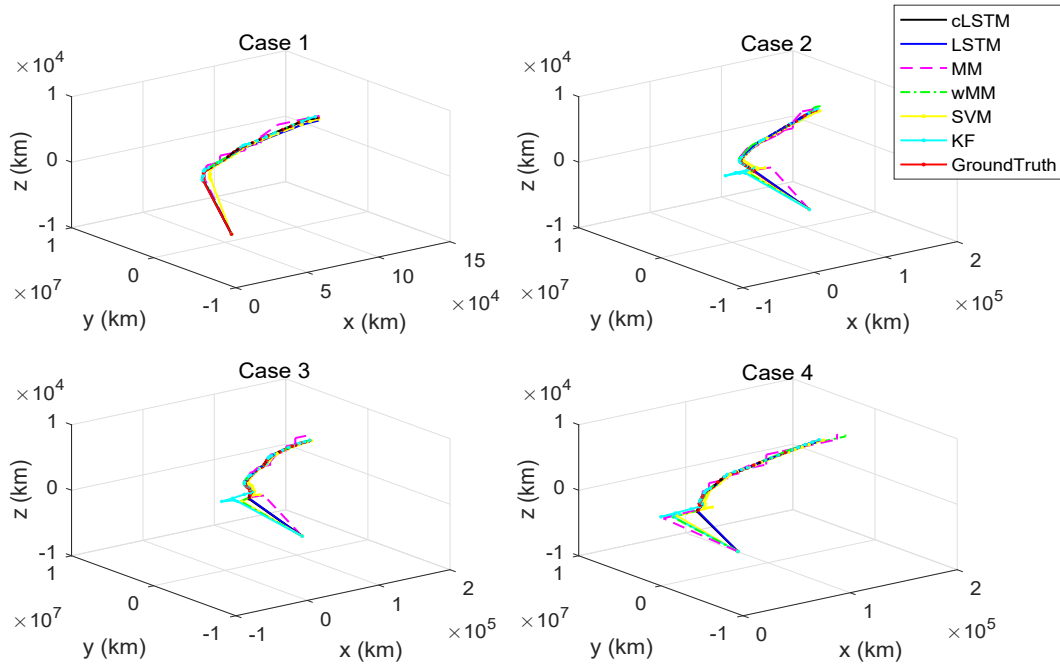


Fig. 4.8 Visualization effect of trajectory prediction in Climbing phase with cLSTM, LSTM, MM, wMM, SVM and KF. (Constraint TOC)

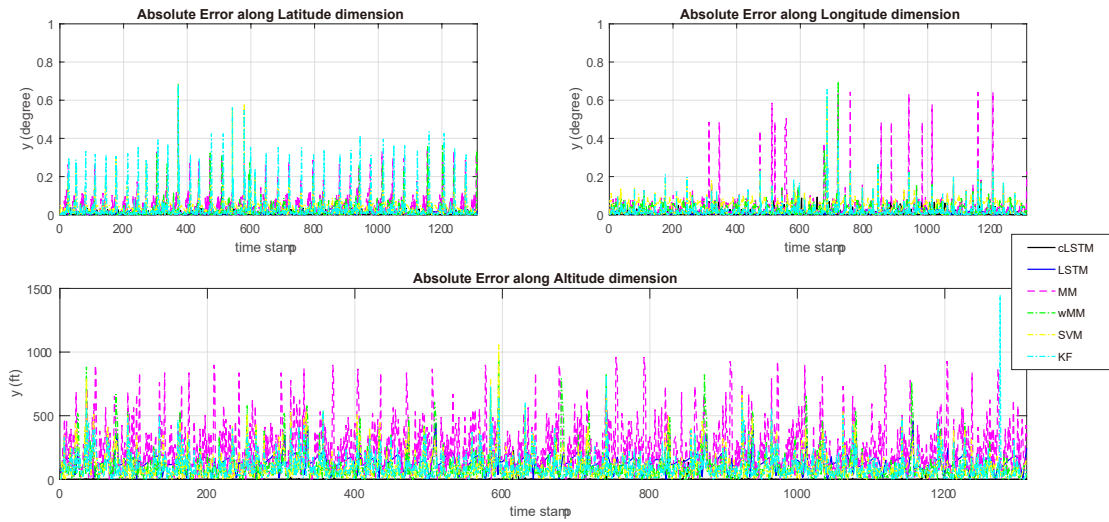


Fig. 4.9 Absolute errors of trajectory prediction in Climbing phase with cLSTM, LSTM, MM, wMM, SVM and KF. (Constraint TOC)

of approximated airway fitted by LLS have the same amount of restriction. They are set to be 0.5 and 0.5, respectively. The loss function in this phase is with the following form, $Loss_{func} = loss_{wpt} = (0.5 \cdot g(d) + 0.5 \cdot h(\theta))^2$.

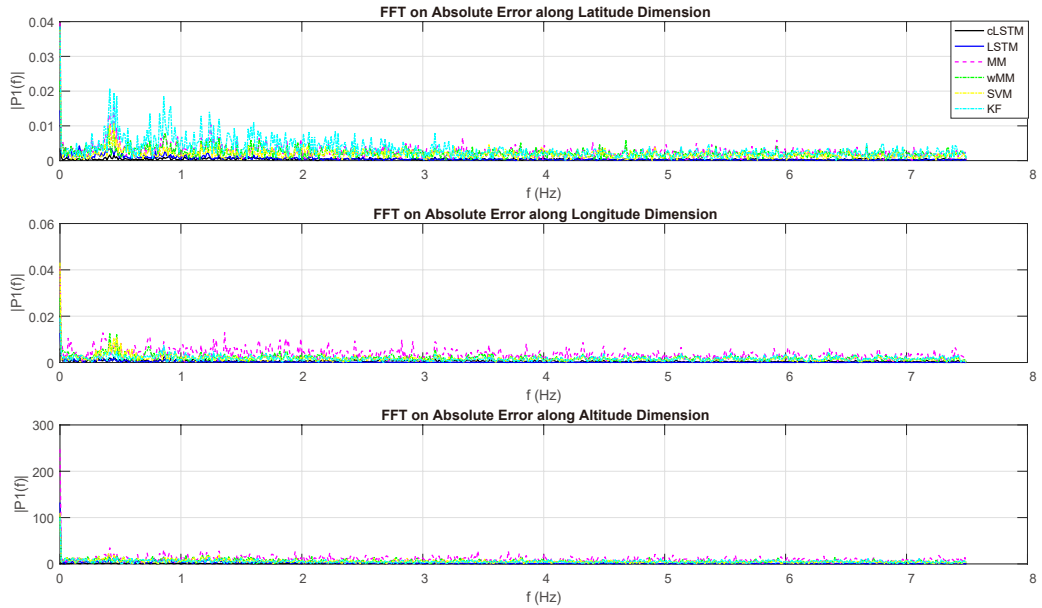


Fig. 4.10 FFT on absolute errors of trajectory prediction in Climbing phase with cLSTM, LSTM, MM, wMM, SVM and KF. (Constraint TOC)

As the cruising phase is projected to the horizontal plane, $h(\theta)$ means the angular deviation between heading of aircraft (ψ in Fig. 4.4) and the direction of fitted airway (ψ_c in Fig. 4.4). The fitted airway is determined by way-points, with the input of discrete way-points, Eq. (4.3) has the following form, $lat = -0.5448 * lon + 84.92$, where parameters a_1 and a_0 are selected from $(-0.6516, -0.4379)$ and $(73.28, 96.56)$, respectively, with 95% confidence level.

The predicted trajectories in cruising phase are shown in Fig. 4.11, and the errors calculated are shown in Fig. 4.12 and Fig. 4.13.

Experiment on Descending/Approaching Phase

In descending/approaching phase, constraints can be diversified that make the situation more complicated. We need to consider distance between aircraft and airport, distance among aircraft and entry point, altitude and heading of the aircraft, and so on.

TOC and WPT are combined to strengthen the constraint applied by RWD for descending/approaching phase. The angular deviation $h(\theta)$ contains both vertical and

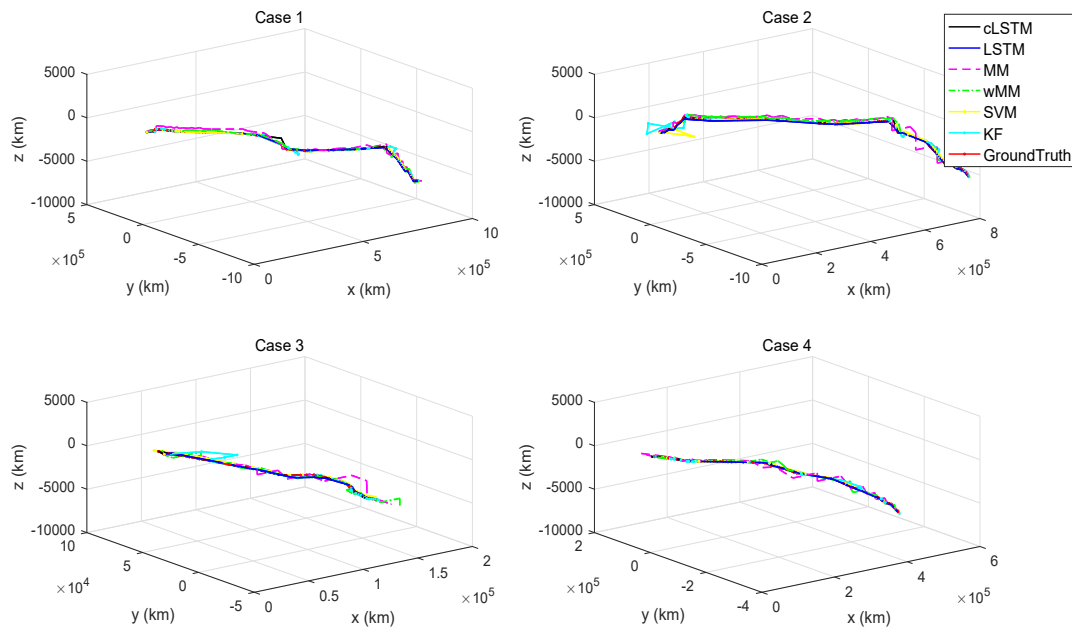


Fig. 4.11 Visualization effect of trajectory prediction in Cruising phase with cLSTM, LSTM, MM, wMM, SVM and KF. (Constraint WPT)

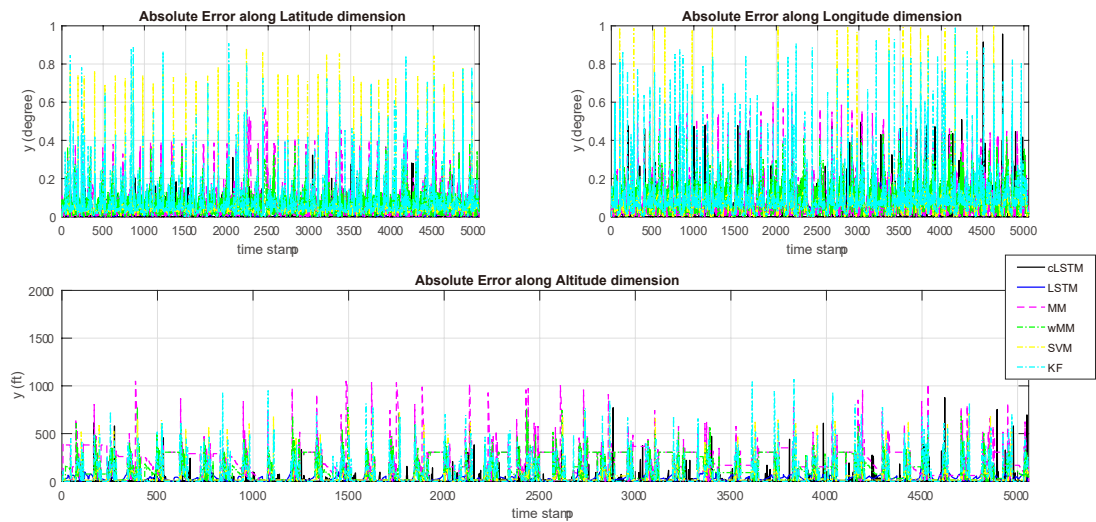


Fig. 4.12 Absolute errors of trajectory prediction in Cruising phase with cLSTM, LSTM, MM, wMM, SVM and KF. (Constraint WPT)

horizontal deviation components, where the horizontal angular deviation consists of errors with way-points and runway, respectively. As indicated in Eq. (4.9), the three

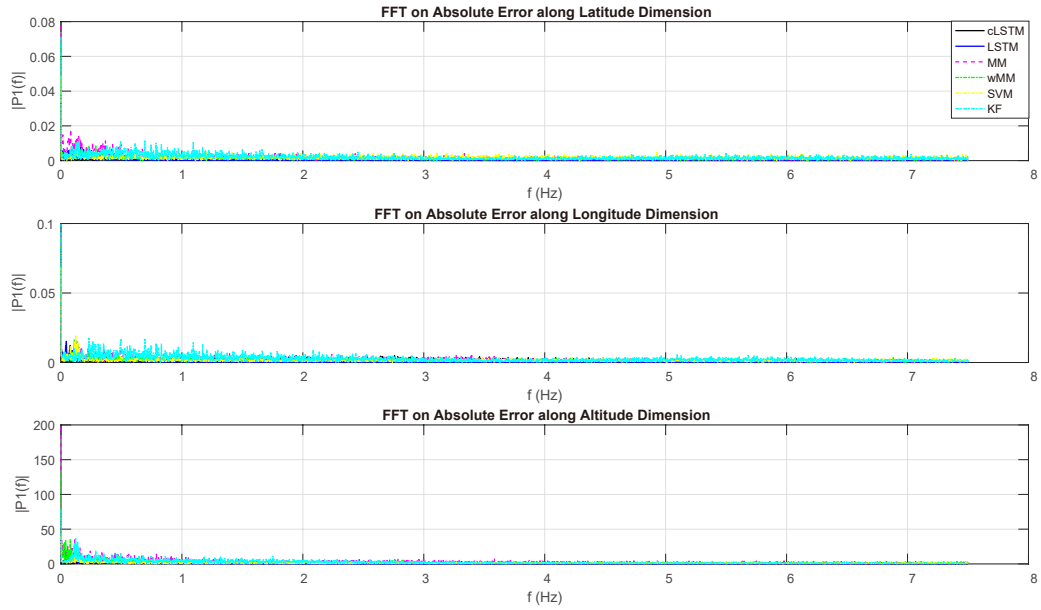


Fig. 4.13 FFT on absolute errors of trajectory prediction in Cruising phase with cLSTM, LSTM, MM, wMM, SVM and KF. (Constraint WPT)

constraints are of equal importance. The loss function is expressed as: $Loss_{func} = 1/3loss_{toc} + 1/3loss_{wpt} + 1/3loss_{rwd}$.

Weights of distance and angular deviations in constraints $loss_{toc}$ and $loss_{wpt}$ are all set to be $[0.6, 0.4]$, respectively. While $loss_{rwd} = (0.6 \cdot g(d) + 0.2 \cdot h(\theta_a) + 0.2 \cdot h(\theta_r))^2$, where, θ_a and θ_r are the components of angular deviations that refer to airway and runway (lines that fitted by LLS), respectively. Different input of LLS results in different approximation. Way-points that located in this phase constitute the approximation as $lat = -2.001 * lon + 238.3$, where parameters a_1 and a_0 are selected from $(-3.802, -0.2007)$ and $(50.83, 425.9)$, respectively. While the entry points and runway direction are fitted as $lat = 2.113 * lon - 189.1$, a_1 and a_0 are selected from $(2.033, 2.194)$ and $(-197.5, -180.7)$, respectively. Parameters are all selected with 95% confidence level.

The effects of prediction on descending/approaching phase are drawn in Fig. 4.14, while errors in time domain and frequency domain are shown in Fig. 4.15 and Fig. 4.16.

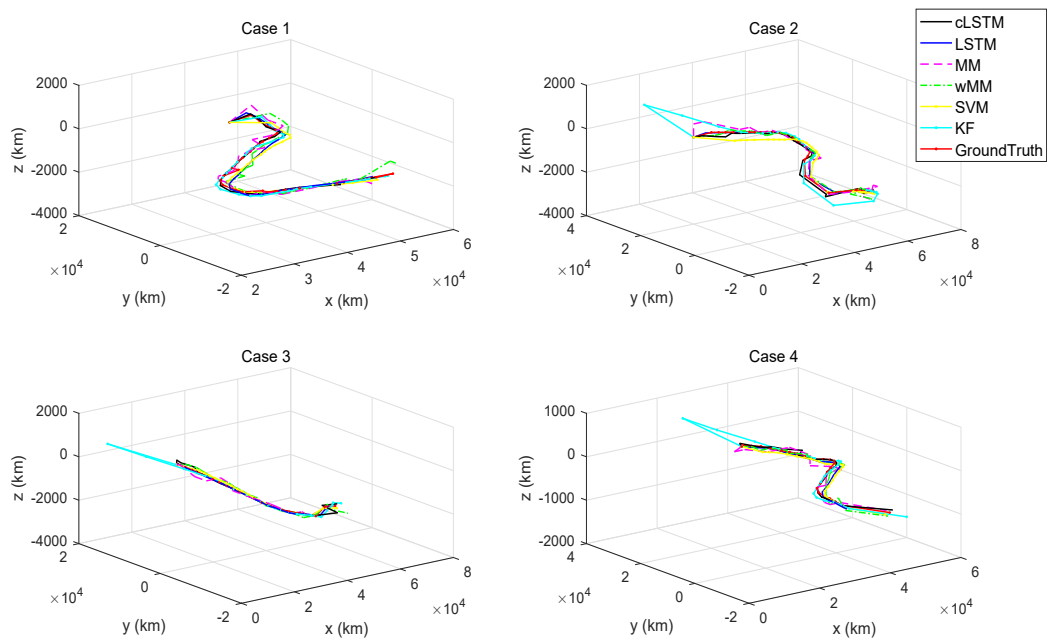


Fig. 4.14 Visualization effect of trajectory prediction in Descending/Approaching phase with cLSTM, LSTM, MM, wMM, SVM and KF. (Constraint TOC, WPT and RWD)

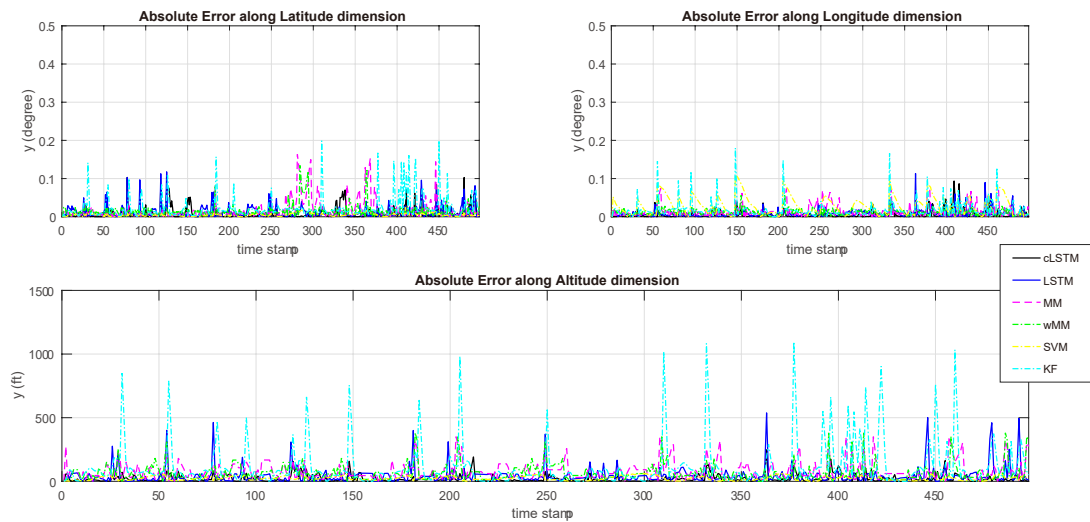


Fig. 4.15 Absolute errors of trajectory prediction in Descending/Approaching phase with cLSTM, LSTM, MM, wMM, SVM and KF. (Constraint TOC, WPT and RWD)

We select one complete track from the test dataset to test and verify the predictive performance of our model. MM is selected as the only comparative model to make our results distinguishable in Fig. 4.17. The prediction effects of cLSTM and MM models

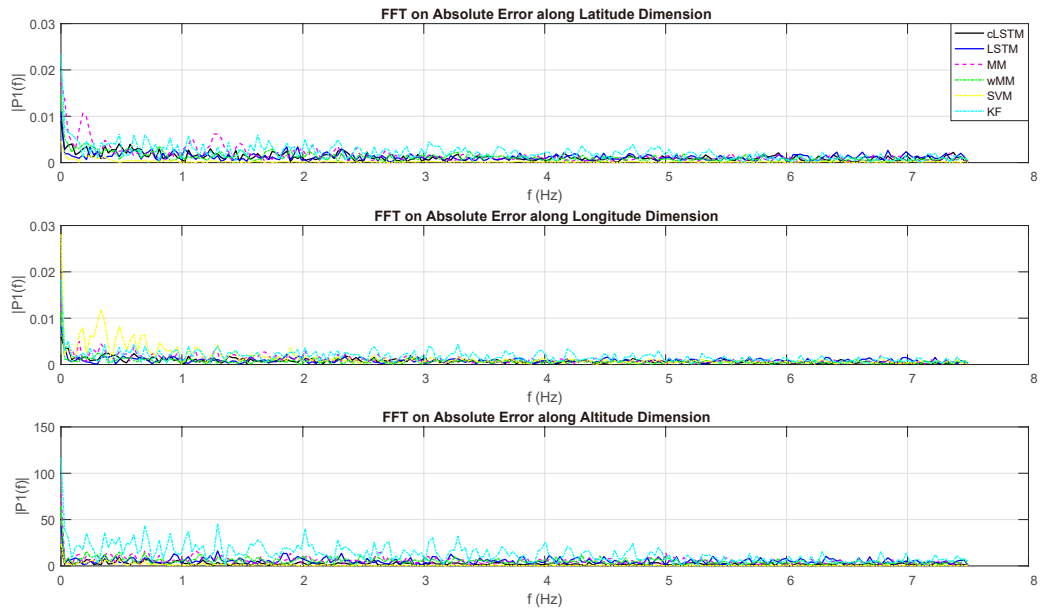


Fig. 4.16 FFT on absolute errors of trajectory prediction in Descending/Approaching phase with cLSTM, LSTM, MM, wMM, SVM and KF. (Constraint TOC, WPT and RWD)

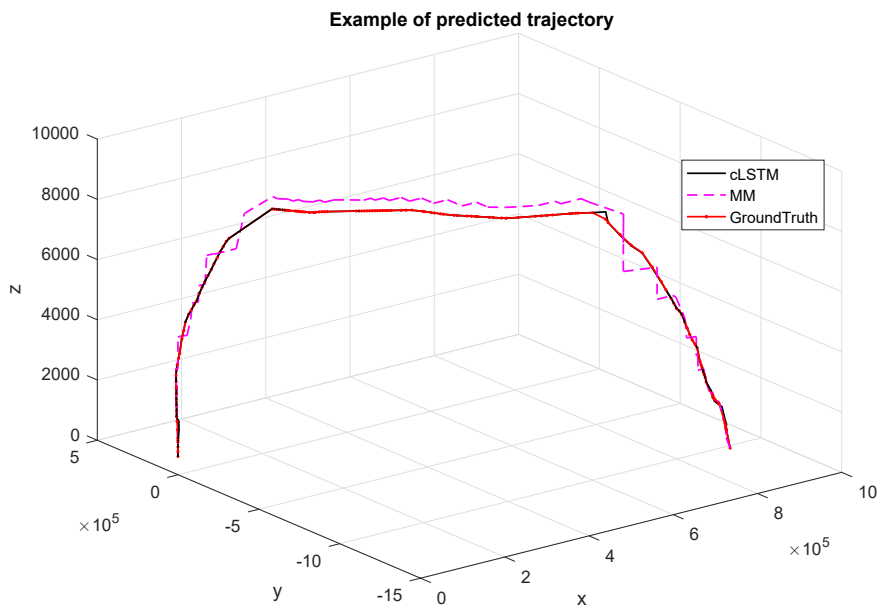


Fig. 4.17 Prediction effect on the whole voyage with cLSTM and MM models.

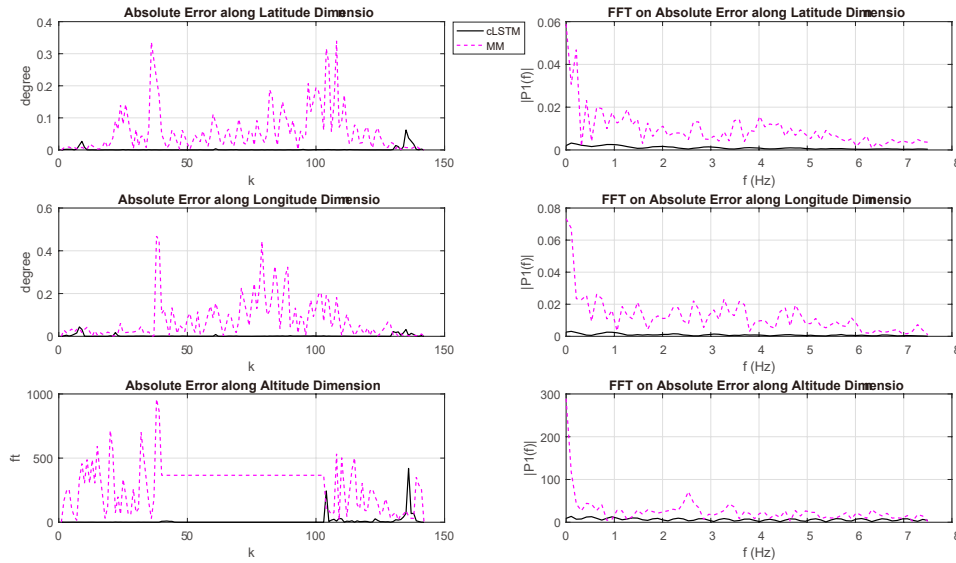


Fig. 4.18 Errors on the whole voyage with cLSTM and MM models.

are analysed in both time domain and frequency domain (Fast Fourier Transform, FFT), respectively, as is shown in Fig. 4.18. The process of parameter-tuning on the weights of distance and angular deviations in each constraint is recorded and drawn in Fig. 4.19. The basis for selecting the weights is the similarity evaluated by DTW distances, which are normalized by Min-Max to values between $[0, 1]$. In order to make Fig. 4.19 concise, we show the proportion of weights on distance and angle, without distinguishing the components of angular deviations to airway and runway.

4.5.7 Quantitative Analysis

In this section, we quantitatively analyze the behaviors of our model with different constraints in corresponding phases. Fig. 4.8, Fig. 4.11, and Fig. 4.14 show three different scenarios of flight traffic, correspond to climbing, cruising, and descending/approaching phases. The increasing of errors of cLSTM model in cruising phase is resulted from the LLS process to accelerate model training. Despite the weakened accuracy in cruising phase, our model still outperforms other methods. The trends drawn in these figures show that the trajectory predicted by our model is closer to the ground truth.

Fig. 4.9, Fig. 4.12, and Fig. 4.15 consistently show our model performs better than others. Markov Models rely too much on the size of group, which affects the prediction accuracy heavily. In addition, their complex and heavy computation load limit their performance on medium/long-term sequence processing. Benefit from our linear assumption between any two timestamps, Kalman Filter predicts fine. But the initial state of KF influences a lot on the prediction effect. The cost of good prediction result of SVM is time and space consumption. We need certain memory space to store the kernel matrix of SVM, and it is quite time consuming to train its model.

LSTM network with sliding windows keeps the smoothness of sequences and maintains characteristics for medium/long-term cases. It performs better than above-mentioned models. However, this is not enough for aviation trajectory prediction, because of the strong maneuvering in trajectories. The cLSTM network makes full use of physical constraints, which significantly narrows the errors between prediction and ground truth.

Both spatial and temporal features of flight trajectory are enrolled and trained which makes our model 4-D predictable. Constraints including dynamic performances of aircraft and static navigational requirements are embedded to adapt to practical application. Losses are calculated in a fast and low-complexity way by Taylor's expansion, which increases accuracy and reduces the computational burden. Compared with the above-mentioned methods, our model has better performance even high non-linearity occurs. Fig. 4.17 and Fig. 4.18 also demonstrate the predictive performance of our model, which can reliably mine the trend of the trajectory.

MAE, MRE, RMSE, and DTW are calculated for all the models. In order to show the errors close to our habits, the errors are listed along latitude, longitude, and altitude directions. The unit used in latitude and longitude directions is degree, while meter is applied in altitude direction. Table 4.1 lists the errors of all test data over the whole voyage, which also indicates our proposed cLSTM model has the lowest prediction error. We can learn from the table that our model performs better especially in the prediction of altitude changes due to the introduction of physical constraints.

For further comparisons with practical models [146] and systems [147], we randomly select one-third of the test data to record the mean errors during different phases.

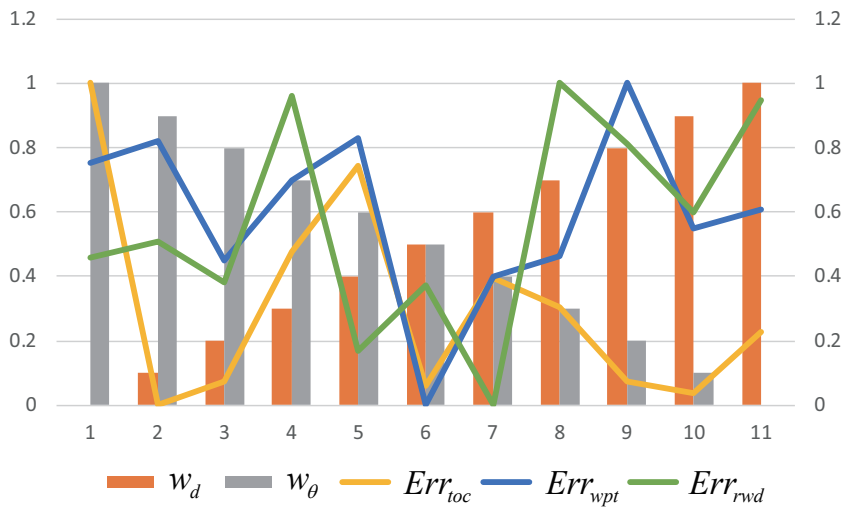


Fig. 4.19 Process of weights selection in loss functions of each constraint.

In cruising phase, the mean errors caused by cLSTM model along the latitude and longitude directions are -0.0116 and 0.0009 degrees, respectively, which are small enough compared with corridor width. While in climbing and descending/approaching phases, the errors along latitude direction will decrease to 0.001 and 0.0011 degrees, respectively. The mean errors along longitude direction in these two phases are 0.0004 and 0.0007 degrees, respectively. During the whole voyage, the mean altitude error is 9.0292m (29.6233 ft). The mean errors in climbing and descending/approaching phases are smaller than those reported in [146], especially along the altitude dimension. Compared with the baselines of practical systems (BADA and CTAS), our model works better than most of the variants. As their absolute mean along-track/cross-track error is between two and three nautical miles, the mean altitude errors can be hundreds of feet [147]. It is indicated that our model outperforms the above-mentioned models/systems during climbing and descending/approaching phases with the lowest altitude error, while in cruising phase our model can still be superior to most of the models with reported horizontal error.

Table 4.1 Performance comparison among cLSTM model and state-of-the-arts models.

Methods	MAE			MRE			RMSE			DTW	
	lat*	lon*	hgt*	lat	lon	hgt	lat	lon	hgt	4-D	
cLSTM	0.0050	0.0105	9.9572	0.0199	0.0094	0.2798	0.0203	0.0482	45.3447	4.9793	
LSTM	0.0286	0.0641	55.6840	0.1122	0.0586	1.7862	0.0382	0.0799	79.8379	27.8421	
SVM	0.0436	0.0609	52.1262	0.1724	0.0554	1.5246	0.0740	0.0888	93.8921	98.9509	
wMM	0.0556	0.0725	119.3041	0.2155	0.0662	2.6723	0.0770	0.0990	168.5243	26.0633	
MM	0.0659	0.0761	197.9012	0.2579	0.0697	4.6956	0.1026	0.1139	257.6596	59.6523	
KF	0.0617	0.0785	85.4935	0.2411	0.0716	2.5085	0.1046	0.1354	157.7501	42.7672	

* *lat, lon, hgt* are abbreviations for *latitude, longitude* and *altitude*, respectively.

4.6 Summary

A constrained LSTM network-based model for 4-D flight trajectory prediction was presented in this chapter. This model was tested and verified by the historical flight trajectories collected by ADS-B devices. Constrained LSTM network introduced reasonable and strict physical constraints while maintaining the long-term dependencies. Applying sliding windows led to a smooth trajectory. Comparison experiments were conducted with LSTM network embedded with sliding windows, Markov Model, weighted Markov Model, Support Vector Machine and Kalman Filter. Quantitative analysis showed our method outperformed those widely used typical algorithms and most of the practical models/systems.

Chapter 5

Situational Awareness and Path Planning

5.1 Overview

Accidents occur frequently when the aircraft take off and land. Even small errors can lead to serious consequences. Driving skills and experience of pilots contribute a lot to our safe travel. The most famous example happened on the plane 3U8633 in 2018, whose wind-shield was broken and felled off, the pilot managed an emergency and safe landing without loss of properties and lives. In addition to the factors of skilled pilots, infrastructures of airports are also crucial, including the construction sites, surrounding environment and corresponding emergency facilities. Any single or combination of the above-mentioned aspects will bring unprecedented challenges to the timeliness and accuracy of ATM. Once an aircraft took off from Hong Kong International Airport (HKG) with abnormal heading, where mountains located just in front of it. The pilot managed to fly over the mountain after receiving a warning from the ground tower. Though no accident occurred, we should raise enough attention to trajectory management and decision-making.

We take the unique geographical environment of HKG as an experimental example, which is surrounded by mountains and sea. 4-D spatial-temporal trajectory predictor is trained by massive historical flight trajectories of climbing phase. Geographical

environment around HKG is modelled as a discrete gridded space by digital elevation model (DEM). A cubic A* algorithm is proposed for aircraft path planning based on the predicted state in 4-D space. Threats between aircraft and the mountains are assessed along the optimally planned path.

The rest of this chapter is organized as follows: Sections 5.2, 5.3 and 5.4 present the models on flight trajectory prediction of climbing aircraft, path planning and threat assessment, respectively. Experimental analysis and discussions are addressed in Section 5.5. Section 5.6 makes a summary of this chapter and provides some possible extensions.

5.2 4-D Trajectory Prediction in Climbing Phase

In the hypothesis of deep learning, a deep and hierarchical structure can improve the expressiveness and efficiency of the neural network [148]. Each layer in the LSTM structure outputs our expected results, which are passed on to next layer [149]. We have optimized the LSTM network by adding its depth in this section to improve its performance.

Two LSTM layers are stacked in our optimized LSTM network, which is followed by a Dense layer before output. Instead of outputting a single value, the first LSTM layer will provide a sequence to the second LSTM layer. The hidden state of each level operates in a different time frame under this structure. Suppose the state of i th hidden layer at time t is expressed as h_t^i ,

$$h_t^i = f(U^i h_{t-1}^i + W^i h_t^{i-1} + b^i) \quad (5.1)$$

where, U^i , W^i and b^i stand for the weight matrices and bias vector of the i th hidden layer, respectively.

Although we extend the hidden layers of our neural network, we cut the number of neurons on corresponding layers to reduce the complexity of network. According to [148], the depth of network can make the model more expressive than that with more neurons in single layer.

Time sequences characterized by time stamps and positions act as the input of LSTM network, whose lengths are controlled by sliding windows. Sliding windows are also embedded into our LSTM network to restrict the spatial span of the input sequences. The length of sliding windows is set according to the rate of climb, but limited to be 10. Windows will shift by one step to keep the characteristics of trajectory.

5.3 Path Planning Model

Many factors need to be aware of when an aircraft performs its task in low-altitude airspace, especially during the take-off and landing phases. Besides the airspace restrictions, such as terrain and no-fly zones, the dynamic performance of the aircraft should also be considered. A path planning model aims to plan before encountering the problem, which compromises between the optimal solution and time consumption. Path-finding in an arbitrary graph will be more complex than the grid-based scenarios. Dijkstra algorithm [150][151] is able to find the shortest paths between nodes in a graph at the cost of certain time consumption. As it repeatedly detect the vertices that are closest but not-yet-extended until reaching the target. Best-First Search algorithm [152] works similarly but with heuristic way. It selects the vertex closet to the target rather than the start node. Though Best-First Search algorithm has lower time consumption than Dijkstra, it cannot guarantee the shortest path. When planning an aircraft trajectory, in addition to the real-time requirements, it is also necessary to consider the dynamic constraints of aircraft (maximum rate of climb, etc.) and flight tasks (voyage and estimated time). In this section, A* search algorithm is first presented, which is followed by the dynamic constraints of aircraft considered in path planning.

A* Search Algorithm

A* search algorithm is a popular method applied in path-finding and graph traversal, which uses a heuristic factor to search a path in a certain direction with the lowest cost (least distance, shortest time, etc). This method integrates the advantages of

Best-First Search and Dijkstra algorithm. It is a method that evaluates the cost of searching location in the state space until reaches the end point.

At each iteration of its loop, A* makes the decision to choose the path to be extended. It finds an optimal path by measuring the cost on current path and estimated cost required to extend to the goal. The estimation function can be generalized as follows,

$$f(n) = g(n) + h(n). \quad (5.2)$$

where n stands for the index of preselected next node on the path, $g(n)$ records the cost between the start node and node n , while $h(n)$ represents a heuristic function that used to estimate the costless extending path. Moreover, Eq. (5.2) follows the characteristics listed below:

- If $g(n) = 0$, it means only the evaluation function $h(n)$ of any node n to the goal is calculated. Then A* turns to be Best-First Search with greedy strategy. The fastest calculation speed we benefit, but we may not get the optimal solution.
- If $h(n)$ is valued less than the actual distance between node n and the target node, the optimal solution can be guaranteed. In addition, the smaller the $h(n)$, the more nodes need to be calculated, which will lead to an inefficient algorithm. Euclidean, Manhattan and Chebyshev distances are the common evaluation functions used in A*.
- If $h(n) = 0$, it is only necessary to find the shortest path $g(n)$ from start to any node n without considering any evaluation function $h(n)$. Then A* is transformed to the single source shortest path problem, namely Dijkstra algorithm.

The search process terminates when the path is well-extended or no path eligible to be extended. In general, there are three types of the commonly used path search direction: 4-direction, 8-direction and 16-direction. As shown in Fig 5.1, different heuristic functions lead to different time complexities of A* search algorithm.

Taking the practical factors into consideration, path planning will be a complex work. A* search algorithm is good at track finding with small expansion space. By referring to the heuristic mechanism, the optimal track is obtained by calculating the

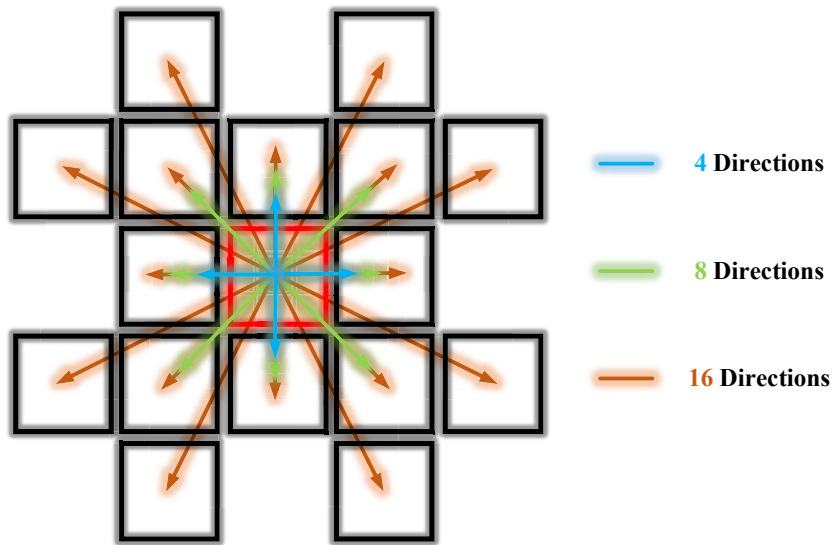


Fig. 5.1 Commonly used three types of path search directions.

cost between current and the target nodes, which is simple in form and suitable for path planning based on gridded space. Many practical factors need to be compromised, which makes it difficult to objectively evaluate the optimal solution. So we have to choose a more reasonable solution according to the situation. A* search algorithm can be optimized by simplifying the search space, optimizing the OPEN table, measuring the heuristic mechanism dynamically, and introducing Newton method or more recent powerball, hyperball method to increase the convergence speed.

Cubic A* Search Model

In this work, we simplify the search space by introducing the dynamic performances to reduce the complexity of search model. Dynamic performances of aircraft should be met when changing their scheduled routes. We should consider the safety, economy and comfort of the flight comprehensively when planning the trajectory.

Force analysis of aircraft in climbing phase is first presented in this section, as is shown in Fig. 5.2. Flight trajectory can be generally divided into lateral and vertical parts. The later part can be described as a function of the performance and configuration of aircraft.

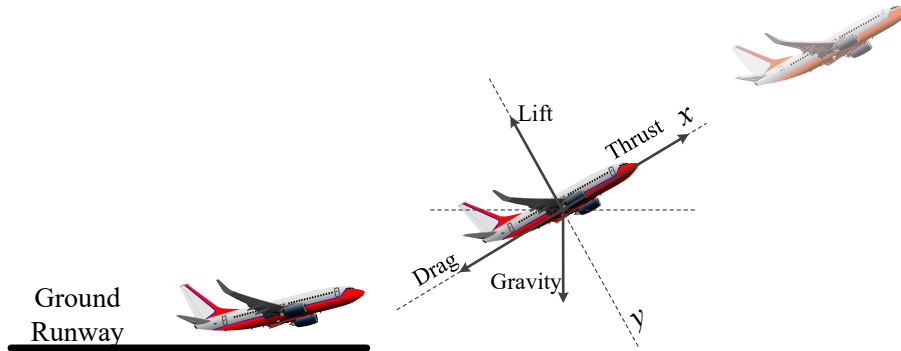


Fig. 5.2 Force analysis of the aircraft during climbing phase.

$$\begin{cases} D = C_D \rho V^2 S / 2 \\ L = C_L \rho V^2 S / 2 \\ Y = C_Y \rho V^2 S / 2 \\ l = C_l \rho V^2 S b / 2 \\ M = C_m \rho V^2 S \bar{c} / 2 \\ N = C_n \rho V^2 S b / 2 \end{cases} \quad (5.3)$$

where, notation ρ represents the density of air, V is the true airspeed (TAS), D , L , Y , l , M , N represent the aerodynamic drag, lift and lateral force, roll, pitch and yaw moments of the aircraft, respectively. C_D , C_L , C_Y , C_l , C_m , C_n represent the coefficients of drag, lift and lateral force, roll, pitch and yaw moment of the aircraft accordingly. S , b , \bar{c} represent the wing area, wing span and the average aerodynamic chord length, respectively. The maximum rate of climb limits the maximum span in the vertical direction, while the maximum yaw angle restricts the horizontal range.

With the help of DEM maps, we extend two-dimensional space to three-dimensional cubic spaces. Each cube stores its inherent geographic coordinates and elevation data. Embedded with constraints and threats, every cube can expand out 26 sub-cubes (8-directional expansion as shown in Fig. 5.1), just like a Rubik's Cube. However, in terms of the aircraft, given certain speed and heading angle, it is impossible for any aircraft to achieve arbitrary rotation within 360 degrees. As we all know, aircraft is subjected to constraints, such as minimum turning radius and maximum angle of climb,

when performing tasks. Then, not all 26 sub-cubes can be reached. The A* search algorithm needs to be modified to adjust to the work on path planning for an aircraft. Moreover, during all the phases of flight, frequent turning will increase the fatigue of pilots and navigation errors, which is not conducive to the safety. Thus frequent turning should be avoided when planning the path.

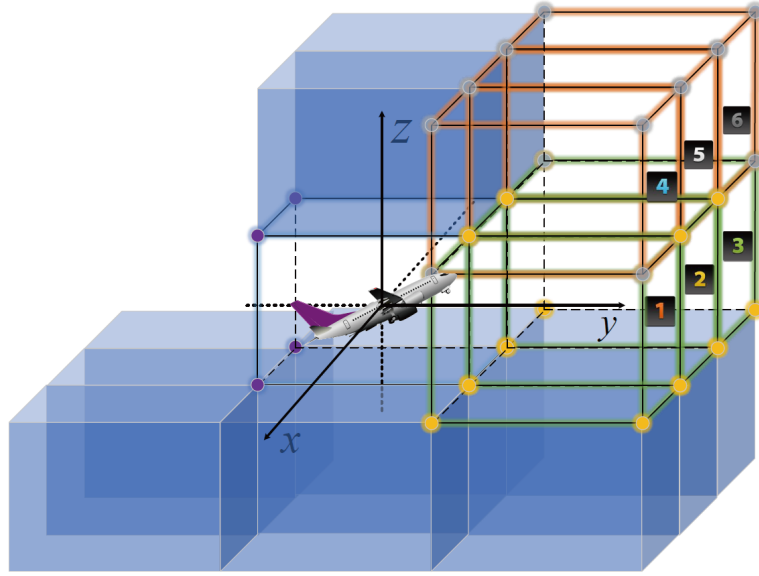


Fig. 5.3 Node expansion of the cubic A* search algorithm.

In this chapter, we take the unique geographical characteristic around HKG airport into consideration. Threats will be raised after the aircraft takes off. Similar to the A* search algorithm, the proposed cubic A* search algorithm also needs to construct OPEN and CLOSED lists, which stores values of the cost. The following two kinds of constraints should be applied to the cubic A* algorithm.

1. Maximum yaw angle ψ . Excessive yaw angle may cause loss of control. Let d_k represent the vector that stores nodes from the parent to current. d_{k+1} stands for the vector that the current node intends to expand. \mathbf{d}_k^h and \mathbf{d}_{k+1}^h are the projections of d_k and d_{k+1} on the horizontal plane, respectively. Then the constraint of maximum yaw angle can be expressed as

$$\frac{\mathbf{d}_k^h \mathbf{d}_{k+1}^h}{\|\mathbf{d}_k^h\| \|\mathbf{d}_{k+1}^h\|} \geq \cos \psi \quad (5.4)$$

2. Maximum rate of climb (RoC). Let θ be the maximum climb angle, the constraint of maximum climb rate can be equivalent to

$$\theta \geq \arctan \frac{|z_k - z_{k+1}|}{\sqrt{(x_k - x_{k+1})^2 + (y_k - y_{k+1})^2}} \quad (5.5)$$

where (x_k, y_k, z_k) marks the current node, $(x_{k+1}, y_{k+1}, z_{k+1})$ is the coordinate of the target node.

With the above-mentioned constraints, any node whose distance difference in the horizontal or vertical direction with current node exceeds the limitations can not be used as a candidate expansion node. We illustrate the node expansion of the cubic A* search algorithm in Fig. 5.3.

5.4 Threat Assessment Model

Data/information fusion is a process proposed for integrating multiple data sources, whose aim is to generate more consistent, accurate and useful information than any independent individual data source. The most famous model of data fusion is the so-called JDL (Joint Directors of Laboratory) data fusion model, which was proposed in the mid-1980s. The Data Fusion Subpanel formed by JDL is now known as the Data Fusion Group. Then the JDL model was expanded to the Data Fusion Information Group (DFIG) model [153][154]. These two models can be illustrated as shown in Fig 5.4. The JDL model refers to level 1-4 as shown in Fig 5.4. While the DFIG model (level 0-5) is a more comprehensive model. Although JDL is still used nowadays, it limits how the data is distributed. Certain shortcomings may exist in these two models, they make the process of data fusion transparent to users. Situational awareness and threat estimation are the key important steps before human-beings or the systems to make decisions.

Threat assessment is a complex problem with multiple factors. Massive information will lead to heavy burden on calculation, and it is impossible to consider all the factors in the threat assessment. Appropriate number of major factors are able to guarantee accurate and timely threat assessment.

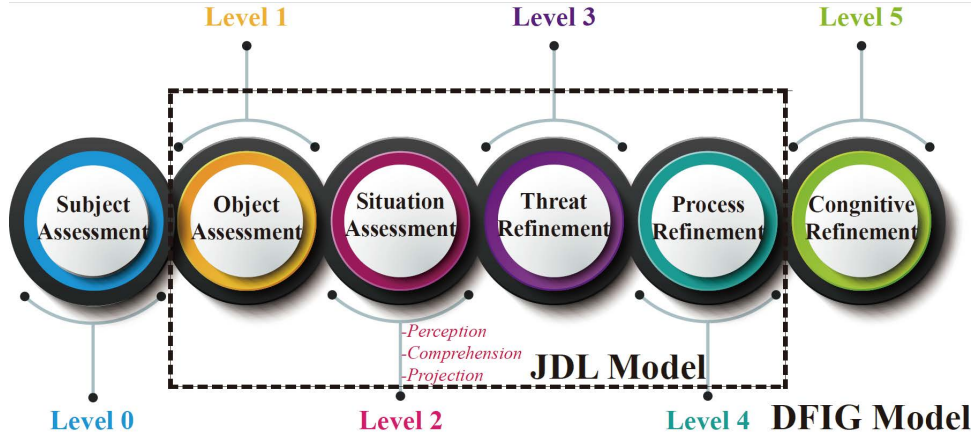


Fig. 5.4 Two classic data fusion models: JDL and DFIG.

For potential threats caused by terrain, the state of aircraft is the key factor when assessing the threats. Speed, altitude and track angle of the aircraft are mainly considered threat factors in this section. As factors are measured and recorded in different units, they must be converted to dimensionless data between 0 and 1.

1. Speed of the aircraft. Distance affects the extent of threat deeply, which is proportional to speed. The shorter the distance or the faster the speed, the higher the threat. In the climbing phase, the threat $\mu(v)$ and speed v can be built in an exponential function as follows.

$$\mu(v) = \begin{cases} 1, & \text{else} \\ 1 - e^{-(v-V_{cl})^2}, & V_{cl,1} \leq v \leq V_{cl,2} \end{cases} \quad (5.6)$$

where, $V_{cl} = (C_{V_{\min}} \cdot (V_{stall})_{TO} + Vd_{CL,k})$ represents the speed when an aircraft takes the climbing phase. $C_{V_{\min}}$ is the minimum speed coefficient and valued 1.3. $(V_{stall})_{TO}$ denotes the take-off stall speed, in our case $(V_{stall})_{TO} = 250knot$ [1]. $Vd_{CL,k}$ stands for the climb speed increment, which increases with the altitude level k . For a jet aircraft, $Vd_{CL,1} = 5knot$ and $Vd_{CL,2} = 10knot$. $[V_{cl,1}, V_{cl,2}]$ indicate the range of climb speed [16].

2. Altitude of the aircraft. Geographical topography has a great influence on take-off phase. Intuitively, the farther away from the ground or obstacle, the safer for an

aircraft to take off. The potential threat caused by mountains is expressed as follows.

$$\mu(z) = \begin{cases} 0, z > Alt_M \\ e^{-(z-Alt_M)^2}, z \leq Alt_M \end{cases} \quad (5.7)$$

where z locates the real-time altitude of the aircraft, while Alt_M stands for the altitude of obstacle when aircraft perform its task in this area.

3. Track angle of the aircraft. The track angle shows the nearly intend of the trajectory. Mountains appear in or closely near the heading direction will lead to great threat to aircraft. The threat is in the form of

$$\mu(\psi) = \begin{cases} 0, else \\ e^{-(\psi-\eta)^2}, z \leq Alt_M \end{cases} \quad (5.8)$$

where ψ stands for the track angle of the aircraft and η represents the angle between aircraft and obstacles.

In summary, the total threat caused by the mountain near the airport is $TA_{cl} = \alpha_1\mu(v) + \alpha_2\mu(z) + \alpha_3\mu(\psi)$. Notations α_1 , α_2 and α_3 are the weights of the three kinds of threats, respectively.

5.5 Experiment and Discussion

We start this section with data collection. According to the data processing flow, 4-DTP model is first performed to generate an accurate prediction of the aircraft. When potential risk appears around the predicted location, the situation of aircraft will be assessed. Path planning and threat assessment models are triggered simultaneously based on the current and predicted states of the aircraft.

5.5.1 Data Collection

Historical Flight Trajectories

The dataset used in this section is part of that collected in Section 4.5.1. Historical flight trajectories are segmented by DBSCAN algorithm in Section 4.5.2. Our 4-DTP model is trained by the dataset belonging to climbing phase.

Terrain Data

It is meaningful that the planned track needs to appeal to the real terrain. Terrains are made up of irregular curved surfaces and cannot be expressed by single or combined surface functions. Digital map is one of the important technologies in trajectory planning, which lays the foundation for rapid development of modern trajectory planning. Geographical attributes, positioning information and hidden relationship of the map elements are stored and used to describe environment in digital form.

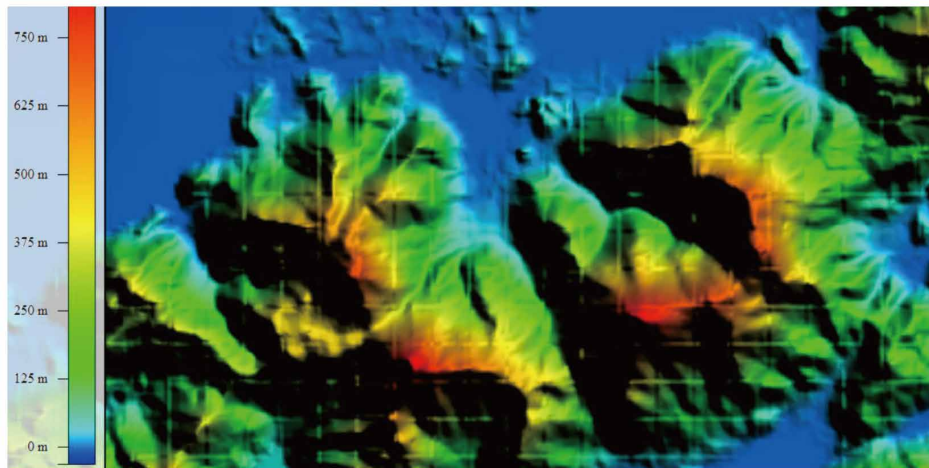


Fig. 5.5 The DEM data near Hong Kong International Airport.

When an aircraft performs its task at a low altitude, both ATC controllers and pilots should monitor the departure/entry routes, intended fly-through way-points and changing parameters of navigational equipment carefully for timely terrain and threat avoidance. For the ground-based air traffic control centre, in order to calculate the terrain's threat to the aircraft, we choose the digital terrain model (DTM) to model

the geographical space around the aircraft. On one hand, DTM provides necessary data for path planning models to obtain an optimal path. On the other hand, DTM manages to display geographical environment that beyond the visual range. In this section, threats raised by topography are taken into consideration. Accordingly, the terrain model we used is characterized by altitude, i.e., the DEM.

Taking the non-analytic features of terrain that mentioned earlier into consideration, the geographical coordinate set $\mathbf{Pos} = (\mathbf{x}, \mathbf{y}, \mathbf{z})$ is scattered into a two-dimensional grid matrix $\mathbf{Pos}_g = (\mathbf{x}_g, \mathbf{y}_g, \mathbf{z}_g)$ in the horizontal plane. Terrains are described as a function of coordinate $(\mathbf{x}_g, \mathbf{y}_g)$. The output of function of terrains will be altitude, i.e., $\mathbf{z}_g = f(\mathbf{x}_g, \mathbf{y}_g)$, where \mathbf{z}_g stands for the series of elevations in the corresponding spatial span. The sparseness of the grid depends on sampling interval, which expressed as grid distance on the digital map. Different sampling intervals result in different resolutions of digital maps. Generally, the smaller the sampling distance, the greater the resolution and the more terrain information the map contains. Airspace around HKG airport is divided into discrete blocks with ultimate Rate of Climb (RoC) of aircraft typed A320. Part of the terrain around HKG airport is shown in Fig. 5.5.

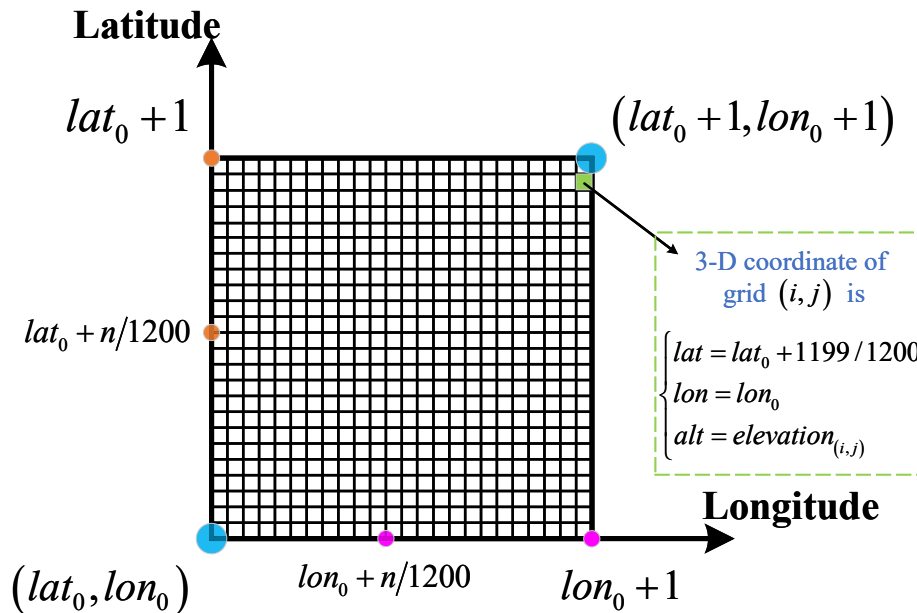


Fig. 5.6 Structure of SRTM-3 data.

Land elevation can be obtained from the NASA's Shuttle Radar Topography Mission (SRTM) data [155]. We select the SRTM data that is sampled at 3 arc-seconds, which means the latitude and longitude are recorded every $1/1200$ degree (90 meters/295 feet). It divides the spatiality into grids with corresponding elevation value. SRTM-3 data is structured as shown in Fig. 5.6.

5.5.2 4-D Trajectory Prediction in Climbing Phase

Taking the scene of HKG into consideration, normally, aircraft take off towards the sea along the direction of runway. However, an aircraft happened to head to the mountain at the beginning of climbing phase. Then the real-time intention/trajectory needs to be well predicted to keep safe.

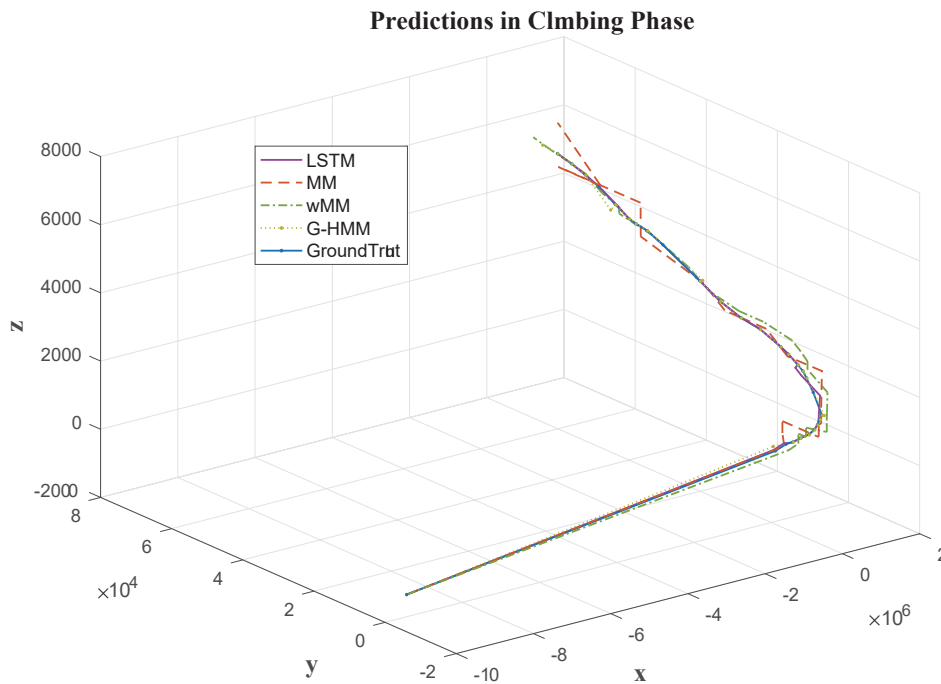


Fig. 5.7 Predictions of trajectory in climbing phase by LSTM, Markov Model, weighted Markov Model and Gaussian Hidden Markov Model.

Two-thirds of the climbing-phase dataset acted as training data, while the rest of it was used for test. We make further optimization on LSTM network as described in Section 5.2. In addition to Markov Model (MM) and weighted Markov Model (wMM)

[126–128], the state-of-the-art Hidden Markov Model (Gaussian Hidden Markov Model, G-HMM) [156][157] is also selected as comparison algorithm. The longest common subsequence distance (LCSS) [158], one way distance (OWD) [159] and dynamic time warping act as our similarity evaluation methods. Table 5.1 lists the similarity evaluations of LSTM, MM, wMM and G-HMM models based on LCSS, OWD and DTW introduced in Section 4.5.5.

1. **Longest Common Subsequence Distance (LCSS)**. Suppose two sequences are represented by $T_1 = (t_1^1, t_1^2, \dots, t_1^m)$ and $T_2 = (t_2^1, t_2^2, \dots, t_2^n)$, respectively. Then the length of longest common subsequence of T_1^i and T_2^j can be calculated by $C[i, j]$, where

$$C[i, j] = \begin{cases} 0, & \text{if } i = 0 \text{ or } j = 0 \\ C[i - 1, j - 1] + 1, & \text{if } i, j > 0 \text{ and } t_1^i = t_2^j \\ \max(C[i, j - 1], C[i - 1, j]), & \text{if } i, j > 0 \text{ and } t_1^i \neq t_2^j \end{cases} \quad (5.9)$$

2. **One Way Distance (OWD)**. Basically, OWD calculates the trajectory similarity piece by piece. For linear trajectories $T = \{t_1, t_2, \dots, t_n\}$, they can be considered as a sequence of segments $LS(T) = \{f_{seg}(t_i, t_{i+1}) | 1 \leq i \leq n - 1\}$. Then the OWD from trajectory T_1 to T_2 is calculated by

$$D_{owd}(T_1, T_2) = \frac{1}{|T_1|} \left(\sum_{s \in LS(T_1)} (D_{owd}(s, T_2) \cdot |s|) \right) \quad (5.10)$$

where $|s|$ indicates the length of line segment s .

Table 5.1 Similarity evaluations of the predicted trajectories and ground truth of the LSTM, MM, wMM and G-HMM models.

Models	LCSS	OWD	DTW
LSTM	0.9655	1.6751	9.7975
G-HMM	0.9310	35.1089	26.3007
wMM	0.9310	77.7938	29.7464
MM	0.8966	169.139	91.1349

LCSS, OWD and DTW have the following features:

- LCSS is suitable for string similarity. It is 1-to-(1 or null) mapping and insensitive to noise, but need to define threshold. Two locations are regarded as equal if they are close (compared to the threshold), which may return dissimilar trajectories. Both LCSS and EDR need to set absolute threshold, which ranges between 0 and 1. Mismatched points in LCSS will be ignored, while they act as penalty in EDR. Two locations are regarded as equal if they are close according to the threshold. The grouped trajectories in Markov Models may lead to unstable performance under LCSS and EDR indicators. Under certain threshold, the performance of wMM seems to be numerically worse than MM under the EDR indicator. While MM is failed to exceed the performance of MM in some cases. In addition, LCSS and EDR are all count-based methods with similar features;
- OWD calculates distance from points Tra_1 and Tra_2 . One trajectory is considered as piece-wise line segment, while the other as discrete samples;
- DTW is suitable for time series distance measure. It is time independent and may be 1-to-many mapping (ignore sampling rates), but sensitive to noise. The weighted Markov Model assigns large weights for the key states, which makes it perform better than MM under the DTW indicator.

The LSTM network is built based on Keras [144]. Neurons of the first and second LSTM layers are assigned with 20 and 10, respectively. Rectified linear unit (ReLU) acts as the activation function. Mean absolute error (MAE) and Adam were selected as the loss function and optimizer, respectively, when compiling the model. Our model is trained with 200 epochs. 4-D position (time stamp, geographical location) acts as the input of LSTM network. While displacement is also added as the input for G-HMM model. We choose speed, heading and accelerate as the hidden states to train G-HMM with the maximum iterations of 100. Each state uses an unrestricted covariance matrix.

Performances of Markov Models are limited by probability selection, which may cause inaccurate estimation of stochastic process. Training process of G-HMM is influenced by the number of hidden states. More states will lead to complex and ineffective model. The initial Gaussian probability also affects a lot to the precision of prediction. Though LCSS is insensitive to noise, it is not easy to define the threshold. The absolute threshold of LCSS is set to be 0.2 experimentally.

Similarity measured by LCSS is normalized to a number between 0 and 1. It is noted that the higher the LCSS value, the more matched point pairs, which indicates the higher similarity. While OWD and DTW record the distance of points, which mean higher similarity with lower value. We can learn from the Fig. 5.7 and Table 5.1 that our LSTM-based 4-DTP model outperforms the comparison models with high accuracy and efficiency.

5.5.3 Path Planning

Path planning for an aircraft is a complex task, which requires to model the known and unknown environment. The one-step predicted state of the aircraft by the stacked LSTM network model acts as the target node of our proposed cubic A* search algorithm, while the current state is used as the start node. Both the start and target nodes are transformed into the expressions in DEM model, i.e., the geographical coordinates are mapped to integer grids. The RoC of the aircraft typed with A320 is considered to divide the vertical plane. The grids are assigned with altitude to become adjacent cubes, thereby dividing the airspace into multiple levels. We set the height of each cube to be the maximum altitude that the aircraft climbs in one second.

The intended path needs to be well planned to avoid dangers. As pointed out in Section 5.3, the intention of an aircraft is limited by physical dynamics, not all of the cubes need to be traversed. Though the number of nodes is multiplied in 3-D geographic space, the amount of calculation is smaller than that of 2-D scene. The projection of the optimal path on the 762-meter-high horizontal plane is shown in Fig. 5.8. Circles with white and magenta colours represent the start and end nodes, respectively, while the cyan line stands for the projected path. The start node is the real-time measurement of the aircraft that collected by ground station. End node is predicted by our 4-DTP model based on the current states. Though A* search algorithm behaves well in path planning of gridded space, it is limited to 2-D scene.

In our case, simple A* search algorithm needs to be performed at each possible height level, which will generate multiple different paths. It is time-consuming and confusing for the operator to make decisions. Our cubic A* search algorithm shows great advantage on trajectory planning under constraints. Taking RoC of the aircraft

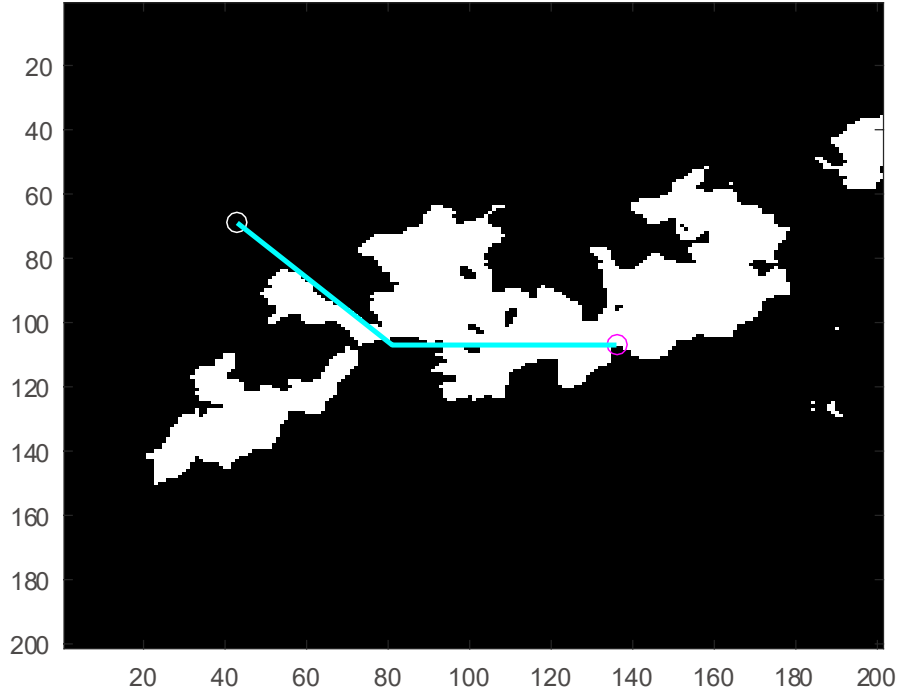


Fig. 5.8 Projection of the optimal path on the 762-meter-high horizontal plane.

into consideration, our model avoids the unnecessary grids, which speeds up the calculation. The planned path is illustrated in Fig .5.9. Before recording the track point at the next time stamp, we can plan the optimal path with a minimum distance of 575.4395m between aircraft and the mountain, which is larger than the safe distance. Time interval for algorithm operation is recorded to be 0.552557 seconds, which is timely enough for an aircraft to take actions.

5.5.4 Threat Assessment

Information entropy is a measurement of disorder or uncertainty in a dataset, which can be expressed as the negative logarithm of probability mass function for each possible data value.

$$S = - \sum_i P_i \log P_i \quad (5.11)$$

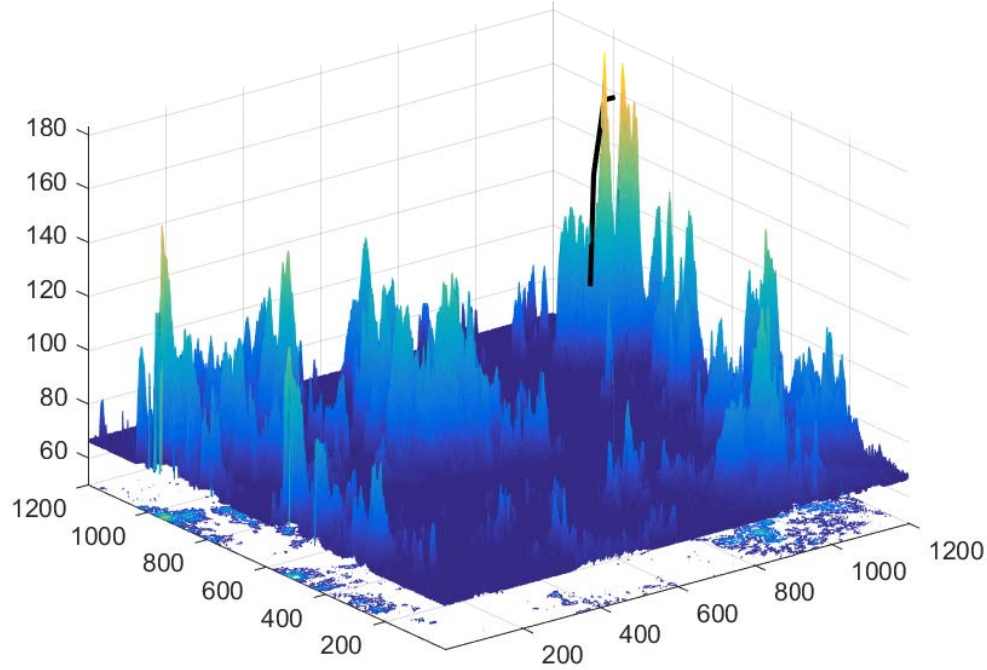


Fig. 5.9 Optimal path planned by cubic A* search algorithm.

where P_i stands for the probability of each data value.

A low-probability value of the data source indicates that it carried more information. The rigor of entropy guarantees its reliability, which makes it able to eliminate the influence of subjective factors.

Static threat caused by the mountain is calculated corresponding to the optimal path. Membership matrix of threat factors $\mathbf{M} = (m_{ij})_{m \times n}$ can be constructed according to section 5.4, where i counts the calculated time stamps, j marks the factors of threat. Weights of the threat factors can be assigned based on the entropy theory. It can be generalized as following steps:

- \mathbf{M} needs to be normalized as $\mathbf{N} = (n_{ij})_{m \times n}$, where $n_{ij} = m_{ij} / \sum_{i=1}^m m_{ij}$, the entropy [160][161] of j th factor is in the form of $e_j = -\frac{1}{\ln m} \sum_{i=1}^m n_{ij} \ln n_{ij}$.

- Then the weights corresponding to each threat factor is calculated by $w_j = \frac{1-e_j}{\sum_{k=1}^n (1-e_k)}$.

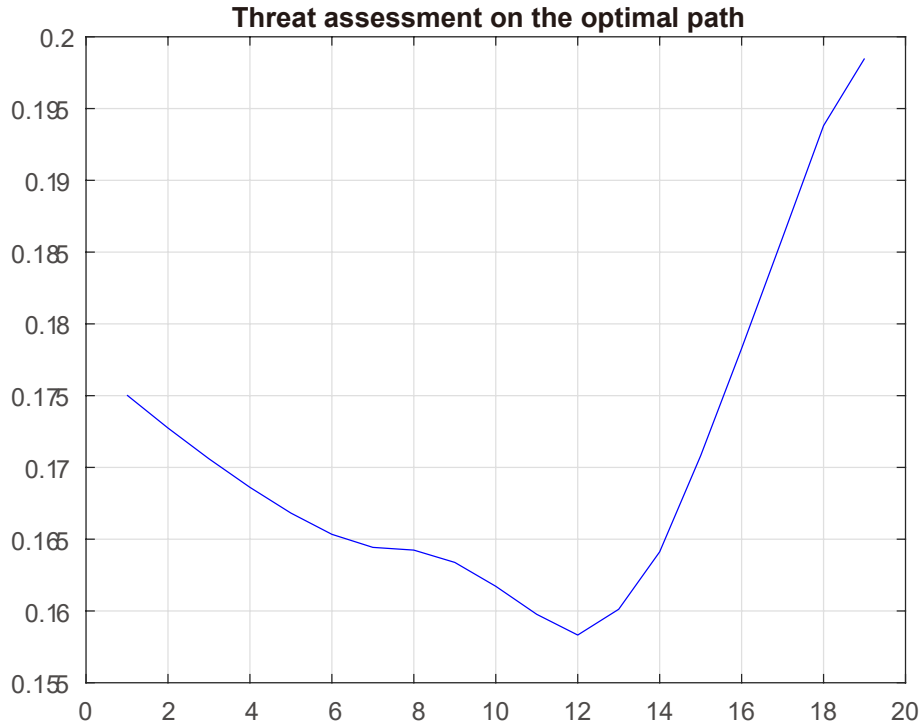


Fig. 5.10 Threat assessment on the optimal path.

We evaluate our planned path by calculating the threats caused by the mountains. Weights of the three proposed threat factors are $w = [0.8449, 0.1361, 0.0191]$. It can be learned from the weight matrix that speed of aircraft is the most important factor in raising threats. Special geographical and discretized airspace weaken the influence of track angle. The weights of altitude and track angle will decrease to zero once the aircraft flies over the mountain. Threats caused by the mountain on the planned path of the aircraft are expressed in the form of weighted linear combinations of the three threat factors. Fig. 5.10 shows the threat assessment on the whole planned path, in which the maximum value is significantly decreased to 0.1985. The rising part in this figure indicates that the aircraft flies along the planned path, but is close to the peak of mountain. When the aircraft follows the guidance of planned path and arrives at the predicted point, the threat of the mountain will be zero as its altitude is higher than

the altitude of mountain. Since the objective of our research is a time series threat caused by static obstacle to single target, our auxiliary decision system outputs the numeric value of threat degree sequentially and displays potential threats prominently.

5.6 Summary

Firstly, the stacked LSTM network was applied to 4-D flight trajectory prediction in climbing phase. Compared with Markov Model, weighted Markov Model and Gaussian Hidden Markov Model, our stacked LSTM network performed well with high accuracy and efficiency. Then, the predicted state of aircraft was used in path planning in 3-D geographical space. Cubic A* search algorithm simplified the complexity by introducing the physical limitation of the aircraft. Finally, potential threats corresponding to the optimal planned path were assessed sequentially.

Chapter 6

Auxiliary Decision Support System and Its Case Studies

6.1 Overview

Over the past few years, with the increasing growth of traffic data in both volumes and types, transportation management and control become data driven and requests significant increasing computing resources. As one important means of modern traffic, civil aviation enjoys a rapid development both in scale and technology. Up to the year 2014, the total number of global civil flights was about 36.5 million, with an average of about 100,000 per day, and has a sustained growth trend. From the year 2014 to 2016, there were 51 wind shear accidents caused by atmospheric fluctuations, which accounted to 19 percent of the total number of accidents. According to the safety report of ICAO [1], accidents in 2018 increased by 11 percent in the total number of accidents compared with 2017, which resulted in a significant increase of fatalities. Though it leads to a convenient and fast trip all around the world, civil aviation brings a huge burden to the current ATM systems.

Situation display is an important branch of visualization. In ATM, this concept was proposed along with the development of collision avoidance systems, regional early warning equipment and data links. The Traffic Situation Display (TSD) was designed by NASA to provide a primary graphical interface for ground operators, which

integrated weather, terrain and special use airspace. It can receive flight plans and flight information that generated by Enhanced Traffic Management System (ETMS, produced by Federal Aviation Administration) to provide assistance. Eurocat-X system displays different symbols through different states of the flight transponder to help operators distinguish flight states. It mainly provides alarms, flight plan conflict detection, traffic flow prediction, terminal arranging and other functions.

Data visualization can help people understand the meaning of information faster. The multidimensional data increases the complexity of visualization. The more dimensions of the data need to be encoded, the more visual attributes we need to use. Colors and icons are carefully selected according to the clients. In ATM, data may appear in multiple types with large amount in the wide detection area. We need to look insight the hidden value, relationship and structure of the dataset. Sequential, dimensional, discrete and dependence features are mined before visualization.

In this chapter, we map information such as numerical values and text descriptions to GIS. According to the dependence relationship with time, we visualize knowledge into static and dynamic expressions. With the foundation of ArcEngine, we design and develop a auxiliary decision support system for air traffic management. Two practical cases are analysed on our system. Firstly, the 3-D path planning for a climbing aircraft in Hong Kong International Airport (HKG) is tested and verified. Secondly, a rerouting path planning for aircraft to avoid bush-fire around Sydney Kingsford Smith Airport (SYD) is visualized in our system. Both these results can provide auxiliary decision support for ATC controllers.

We schedule this chapter as follows: Data base of the basic data is built firstly and knowledge visualization is presented in Section 6.2. Section 6.3 explains the construction of our auxiliary decision support system. Case studies in HKG and SYD are shown in Section 6.4 to prove the effectiveness and practicality of our system. Section 6.5 sums up this chapter.

6.2 Visualization of Knowledge

Data/knowledge is of importance in model training and decision making. However, data can be existed and represented in various modal. We extracted data into knowledge and visualized it in a GIS system.

The basic data is divided into static and dynamic categories according to its dependence on time. Static data keeps attributes unchanged over time, such as basic map/terrain data, fixed way-points, fixed airways, no-fly/special action zones, flight plans, aircraft types, engine types, regulations and to name but a few. Dynamic data in this research refers to measurements that change in geographic location over time, including ADS-B records, ATC measurements, traffic flow, weather, etc.

Generally, the basic information is expressed in plain text. While some are coded, such as the weather conditions of airports in flight plans. We take the METAR code of Sydney Airport as example, "*YSSY 070000Z 09015KT 4000 +SHRA FEW012 BKN022 BKN028 20/19 Q1021*". This code is decoded in detail as follows. We need to parse and map those complex encoded data into reasonable visual symbols that can be described mathematically.

- YSSY, the airport code in ICAO for Sydney Airport,
- 070000Z, report time: 00:00, February 07, 2020,
 - 07, days,
 - 00, hours,
 - 00, minutes,
 - Z, Zulu time (Coordinated Universal Time).
- 09015KT, wind with direction of 90 degrees at speed of 15 knots,
- 4000, visibility in meters,
- +SHRA, rain showers at heavy intensity,
- FEW012, cloud cover and heights, cloud base at 360 m,

- BKN030 BKN040, broken cloud layer at 3000 and 4000 ft above ground level,
- 20/19, temperature/dew point in Celsius,
- Q1021, current altimeter setting with 1021 hPa.

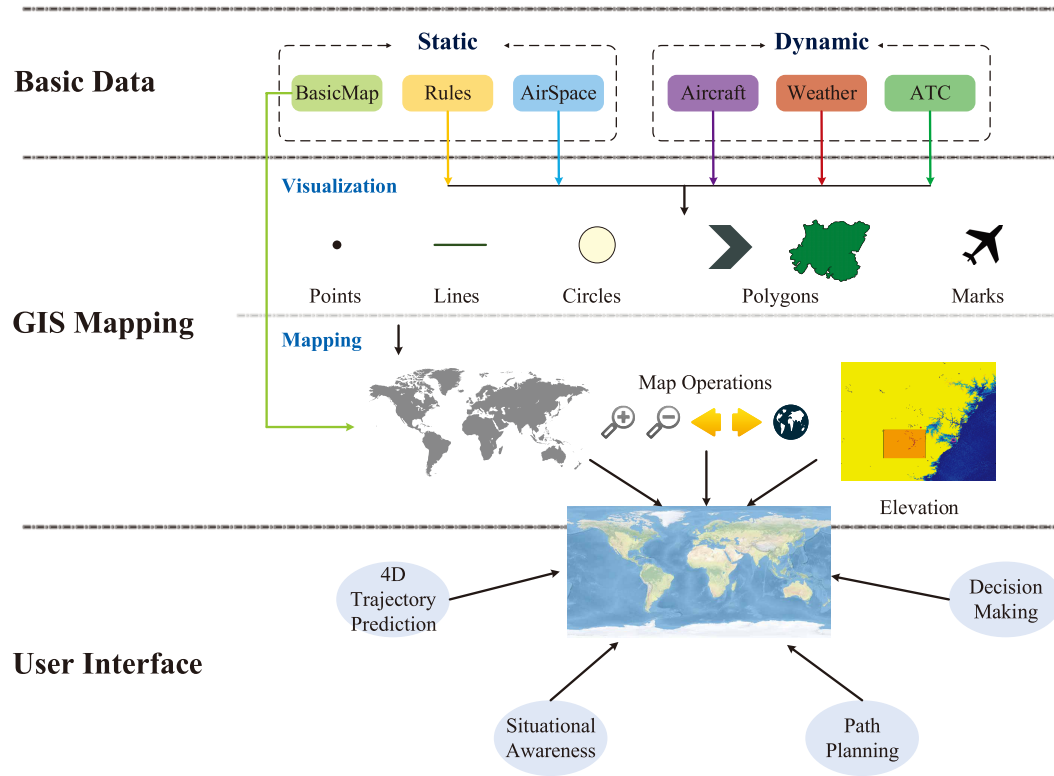


Fig. 6.1 Data visualization process.

As we can sense and see in the real world, the topographic information of the base map is mainly composed of longitude and latitude grids, oceans, lakes, rivers, continents, national/province/state boundaries, vegetation, transportation networks and residential areas. Graphics in the base map contain geographic data and elements, both of which are characterized with Geometry attributes. The higher the accuracy of base map, the richer the elements will be displayed. We design our system to load low-precise map in initialization to reduce resource consumption. It will be sufficient for ATM, which is with large spatial spans. When emergency or bad weather occur in certain airspace, we provide a high-precise map to zoom to monitor the situation. Static data is visualized by points, lines, circles, polygons and marks as shown in Fig.

6.1. These visual features are transformed by geographic coordinates and mapped onto the base map. Operations, such as zoom in/out, pan, load, delete are also developed in our system. Since our system currently provides and supports two-dimensional (2-D) display and operations, when three-dimensional (3-D) scenes need to be considered, we introduce elevation information for assistance.

The spatial span of monitoring area determines the amount of static data. We first build a geographical database (GeoDatabase/GDB), which is the key of GIS. GeoDatabase organizes spatial data based on hierarchical data objects, which include object class, feature class and feature dataset. We design our system to load the static data only once when initializing. Data is mapped and stored as an SHP file. It is time-saving and effective to load SHP file directly and can greatly reduce occupation of computing resource. Once any changes (add/delete) occur in the static database, our system will automatically load the new database and create new SHP files.

Dynamic data will be delivered to our system according to the period of data collection. Flight trajectory and weather information will be displayed on the user interface and update over time. Functions such as real-time display, attribute query and replay can be achieved by dynamic layer. The dynamic layer based on ArcEngine component library is a user-defined layer and inherits three interfaces of ILayer, IDynamiclayer and IGeoDataset. These three interfaces consist of seven sub-interfaces:

- IDynamicMap: Controlling dynamic display,
- IDynamicLayer: Dynamic drawing,
- IDynamicScreenDisplay: Controlling dynamic display,
- IDynamicGlyph: Managing display resources,
- IDynamicGlyphFactory: Managing dynamic symbols,
- IDynamicSymbolProperties: Managing symbol attribute information,
- IDynamicDisplay: Collaboratively applied with IDynamicSymbolProperties.

The dynamic layer performs according to fixed clock step and displays the airspace information in real time and dynamically.

Fig. 6.1 vividly illustrates the visualization process of multi-modal data. The process can be defined as three parts, i.e., Basic data, GIS mapping and User interface. Data is expressed in different layers (static SHP and dynamic layer), users can perform various functional models and check the results in a visualized way, which can greatly improve the efficiency.

6.3 Development of Auxiliary Decision Support System

We design our auxiliary decision system (ADSS) based on the secondary development of ArcGIS platform with .Net framework. As described in Section 6.2, AcrEngine provides us with the foundation of map operations. The primary function is to visually display data in the geographical environment. This ADSS is structured into five main functions, including data processing function, layer management function, 2-D terrain display function, feature inquiry function and user-defined function, as illustrated in Fig. 6.2. These functions are designed with the following mechanisms:

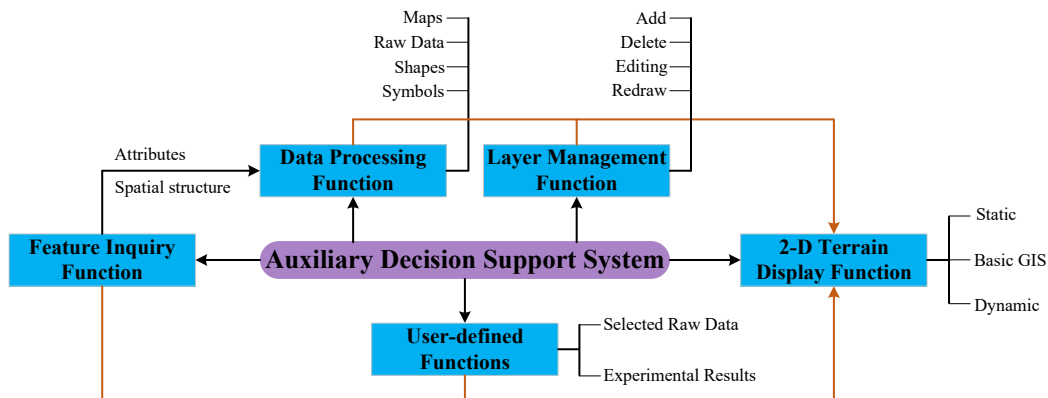


Fig. 6.2 Functions of our auxiliary decision support system.

1. Data Processing Function:

- Searching the database of basic data shown in Fig. 6.1,
- Extracting features of different data to create DBF files,

- Visualizing the static information including way-points, airports, airways, and mountains,
- Embedding the symbols and geographical features into SHP file.

2. Layer Management Function:

- Add/delete certain layers, which include both static and dynamic layers,
- Editing visualization symbols of layers,
- Redrawing layers.

3. 2-D Terrain Display Function:

- Primarily display the base map,
- Selectively display static layers according to application requirements,
- Dynamic flight trajectories are drawn with Dynamiclayer.

4. Feature Inquiry Function:

- Inquiry on the properties of visual symbols,
- Inquiry on the spatial features.

5. User-Defined Function:

- 4-D trajectory prediction model,
- Path planning model,
- Threat assessment model,
- Comparison between raw data and experimental results.

Our ADSS is able to display massive data simultaneously in a large scale (over 2000 tracks can be displayed and managed at the same time by testing). In the initialization process, we first load a low-precise world map as the base map. It is precise enough for the application of ATM, which can cover a range of 200 nautical miles (370 km). Once encountered with an abnormal or dangerous situation, our system will enlarge the selected region by operators to show the map with higher accuracy. As is shown in Fig. 6.3, both static and dynamic data are projected to the map.

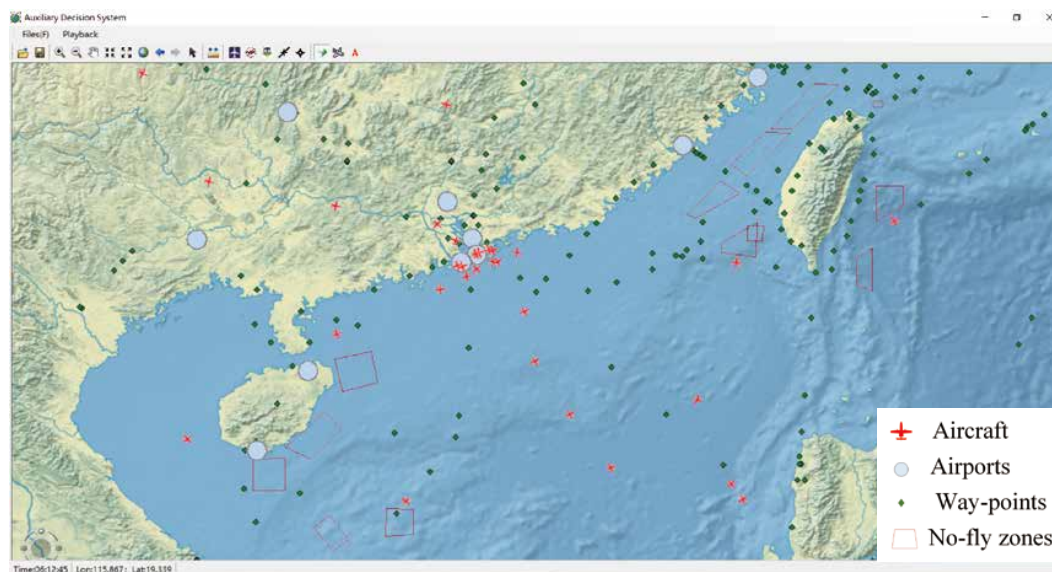


Fig. 6.3 Fundamental functions of our auxiliary decision support system.

We can learn from Fig. 6.3 that, short-cuts of functional tools are arranged on the top of user interface. It can be divided into map operations and layer management. Map operations include (fixed) zoom in/out, pan, measure and certain extent. While layer management include elements selection and add/delete layers. When selecting symbols on the base map, their features will be displayed beside the symbols. Layers in our system consist of static and dynamic layers. The former layers contain airport layer in grey circles, no-fly zones in red polygons, way-points in green dots and airways in blue lines, respectively. While the dynamic layer depicts the real-time trajectory, where the head of tracks are labelled with red plane marks. We have omitted the tails of trajectories to make Fig. 6.3 distinguishable. The base map is refreshed within recompile rate to show how the trajectory changes over time and spatial spans. The lower left corner of our interface shows the system time and geographic locations corresponding to the position of mouse. Left button of mouse is activated to select items and inquire detailed text information, including flight number, departing and landing airports.

Experimental results in Chapters 4 and 5 are displayed on our ADSS. It displays real scene and experimental results to operators to detect anomalies, make decisions and early-warning. We reproduce practical cases our system to test and verify its capability and robustness.

6.4 Case Studies

6.4.1 Case 1: Path Planning in HKG Airport

As discussed in Chapter 5, we considered the potential threat caused by static terrain to take-off flights in the HKG airport. As is shown in Fig. 5.5, HKG is surrounded by mountains and sea, while the mountains will raise potential risks for departing and arriving aircraft as the pilots will burden the responsibility for safe flight under the guidance of ATC centre. Section 1.2.2 has stated the importance of the strategic location of airports and their influences on safe flight. Mountains mainly affect the sight of pilots, situations will be exacerbated and worsened at night or encountered with bad weather and natural disasters.

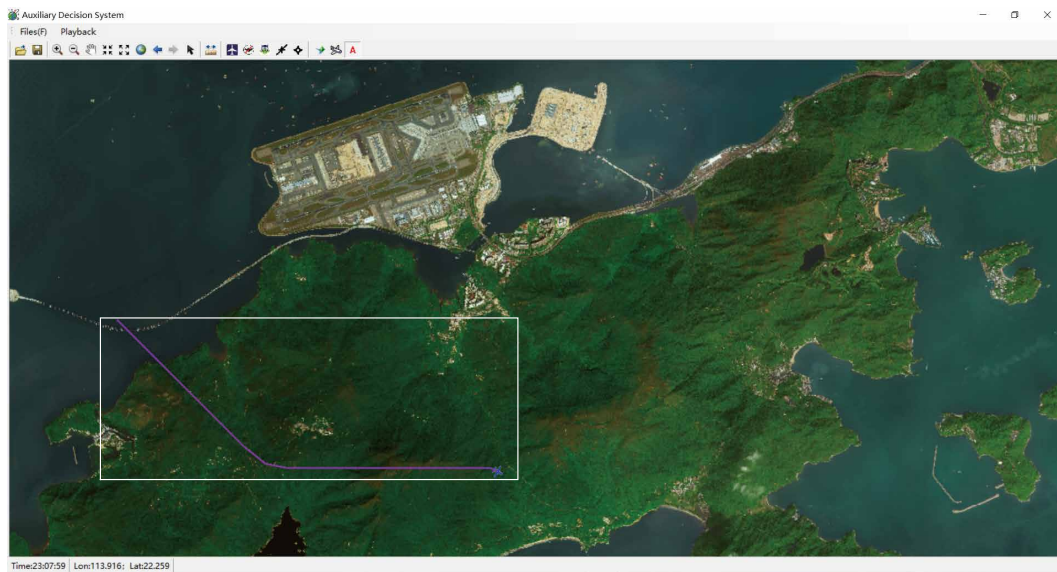


Fig. 6.4 Climbing flight path planning for obstacle avoidance in Hong Kong International Airport.

Fig. 6.3 shows the primary functions of our ADSS in the scope of air traffic monitoring and traffic flow management. When we need to monitor air traffic flow or special circumstances in the airspace around airport, we enlarge the map and load the high-precision airport map to show detailed terrain information. As is shown in Fig. 6.4, we show the HKG runways and mountains near it. In our ADSS, we map airports such as HKG with 17-level precision maps to show the terrains, transportation networks and residential areas. Static layer with elevation can be added manually when the altitude

information is needed. Low-precise world map is loaded in system initialization, we can monitor the scene within detection scope. But it will be blurred when it is partially enlarged to clearly display airports.

Operators should attach great importance to trajectories during climbing and descending phases, which have high accident rate. During these phases, 4-D trajectories are predicted by our pre-tuned 4-DTP model for climbing phase illustrated in Section 5.2, once they are recorded by ground-based equipment. Threat must be assessed if there are aircraft flying towards the mountain. Path planning and threat assessment models in Sections 5.3 and 5.4 are triggered automatically when aircraft fly near the special areas, such as no-fly zones and mountains. Our system will give a warning by partial enlargement as well as change the color of aircraft icons if dangerous appear.

In our experimental scenario, an aircraft happened to deviate from normal trajectories and flew towards the mountain. Our models manage to plan a 3-D path for this aircraft in a very short time. The planned path is evaluated by threat assessment. The result is shown in the white rectangular frame in Fig. 6.4. The blue airplane represents the predicted position in the next record time and purple line indicates the planned path. Our system will raise a warning to the ATC operators, then he will make decisions and take actions accordingly to ensure the safety.

6.4.2 Case 2: Rerouting Suggestion in SYD Airport

Weather and natural disasters have a serious impact on public transportation, which will lead to varying degrees of delays and even congestions of the transportation network. In aviation activities, visibility, crosswinds, clouds, navigational facility failures and traffic management are key important factors especially for the taking-off and landing aircraft.

As is well known, the Australian bush-fire lasted for almost half a year, which has caused a series of subsequent effects. Inevitably, civil aviations were also affected, mainly by frequent changes in temperature and visibility. The high-temperature smoke generated by bush-fire will result in a high-speed air flow field when it diffuses, which will surely cause violent bumps when an aircraft fly through this area. Civil aviation

transportation will be more or less interfered by these natural phenomena. Fig. 6.5 summarizes the flight volume and on-time rates of Sydney Kingsford Smith Airport in the year 2019.

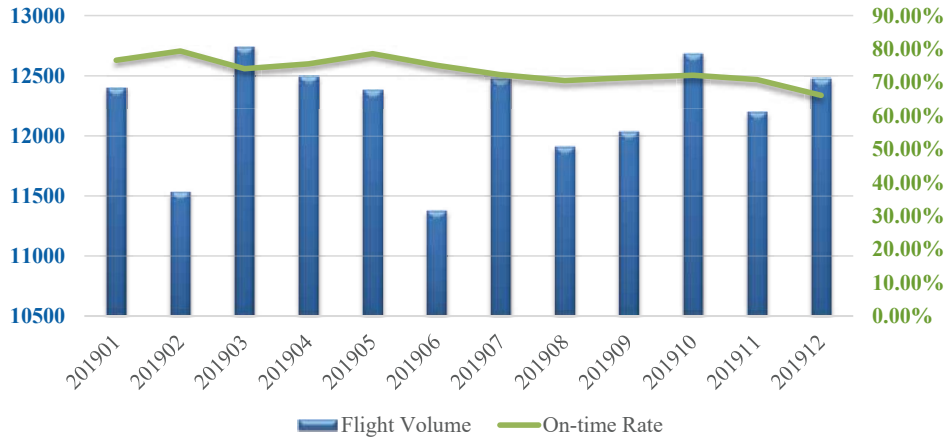


Fig. 6.5 Flight volume and on-time rate of Sydney Kingsford Smith Airport in the year 2019.

Compared with cumulonimbus clouds, the direction and speed of the spread of bush-fire are not only related to the wind, but more importantly, they are closely related to the geographical distribution of combustible. Therefore, in this case, we build the restricted flight zone according to the geographical location of combustibles. Once the restricted flight zone is established, all the in-flight aircraft at every flight level need to avoid this zone.

Many restricted flight zones are designed with simple polygons, however, the concave polygons leave hidden dangers that the aircraft will fly into the zone. In addition, the fly-by distance will be longer if the aircraft performs in simple polygons, so we set the restricted zone as a convex polygon. As is shown in Fig. 6.6, the rerouting flight path is described in 2-D space. We model the restricted flight zone as a convex polygon. Suppose Eq. (6.1) stands for the sequence of way-points to pass in a flight plan.

$$\mathbf{wp} = \{wp_1, wp_2, \dots, wp_n\} \quad (6.1)$$

Points $\{wp_k, \dots, wp_l\}, k < l < n$ fall into the convex polygon. For ATC controllers, they need to find a temporary alternative point to guide the aircraft from wp_{k-1} to

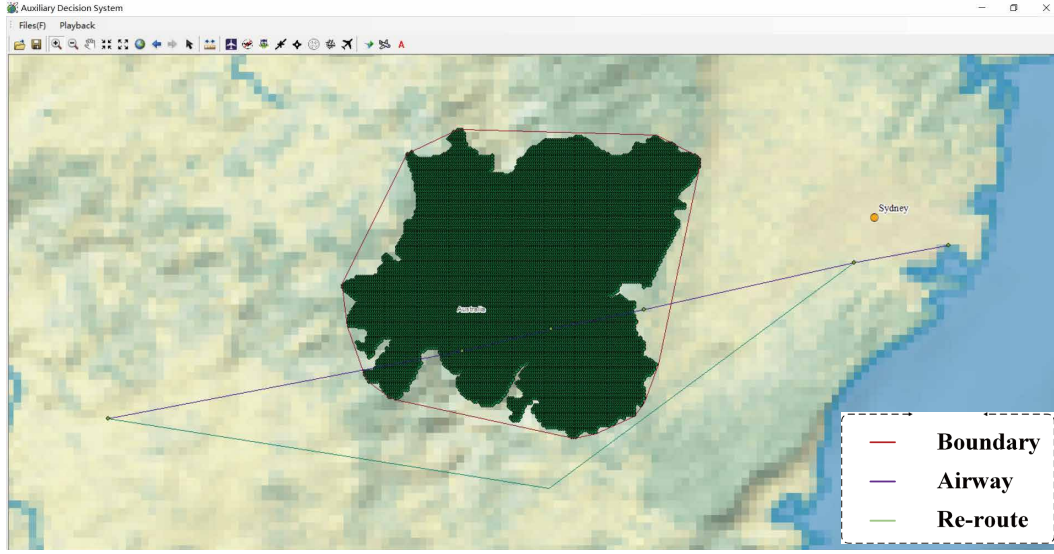


Fig. 6.6 Rerouting suggestion for the departure and landing aircraft around Sydney Kingsford Smith Airport.

wp_{l+1} . We manage to provide a rerouting point r with the consideration of less voyage and less number of turning points [162].

There are many factors to evaluate the effectiveness and availability of the rerouting path. Generally, they can be concluded in four aspects, i.e., effective avoidance, turning angle, rerouting voyage and number of rerouting points. Firstly, the rerouting path does not cross the restricted zone. Secondly, it meets the requirement of restrictions on the amount of turn and flight segment (6.2).

$$\begin{cases} \angle (wp_{k-1}, r, wp_{l+1}) > 90^\circ \\ d(wp_{k-1}, r) > d_{norm} \\ d(r, wp_{l+1}) > d_{norm} \end{cases} \quad (6.2)$$

where, $d(a, b)$ stands for the Euclidean distance of points a and b . d_{norm} is a constant, which is usually assigned with the width of airway. The recommended rerouting point is represented by d . Suppose an aircraft will or scheduled to fly along the airway (labelled purple in Fig. 6.6), if there exists a bush-fire, the ATC controllers can make a rerouting path (labelled green in Fig. 6.6) for pilots in advance. In this case, we happen to get one rerouting point due to the sparse distributed way-points. While in

other cases, if we get several points, we need to merge some of them under certain rules to guarantee fewer rerouting points.

6.5 Summary

An auxiliary decision support system based on ArcGIS 10.0 for 4-D trajectory management was presented in this chapter. We aim to provide auxiliary decisions or options for the operators in ATM systems. Geometry symbols were applied to visualize the knowledge to make it concise and editable. Static geographic elements and dynamic flight trajectories were simultaneously mapped to the GIS system to provide auxiliary information.

The primary function of our system is to display flight trajectories in real-time. 4-D trajectory prediction function always performs during the climbing and descending phases. Path planning and threat assessment functions will be triggered when aircraft performing tasks within a special geographical environment. Once encountered with an abnormal or dangerous situation, our system will spontaneously send a warning and provide a planned path for the operator, thereby offers auxiliary decision support. For some natural disasters, which have continuously serious influence on the safe aviation activities. We provide the rerouting function before taking off and landing if dangers appear along the predicted trajectory or scheduled flight plans. Information is visualized in our system, which reduces the time required for data analysis thus shortens the steps to make decisions.

Chapter 7

Conclusions and Future Work

7.1 Conclusions

We conclude our works in this section.

Chapter 4 proposes a LSTM network based 4-D flight trajectory predictor, which is embedded with physical constraints in corresponding flight phases. In addition to the historical training dataset, the geographical environment and the dynamic performance of the aircraft also have important consequences on the model accuracy. The proposed constraints limit the predicted flight trajectory in both distance and angle. Different combinations of constraint items optimize the LSTM network at different flight phases. Our model outperforms most models/variants of BADA, practical systems and conventional methods, which lays a solid foundation for air traffic management.

Chapter 5 evaluates the geographical situation of specific airport for a taking-off aircraft, which is located near the mountains and sea. Terrains including mountains and seas are modelled by DEM, while the airspace is divided into adjacent cubes according to the dynamic performance of aircraft (type A320, BADA family 3). When terrains raise certain threats to departure aircraft, 4DTP model provides a precise one-step predicted location of the aircraft. Then cubic A* search algorithm will plan an optimal path for the aircraft heading to the mountain in a very short time. We also assess the planned path to provide auxiliary information to operators to make decisions.

Chapter 6 constructs a GIS-based decision support system, which visualizes the knowledge and provides key information for ATC controllers to make decisions. Based on ArcEngine, static terrains, oceans, and airspace and dynamic trajectories are modelled and mapped as visual elements to provide intuitively data understanding and analysis. Two practical cases are studied and tested on this system, which shows how the natural environment applies its influence on civil aviation.

7.2 Future work

Interesting directions for future work are presented in the following.

- In Chapter 4, Airports appear to be the busiest and most important part in aviation activities. Attitude in climbing and descending/approaching phases are forecast step by step to provide a precise prediction in current work. In the cruising phase, our proposed model can predict 10 steps ahead with good accuracy. While the state-of-the-arts algorithms suffer divergent predictions once aircraft manoeuvring non-linearly (sharp turning). In our future work, we will embed intersected airways, the regulations/guidance of ATM and weather conditions to provide accurate long-term arrival reminder. Different scenarios also need to be well-defined and considered in aviation activities, such as severe deviation from airways and emergency landing. We can predict trajectories that exactly follow the airway precisely, and errors will increase within acceptable scope when handling with severe deviations with the same values for weights in the loss function. This error will be reduced when adjusting the length of output. In future, the framework will be improved to be robust for unexpected situations. Meteorological factors, geographical features and BADA variants will be considered in our next work. Also, some new evaluation indicators could be introduced in the future.
- In Chapter 5, the aircraft is still under the guidance/control of the airport's control tower in the experimental scenario. The role of pilot is weakened in this short scene. Human factors need to be modelled in the following work to analyse the behaviours of aircraft. Reactions of pilots can be different when encountering

emergencies, such as bad weathers, traffic jams in cross routes or aircraft failures, which may raise potential risks for aviation activities. Inspired by the work in [163], we will consider the reactions of pilots for long-term trajectory management, especially for the unexpected situations.

- In Chapter 6, our system is tested on some practical cases. However, it is a 2-D display platform, when dealing with 3-D scenes, we need to load the elevation map to provide the altitude information, which will pull down the efficiency and increase the consumption of computer sources. The visual symbols also need to be well-designed and arranged to express the information comprehensively. For the weather conditions and natural disasters, the spatial and temporal characteristics need to be considered simultaneously to ensure the timeliness of the user functions. More functions will be embedded in our system, including compatibility of multi-modal data and more application scenarios.

References

- [1] UN Specialized Agency, “Administration and governance of the Convention on International Civil Aviation (Chicago Convention), <https://www.icao.int>,” 1994.
- [2] C. Montreal, “The trade association for the world’s airlines,” [Online]. Available: <https://www.iata.org>, 1945.
- [3] I. A. T. Association, “Annual Review 2019.” Website, 2019. <https://www.iata.org/publications/Documents/iata-annual-review-2019.pdf>.
- [4] VariFlight, “World’s airport and on-time report 2019.” Website, 2019. <http://www.variflight.com/>.
- [5] F. S. Foundation, “Aviation safety.” Website, January, 1996. <https://aviation-safety.net/>.
- [6] T. A. Lewis, A. S. Aweiss, N. M. Guerreiro, and R. J. Daiker, “A review of function allocation and En Route separation assurance,” 2016.
- [7] D. ICAO, “Draft 2016-2030 Global Air Navigation Plan,” tech. rep., Doc 9750-AN/963, Fifth Edition, 2016., Montreal, Canada.
- [8] Z. Jiang, “A survey on spatial prediction methods,” *IEEE Transactions on Knowledge and Data Engineering*, vol. 31, no. 9, pp. 1645–1664, 2018.
- [9] Q. Lv, Y. Qiao, N. Ansari, J. Liu, and J. Yang, “Big data driven hidden Markov model based individual mobility prediction at points of interest,” *IEEE Transactions on Vehicular Technology*, vol. 66, no. 6, pp. 5204–5216, 2016.
- [10] C. Johnson, A. Rusu, A. Breitzman, J. Bucknam, and N. Laposta, “Phase of flight and rule of flight calculator,” in *7th International Conference on Research in Air Transportation, ICRAT*, 2016.
- [11] S. Aditya, A. F. Molisch, and H. M. Behairy, “A survey on the impact of multipath on wideband time-of-arrival based localization,” *Proceedings of the IEEE*, vol. 106, no. 7, pp. 1183–1203, 2018.
- [12] Airservices, “How ADS-B works,” *Australia*, Nov. 2012.
- [13] R. Alligier and D. Gianazza, “Learning aircraft operational factors to improve aircraft climb prediction: A large scale multi-airport study,” *Transportation Research Part C: Emerging Technologies*, vol. 96, pp. 72–95, 2018.

- [14] M. Aguiar, A. Stolzer, and D. D. Boyd, “Rates and causes of accidents for general aviation aircraft operating in a mountainous and high elevation terrain environment,” *Accident Analysis & Prevention*, vol. 107, pp. 195–201, 2017.
- [15] M. Ayres Jr, H. Shirazi, R. Carvalho, J. Hall, R. Speir, E. Arambula, R. David, J. Gadzinski, R. Caves, D. Wong, *et al.*, “Modelling the location and consequences of aircraft accidents,” *Safety Science*, vol. 51, no. 1, pp. 178–186, 2013.
- [16] E. E. Center, “User manual for the Base of Aircraft Data (BADA), Revision 3.6,” *EEC Note*, no. 10/04, 2011.
- [17] D. Washington, “Federal Aviation Administration NextGen implementation plan,” [Online]. Available: <https://www.faa.gov/nextgen/>, 1990.
- [18] E. European Union, “European ATM master plan,” [Online]. Available: <https://www.sesarju.eu/>, 2007.
- [19] T. Yong, W. Honggang, X. Zhili, and H. Zhongtao, “ADS-B and SSR data fusion and application,” in *2012 IEEE International Conference on Computer Science and Automation Engineering (CSAE)*, vol. 2, pp. 255–258, IEEE, 2012.
- [20] J. A. Besada, J. Garcia, G. De Miguel, F. Jimenez, G. Gavin, and J. Casar, “Data fusion algorithms based on radar and ADS measurements for ATC application,” in *Record of the IEEE 2000 International Radar Conference [Cat. No. 00CH37037]*, pp. 98–103, IEEE, 2000.
- [21] D. Jeon, Y. Eun, and H. Kim, “Estimation fusion with radar and ADS-B for air traffic surveillance,” *International Journal of Control, Automation and Systems*, vol. 13, no. 2, pp. 336–345, 2015.
- [22] J. Roskam, *Airplane flight dynamics and automatic flight controls*. DARcorporation, 1998.
- [23] J. C. Cheung, “Flight planning: node-based trajectory prediction and turbulence avoidance,” *Meteorological Applications*, vol. 25, no. 1, pp. 78–85, 2018.
- [24] N. Takeichi, “Adaptive prediction of flight time uncertainty for ground-based 4D trajectory management,” *Transportation Research Part C: Emerging Technologies*, vol. 95, pp. 335–345, 2018.
- [25] V. Courchelle, M. Soler, D. González-Arribas, and D. Delahaye, “A simulated annealing approach to 3D strategic aircraft deconfliction based on En-Route speed changes under wind and temperature uncertainties,” *Transportation Research Part C: Emerging Technologies*, vol. 103, pp. 194–210, 2019.
- [26] A. Nuic, “User manual for the Base of Aircraft Data (BADA)–Revision 3.10, EUROCONTROL, EEC Technical,” tech. rep., Scientific Report, 2012.
- [27] A. Harada, N. Takeichi, and K. Oka, “An optimal trajectory-based trajectory prediction method for automated traffic flow management,” in *AIAA Scitech 2019 Forum*, p. 1360, 2019.

- [28] Y. Liu and X. R. Li, "Intent based trajectory prediction by multiple model prediction and smoothing," in *AIAA Guidance, Navigation, and Control Conference*, p. 1324, 2015.
- [29] Japan, "Japan meteorological business support center online data service, <http://www.jmbsec.or.jp/>," 2018.
- [30] B. Musialek, C. F. Munafo, H. Ryan, and M. Paglione, "Literature survey of trajectory predictor technology," *Federal Aviation Administration, William J. Hughes Technical Center, Tech. Rep*, 2010.
- [31] E. Gallo, J. Lopez-Leones, M. A. Vilaplana, F. A. Navarro, and A. Nuic, "Trajectory computation infrastructure based on BADA aircraft performance model," in *2007 IEEE/AIAA 26th Digital Avionics Systems Conference*, pp. 1–C, IEEE, 2007.
- [32] J. Sun, J. Ellerbroek, and J. Hoekstra, "Modeling and inferring aircraft takeoff mass from runway ADS-B data," in *7th International Conference on Research in Air Transportation*, 2016.
- [33] M. Uzun and E. Koyuncu, "Data-driven trajectory uncertainty quantification for climbing aircraft to improve ground-based trajectory prediction," *Anadolu Üniversitesi Bilim Ve Teknoloji Dergisi A-Uygulamalı Bilimler ve Mühendislik*, vol. 18, no. 2, pp. 323–345, 2017.
- [34] D. Boyle and G. Chamitoff, "Robust nonlinear lasso control: a new approach for autonomous trajectory tracking," in *AIAA Guidance, Navigation, and Control Conference and Exhibit*, p. 5518, 2003.
- [35] M. Porretta, M. D. Dupuy, W. Schuster, A. Majumdar, and W. Ochieng, "Performance evaluation of a novel 4D trajectory prediction model for civil aircraft," *Journal of Navigation*, vol. 61, no. 3, pp. 393–420, 2008.
- [36] I. Hwang, J. Hwang, and C. Tomlin, "Flight-mode-based aircraft conflict detection using a residual-mean interacting multiple model algorithm," in *AIAA Guidance, Navigation, and Control Conference and Exhibit*, p. 5340, 2003.
- [37] R. Slattery and Y. Zhao, "Trajectory synthesis for air traffic automation," *Journal of Guidance, Control, and Dynamics*, vol. 20, no. 2, pp. 232–238, 1997.
- [38] L. A. Weitz, "Derivation of a point-mass aircraft model used for fast-time simulation," *MITRE Corporation*, 2015.
- [39] J. Lovera Yepes, I. Hwang, and M. Rotea, "An intent-based trajectory prediction algorithm for air traffic control," in *AIAA Guidance, Navigation, and Control Conference and Exhibit*, p. 5824, 2005.
- [40] X. Tang, P. Chen, and Y. Zhang, "4D trajectory estimation based on nominal flight profile extraction and airway meteorological forecast revision," *Aerospace Science and Technology*, vol. 45, pp. 387–397, 2015.

-
- [41] M. Hrastovec and F. Solina, “Prediction of aircraft performances based on data collected by air traffic control centers,” *Transportation Research Part C: Emerging Technologies*, vol. 73, pp. 167–182, 2016.
- [42] J. Krozel and D. Andrisani, “Intent inference and strategic path prediction,” in *AIAA Guidance, Navigation, and Control Conference and Exhibit*, p. 6450, 2005.
- [43] J. V. Benavides, J. Kaneshige, S. Sharma, R. Panda, and M. Steglinski, “Implementation of a trajectory prediction function for trajectory based operations,” in *AIAA Atmospheric Flight Mechanics Conference*, p. 2198, 2014.
- [44] P. Pradeep and P. Wei, “Predictability, variability and operational feasibility aspect of CDA,” in *Aerospace Conference, 2017 IEEE*, pp. 1–14, IEEE, 2017.
- [45] J. Sun, J. Ellerbroek, and J. Hoekstra, “Modeling aircraft performance parameters with open ADS-B data,” in *Proceedings of the 12th USA/Europe Air Traffic Management Research and Development Seminar*, FAA/EUROCONTROL, 2017.
- [46] M. Elhoushi, J. Georgy, A. Noureldin, and M. J. Korenberg, “A survey on approaches of motion mode recognition using sensors,” *IEEE Transactions on Intelligent Transportation Systems*, vol. 18, no. 7, pp. 1662–1686, 2017.
- [47] T. Radišić, D. Novak, and B. Juričić, “Reduction of air traffic complexity using trajectory-based operations and validation of novel complexity indicators,” *IEEE Transactions on Intelligent Transportation Systems*, vol. 18, no. 11, pp. 3038–3048, 2017.
- [48] C. Ordóñez, F. S. Lasheras, J. Roca-Pardiñas, and F. J. de Cos Juez, “A hybrid ARIMA–SVM model for the study of the remaining useful life of aircraft engines,” *Journal of Computational and Applied Mathematics*, vol. 346, pp. 184–191, 2019.
- [49] S. V. Kumar, “Traffic flow prediction using Kalman filtering technique,” *Procedia Engineering*, vol. 187, pp. 582–587, 2017.
- [50] C. D. Zuluaga, M. A. Alvarez, and E. Giraldo, “Short-term wind speed prediction based on robust Kalman filtering: An experimental comparison,” *Applied Energy*, vol. 156, pp. 321–330, 2015.
- [51] L. Song, D. Kotz, R. Jain, and X. He, “Evaluating location predictors with extensive Wi-Fi mobility data,” in *IEEE INFOCOM*, vol. 2, pp. 1414–1424, IEEE, 2004.
- [52] D. Ashbrook and T. Starner, “Using GPS to learn significant locations and predict movement across multiple users,” *Personal and Ubiquitous Computing*, vol. 7, no. 5, pp. 275–286, 2003.
- [53] S. Ayhan and H. Samet, “Aircraft trajectory prediction made easy with predictive analytics,” in *Proceedings of the 22nd ACM SIGKDD International Conference on Knowledge Discovery and Data Mining*, pp. 21–30, ACM, 2016.

- [54] S. Ayhan and H. Samet, "Time series clustering of weather observations in predicting climb phase of aircraft trajectories," in *Proceedings of the 9th ACM SIGSPATIAL International Workshop on Computational Transportation Science*, pp. 25–30, ACM, 2016.
- [55] S. Ayhan, P. Costas, and H. Samet, "A data-driven framework for long-range aircraft conflict detection and resolution," *ACM Transactions on Spatial Algorithms and Systems (TSAS)*, vol. 5, no. 4, pp. 1–23, 2019.
- [56] X. Feng, X. Ling, H. Zheng, Z. Chen, and Y. Xu, "Adaptive multi-kernel SVM with spatial-temporal correlation for short-term traffic flow prediction," *IEEE Transactions on Intelligent Transportation Systems*, no. 99, pp. 1–13, 2018.
- [57] I. Goodfellow, Y. Bengio, A. Courville, and Y. Bengio, *Deep learning*, vol. 1. MIT press Cambridge, 2016.
- [58] T. Fernando, S. Denman, S. Sridharan, and C. Fookes, "Soft+ hardwired attention: An LSTM framework for human trajectory prediction and abnormal event detection," *Neural Networks*, vol. 108, pp. 466–478, 2018.
- [59] Z. Zhao, W. Chen, X. Wu, P. C. Chen, and J. Liu, "LSTM network: a deep learning approach for short-term traffic forecast," *IET Intelligent Transport Systems*, vol. 11, no. 2, pp. 68–75, 2017.
- [60] P. Lingras, S. Sharma, and M. Zhong, "Prediction of recreational travel using genetically designed regression and time-delay neural network models," *Transportation Research Record: Journal of the Transportation Research Board*, no. 1805, pp. 16–24, 2002.
- [61] Y. Kim, Y. Jernite, D. Sontag, and A. M. Rush, "Character-aware neural language models," in *AAAI*, pp. 2741–2749, 2016.
- [62] A. Graves and N. Jaitly, "Towards end-to-end speech recognition with recurrent neural networks," in *International Conference on Machine Learning*, pp. 1764–1772, 2014.
- [63] I. Sutskever, O. Vinyals, and Q. V. Le, "Sequence to sequence learning with neural networks," in *Advances in Neural Information Processing Systems*, pp. 3104–3112, 2014.
- [64] J. Donahue, L. Anne Hendricks, S. Guadarrama, M. Rohrbach, S. Venugopalan, K. Saenko, and T. Darrell, "Long-term recurrent convolutional networks for visual recognition and description," in *Proceedings of the IEEE conference on Computer Vision and Pattern Recognition*, pp. 2625–2634, 2015.
- [65] Y. Tian, K. Zhang, J. Li, X. Lin, and B. Yang, "LSTM-based traffic flow prediction with missing data," *Neurocomputing*, vol. 318, pp. 297–305, 2018.
- [66] Q. Liu, S. Wu, L. Wang, and T. Tan, "Predicting the next location: A recurrent model with spatial and temporal contexts," in *AAAI*, pp. 194–200, 2016.

- [67] Y. Bengio, P. Frasconi, and P. Simard, "The problem of learning long-term dependencies in recurrent networks," in *Neural Networks, 1993., IEEE International Conference on*, pp. 1183–1188, IEEE, 1993.
- [68] D. H. Douglas, "Least-cost path in GIS using an accumulated cost surface and slopelines," *Cartographica: the International Journal for Geographic Information and Geovisualization*, vol. 31, no. 3, pp. 37–51, 1994.
- [69] A. Y. Chang, M. E. Parrales, J. Jimenez, M. E. Sobieszczyk, S. M. Hammer, D. J. Copenhagen, and R. P. Kulkarni, "Combining Google Earth and GIS mapping technologies in a dengue surveillance system for developing countries," *International Journal of Health Geographics*, vol. 8, no. 1, p. 49, 2009.
- [70] P. B. Keenan and P. Jankowski, "Spatial decision support systems: Three decades on," *Decision Support Systems*, vol. 116, pp. 64–76, 2019.
- [71] S. Ruiz, M. A. Piera, and I. Del Pozo, "A medium term conflict detection and resolution system for terminal maneuvering area based on spatial data structures and 4D trajectories," *Transportation Research Part C: Emerging Technologies*, vol. 26, pp. 396–417, 2013.
- [72] X. Qian, J. Mao, C.-H. Chen, S. Chen, and C. Yang, "Coordinated multi-aircraft 4D trajectories planning considering buffer safety distance and fuel consumption optimization via pure-strategy game," *Transportation Research Part C: Emerging Technologies*, vol. 81, pp. 18–35, 2017.
- [73] B. Yan, P. Shi, C.-C. Lim, C. Wu, and Z. Shi, "Optimally distributed formation control with obstacle avoidance for mixed-order multi-agent systems under switching topologies," *IET Control Theory & Applications*, vol. 12, no. 13, pp. 1853–1863, 2018.
- [74] L. Nilim, Arnab ; El Ghaoui, "Robustness in Markov decision problems with uncertain transition matrices," in *17th Annual Conference on Neural Information Processing Systems (NIPS)*, pp. 1–7, NIPS, 2003.
- [75] J. Pannequin, A. Bayen, I. Mitchell, H. Chung, and S. Sastry, "Multiple aircraft deconflicted path planning with weather avoidance constraints," in *AIAA Guidance, Navigation and Control Conference and Exhibit*, p. 6588, 2007.
- [76] F. Vormer, M. Mulder, R. V. Paassen, and J. Mulder, "Optimization of flexible approach trajectories using a genetic algorithm," *Journal of Aircraft*, vol. 43, no. 4, pp. 941–952, 2006.
- [77] P. E. Hart, N. J. Nilsson, and B. Raphael, "A formal basis for the heuristic determination of minimum cost paths," *IEEE transactions on Systems Science and Cybernetics*, vol. 4, no. 2, pp. 100–107, 1968.
- [78] M. Randour, J.-F. Raskin, and O. Sankur, "Variations on the stochastic shortest path problem," in *International Workshop on Verification, Model Checking, and Abstract Interpretation*, pp. 1–18, Springer, 2015.

- [79] S. Bokadia and J. Valasek, "Severe weather avoidance using informed heuristic search," *AIAA Paper*, vol. 4232, 2001.
- [80] L. Zuo, Q. Guo, X. Xu, and H. Fu, "A hierarchical path planning approach based on A* and least-squares policy iteration for mobile robots," *Neurocomputing*, vol. 170, pp. 257–266, 2015.
- [81] M. R. Endsley, "Automation and situation awareness," in *Automation and Human Performance*, pp. 183–202, Routledge, 2018.
- [82] G. Ioannou, P. Louvieris, and N. Clewley, "A Markov multi-phase transferable belief model for cyber situational awareness," *IEEE Access*, 2019.
- [83] L. Snidaro, I. Visentini, and K. Bryan, "Fusing uncertain knowledge and evidence for maritime situational awareness via Markov logic networks," *Information Fusion*, vol. 21, pp. 159–172, 2015.
- [84] Y. Han and Y. Deng, "An evidential fractal analytic hierarchy process target recognition method," *Defence Science Journal*, vol. 68, no. 4, pp. 367–373, 2018.
- [85] G. Xie, H. Gao, B. Huang, L. Qian, and J. Wang, "A driving behavior awareness model based on a dynamic Bayesian network and distributed genetic algorithm," *International Journal of Computational Intelligence Systems*, vol. 11, no. 1, pp. 469–482, 2018.
- [86] W. Zhang, X. Ji, Y. Yang, J. Chen, Z. Gao, and X. Qiu, "Data fusion method based on improved DS evidence theory," in *2018 IEEE International Conference on Big Data and Smart Computing (BigComp)*, pp. 760–766, IEEE, 2018.
- [87] D. Karaboga and E. Kaya, "Adaptive network based fuzzy inference system (ANFIS) training approaches: a comprehensive survey," *Artificial Intelligence Review*, pp. 1–31, 2018.
- [88] J. Tang, "Analysis and improvement of traffic alert and collision avoidance system," *IEEE Access*, vol. 5, pp. 21419–21429, 2017.
- [89] A. T. McCartt and J. Rohrbaugh, "Evaluating group decision support system effectiveness: A performance study of decision conferencing," *Decision Support Systems*, vol. 5, no. 2, pp. 243–253, 1989.
- [90] E. Koksalmis and Ö. Kabak, "Deriving decision makers' weights in group decision making: an overview of objective methods," *Information Fusion*, vol. 49, pp. 146–160, 2019.
- [91] D. Wu and Y. Cui, "Disaster early warning and damage assessment analysis using social media data and geo-location information," *Decision Support Systems*, vol. 111, pp. 48–59, 2018.
- [92] N. Sahebjamnia, S. A. Torabi, and S. A. Mansouri, "A hybrid decision support system for managing humanitarian relief chains," *Decision Support Systems*, vol. 95, pp. 12–26, 2017.

- [93] P. Srisawat, N. Kronprasert, and K. Arunotayanun, "Development of decision support system for evaluating spatial efficiency of regional transport logistics," *Transportation Research Procedia*, vol. 25, pp. 4832–4851, 2017.
- [94] L. Jayarathna, D. Rajapaksa, S. Managi, W. Athukorala, B. Torgler, M. A. Garcia-Valiñas, R. Gifford, and C. Wilson, "A gis based spatial decision support system for analysing residential water demand: A case study in Australia," *Sustainable Cities and Society*, vol. 32, pp. 67–77, 2017.
- [95] S. Biswas and R. V. Babu, "Anomaly detection via short local trajectories," *Neurocomputing*, vol. 242, pp. 63–72, 2017.
- [96] S. J. Landry, X. W. Chen, and S. Y. Nof, "A decision support methodology for dynamic taxiway and runway conflict prevention," *Decision Support Systems*, vol. 55, no. 1, pp. 165–174, 2013.
- [97] M. Liang, D. Delahaye, and P. Marechal, "Conflict-free arrival and departure trajectory planning for parallel runway with advanced point-merge system," *Transportation Research Part C: Emerging Technologies*, vol. 95, pp. 207–227, 2018.
- [98] J. Tang, F. Zhu, and M. A. Piera, "A causal encounter model of traffic collision avoidance system operations for safety assessment and advisory optimization in high-density airspace," *Transportation Research Part C: Emerging Technologies*, vol. 96, pp. 347–365, 2018.
- [99] C. Di Ciccio, H. Van der Aa, C. Cabanillas, J. Mendling, and J. Prescher, "Detecting flight trajectory anomalies and predicting diversions in freight transportation," *Decision Support Systems*, vol. 88, pp. 1–17, 2016.
- [100] F. A. A. (FAA), "Pilot's handbook of aeronautical knowledge FAA-H-8083-25A," 2004.
- [101] I. C. A. Organization, *Manual of the ICAO Standard Atmosphere: extended to 80 kilometres (262 500 feet)*, vol. 7488. International Civil Aviation Organization, 1993.
- [102] C. ICAO, "Phase of flight, definitions and usage notes," *CAST/ICAO Common Taxonomy Team*, <http://www.intlaviationstandards.org/Documents/PhaseofFlightDefinitions.pdf>, *Tech. Rep*, 2013.
- [103] I. Annex, "Aeronautical telecommunications," *Catalogue of ICAO Publications*, vol. 1, p. I02, 2002.
- [104] Canberra, "Airservices Australia." Website, 1995. <http://www.airservicesaustralia.com/>.
- [105] P. ICAO, "Air traffic management," *Doc-4444*, 2007.
- [106] Seattle, "Skyvector." Website, 2006. <https://skyvector.com>.

- [107] N. Xu, G. Donohue, K. B. Laskey, and C.-H. Chen, "Estimation of delay propagation in the national aviation system using Bayesian networks," in *6th USA/Europe Air Traffic Management Research and Development Seminar*, FAA and Eurocontrol Baltimore, MD, 2005.
- [108] J. J. Rebollo and H. Balakrishnan, "Characterization and prediction of air traffic delays," *Transportation Research Part C: Emerging Technologies*, vol. 44, pp. 231–241, 2014.
- [109] Y. J. Kim, S. Choi, S. Briceno, and D. Mavris, "A deep learning approach to flight delay prediction," in *Digital Avionics Systems Conference (DASC), 2016 IEEE/AIAA 35th*, pp. 1–6, IEEE, 2016.
- [110] W. Haiyan and W. Youzhen, "Vessel traffic flow forecasting with the combined model based on support vector machine," in *Transportation Information and Safety (ICTIS), 2015 International Conference on*, pp. 695–698, IEEE, 2015.
- [111] D. Huang, Z. Deng, L. Zhao, and B. Mi, "A short-term traffic flow forecasting method based on Markov chain and grey Verhulst model," in *Data Driven Control and Learning Systems (DDCLS), 2017 6th*, pp. 606–610, IEEE, 2017.
- [112] A. Abadi, T. Rajabioun, P. A. Ioannou, *et al.*, "Traffic flow prediction for road transportation networks with limited traffic data," *IEEE Transactions Intelligent Transportation Systems*, vol. 16, no. 2, pp. 653–662, 2015.
- [113] S. Qiao, D. Shen, X. Wang, N. Han, and W. Zhu, "A self-adaptive parameter selection trajectory prediction approach via hidden Markov models," *IEEE Transactions on Intelligent Transportation Systems*, vol. 16, no. 1, pp. 284–296, 2015.
- [114] D. Jeong, M. Baek, and S.-S. Lee, "Long-term prediction of vehicle trajectory based on a deep neural network," in *Information and Communication Technology Convergence (ICTC), 2017 International Conference on*, pp. 725–727, IEEE, 2017.
- [115] D. Runle, L. Jiaqi, G. Lu, L. Zhifeng, and Z. Li, "Long term trajectory prediction based on advanced guidance law recognition," in *Metrology for AeroSpace (MetroAeroSpace), 2017 IEEE International Workshop on*, pp. 456–461, IEEE, 2017.
- [116] C. Yuan, D. Li, and Y. Xi, "Medium-term prediction of urban traffic states using probability tree," in *Control Conference (CCC), 2016 35th Chinese*, pp. 9246–9251, IEEE, 2016.
- [117] D. Chen, M. Hu, K. Han, H. Zhang, and J. Yin, "Short/medium-term prediction for the aviation emissions in the En Route airspace considering the fluctuation in air traffic demand," *Transportation Research Part D: Transport and Environment*, vol. 48, pp. 46–62, 2016.
- [118] P. Duan, G. Mao, W. Liang, and D. Zhang, "A unified spatio-temporal model for short-term traffic flow prediction," *IEEE Transactions on Intelligent Transportation Systems*, 2018.

-
- [119] H. Tan, Y. Wu, B. Shen, P. J. Jin, and B. Ran, "Short-term traffic prediction based on dynamic tensor completion," *IEEE Transactions on Intelligent Transportation Systems*, vol. 17, no. 8, pp. 2123–2133, 2016.
- [120] Z. Zhou, J. Chen, B. Shen, Z. Xiong, H. Shen, and F. Guo, "A trajectory prediction method based on aircraft motion model and grey theory," in *Advanced Information Management, Communicates, Electronic and Automation Control Conference (IMCEC), 2016 IEEE*, pp. 1523–1527, IEEE, 2016.
- [121] Y. Song, P. Cheng, and C. Mu, "An improved trajectory prediction algorithm based on trajectory data mining for air traffic management," in *Information and Automation (ICIA), 2012 International Conference on*, pp. 981–986, IEEE, 2012.
- [122] C. Zhang, X. Zhang, C. Shi, and W. Liu, "Aircraft trajectory prediction based on genetic programming," in *2016 3rd International Conference on Information Science and Control Engineering (ICISCE)*, pp. 158–162, IEEE, 2016.
- [123] S. V. Kumar and L. Vanajakshi, "Short-term traffic flow prediction using seasonal ARIMA model with limited input data," *European Transport Research Review*, vol. 7, no. 3, p. 21, 2015.
- [124] A. Anand, G. Ramadurai, and L. Vanajakshi, "Data fusion-based traffic density estimation and prediction," *Journal of Intelligent Transportation Systems*, vol. 18, no. 4, pp. 367–378, 2014.
- [125] C.-C. Lu and X. Zhou, "Short-term highway traffic state prediction using structural state space models," *Journal of Intelligent Transportation Systems*, vol. 18, no. 3, pp. 309–322, 2014.
- [126] C. Yuan, D. Li, and Y. Xi, "Campus trajectory forecast based on human activity cycle and Markov method," in *Cyber Technology in Automation, Control, and Intelligent Systems (CYBER), 2015 IEEE International Conference on*, pp. 941–946, IEEE, 2015.
- [127] B. Wang, Y. Hu, G. Shou, and Z. Guo, "Trajectory prediction in campus based on Markov chains," in *International Conference on Big Data Computing and Communications*, pp. 145–154, Springer, 2016.
- [128] M. A. Awad and I. Khalil, "Prediction of user's web-browsing behavior: Application of Markov model," *IEEE Transactions on Systems, Man, and Cybernetics, Part B (Cybernetics)*, vol. 42, no. 4, pp. 1131–1142, 2012.
- [129] S. Sun, C. Zhang, and Y. Zhang, "Traffic flow forecasting using a spatio-temporal Bayesian network predictor," in *International Conference on Artificial Neural Networks*, pp. 273–278, Springer, 2005.
- [130] G. A. Davis and N. L. Nihan, "Nonparametric regression and short-term freeway traffic forecasting," *Journal of Transportation Engineering*, vol. 117, no. 2, pp. 178–188, 1991.

- [131] P. Cai, Y. Wang, G. Lu, P. Chen, C. Ding, and J. Sun, "A spatiotemporal correlative K-nearest neighbor model for short-term traffic multistep forecasting," *Transportation Research Part C: Emerging Technologies*, vol. 62, pp. 21–34, 2016.
- [132] X. Zeng and Y. Zhang, "Development of recurrent neural network considering temporal-spatial input dynamics for freeway travel time modeling," *Computer-Aided Civil and Infrastructure Engineering*, vol. 28, no. 5, pp. 359–371, 2013.
- [133] M. Gariel, A. N. Srivastava, and E. Feron, "Trajectory clustering and an application to airspace monitoring," *IEEE Transactions on Intelligent Transportation Systems*, vol. 12, no. 4, pp. 1511–1524, 2011.
- [134] A. Sternberg, J. Soares, D. Carvalho, and E. Ogasawara, "A review on flight delay prediction," *arXiv preprint arXiv:1703.06118*, 2017.
- [135] X. Tang, J. Gu, Z. Shen, and P. Chen, "A flight profile clustering method combining twed with K-means algorithm for 4D trajectory prediction," in *Integrated Communication, Navigation, and Surveillance Conference (ICNS), 2015*, pp. S3–1, IEEE, 2015.
- [136] Z. Shi, M. Xu, Q. Pan, B. Yan, and H. Zhang, "LSTM-based flight trajectory prediction," in *2018 International Joint Conference on Neural Networks (IJCNN)*, pp. 1–8, IEEE, 2018.
- [137] D. Birant and A. Kut, "ST-DBSCAN: An algorithm for clustering spatial-temporal data," *Data & Knowledge Engineering*, vol. 60, no. 1, pp. 208–221, 2007.
- [138] M. Thelwall, "The precision of the arithmetic mean, geometric mean and percentiles for citation data: An experimental simulation modelling approach," *Journal of Informetrics*, vol. 10, no. 1, pp. 110–123, 2016.
- [139] C.-C. Chang and C.-J. Lin, "LIBSVM: a library for support vector machines," *ACM Transactions on Intelligent Systems and Technology (TIST)*, vol. 2, no. 3, p. 27, 2011.
- [140] W. Richards, K. O'Brien, and C. Dean, "New air traffic surveillance technology. Boeing Aero Quarterly 2," 2014.
- [141] G. Gugliotta, "An air-traffic upgrade to improve travel by plane," *The New York Times*, vol. 17, 2009.
- [142] "SESAR ADS-B." Website, 2014. <http://www.aai.aero/misc/AIPS-2014-18.pdf>.
- [143] E. Kelly, "Australia and Indonesia swap ADS-B data," *Flight International*, vol. 178, no. 5268, pp. 12–12, 2010.
- [144] F. Chollet *et al.*, "Keras," 2015.
- [145] P. Senin, "Dynamic time warping algorithm review," *Information and Computer Science Department University of Hawaii at Manoa Honolulu, USA*, vol. 855, no. 1-23, p. 40, 2008.

- [146] Y. Lin, J.-w. Zhang, and H. Liu, "An algorithm for trajectory prediction of flight plan based on relative motion between positions," *Frontiers of Information Technology & Electronic Engineering*, vol. 19, no. 7, pp. 905–916, 2018.
- [147] M. Abramson and K. Ali, "Integrating the Base of Aircraft Data (BADA) in CTAS trajectory synthesizer," 2012.
- [148] R. Pascanu, C. Gulcehre, K. Cho, and Y. Bengio, "How to construct deep recurrent neural networks," *arXiv preprint arXiv:1312.6026*, 2013.
- [149] M. Hermans and B. Schrauwen, "Training and analysing deep recurrent neural networks," in *Advances in Neural Information Processing Systems*, pp. 190–198, 2013.
- [150] M. J. De Smith, M. F. Goodchild, and P. Longley, *Geospatial analysis: a comprehensive guide to principles, techniques and software tools*. Troubador Publishing Ltd, 2007.
- [151] M. L. Hetland, *Python algorithms: mastering basic algorithms in the Python language*. Apress, 2014.
- [152] R. Dechter and J. Pearl, "Generalized best-first search strategies and the optimality of A," *Journal of the ACM (JACM)*, vol. 32, no. 3, pp. 505–536, 1985.
- [153] E. Blasch, É. Bossé, and D. A. Lambert, *High-level information fusion management and systems design*. Artech House, 2012.
- [154] B. Khaleghi, A. Khamis, F. O. Karray, and S. N. Razavi, "Multisensor data fusion: A review of the state-of-the-art," *Information Fusion*, vol. 14, no. 1, pp. 28–44, 2013.
- [155] T. G. Farr, P. A. Rosen, E. Caro, R. Crippen, R. Duren, S. Hensley, M. Kobrick, M. Paller, E. Rodriguez, L. Roth, *et al.*, "The shuttle radar topography mission," *Reviews of Geophysics*, vol. 45, no. 2, 2007.
- [156] Y. Lin, B. Yang, J. Zhang, and H. Liu, "Approach for 4-D trajectory management based on hmm and trajectory similarity," *Journal of Marine Science and Technology*, vol. 27, no. 3, pp. 246–256, 2019.
- [157] N. Ye, Y. Zhang, R. Wang, and R. Malekian, "Vehicle trajectory prediction based on hidden Markov model.," *KSII Transactions on Internet & Information Systems*, vol. 10, no. 7, 2016.
- [158] D. S. Hirschberg, "A linear space algorithm for computing maximal common subsequences," *Communications of the ACM*, vol. 18, no. 6, pp. 341–343, 1975.
- [159] B. Lin and J. Su, "One way distance: For shape based similarity search of moving object trajectories," *GeoInformatica*, vol. 12, no. 2, pp. 117–142, 2008.
- [160] G. Yang and W. Huang, "Application of the TOPSIS based on entropy-AHP weight in nuclear power plant nuclear-grade equipment supplier selection," in *2009 International Conference on Environmental Science and Information Application Technology*, vol. 3, pp. 633–636, IEEE, 2009.

-
- [161] K. Zhang, P. Liu, K. Li, W. Kong, and J. Zhang, “Multi-target threat assessment in air combat based on entropy and VIKOR,” in *2017 Ninth International Conference on Advanced Computational Intelligence (ICACI)*, pp. 175–179, IEEE, 2017.
- [162] B. Sridhar, G. Chatterji, S. Grabbe, and K. Sheth, “Integration of traffic flow management decisions,” in *AIAA Guidance, Navigation, and Control Conference and Exhibit*, p. 5014, 2002.
- [163] Y. Wu, H. Tan, X. Chen, and B. Ran, “Memory, attention and prediction: a deep learning architecture for car-following,” *Transportmetrica B: Transport Dynamics*, vol. 7, no. 1, pp. 1553–1571, 2019.

